Describing the relationship between three ice hockey helmet impact tests and reconstructions of concussive injuries in professional ice hockey

Andrew Meehan

A thesis submitted to the Faculty of Graduate and Postdoctoral Studies
In partial fulfillment of the requirements for the degree of

MASTER OF SCIENCE IN HUMAN KINETICS

Supervisor
T. Blaine Hoshizaki, PhD

Committee Members
Patrick Bishop, PhD
Gordon Robertson, PhD

School of Human Kinetics
Faculty of Health Sciences
University of Ottawa

Acknowledgements

I would like to start by thanking my thesis supervisor, Dr. Blaine Hoshizaki, who has supported me throughout the completion of this thesis. Thank you for welcoming me into your laboratory as an undergraduate student and introducing me to the world of research. Your patience and guidance have helped me become a stronger student and researcher. Thank you for helping develop this project into something that I am passionate about and proud of.

I would also like to thank my committee members, Dr. Patrick Bishop and Dr. Gordon Robertson. Thank you for volunteering your time to read and provide feedback on this thesis. Your insightful questions and ideas have enriched the quality of this project, and I am grateful for your assistance. Thank you to CCM for providing the ice hockey helmets used in this thesis.

Next, I would like to extend my gratitude to Dr. Andrew Post for his assistance and mentorship. I appreciate all your help with my undergraduate and graduate research projects. Thank you for taking the time to answer my questions, keeping the laboratory equipment in working order, and reminding me to always clean up my tools. I would also like to thank Dr. David Koncan, for always answering my questions by asking me more questions. Thank you for being patient and helping me solve problems logically.

I would also like to thank the rest of my colleagues, past and present, at the Neurotrauma Impact Science Laboratory: Dr. Marshall Kendal, Dr. Anna Oeur, Dr. Karen Taylor, Dr. Janie Cournoyer, Dr. Michio Clark, Clara Karton, Lauren Dawson, Talia Ignacy, Bianca Rock, Wes Chen, Bianca Paiement, Kevin Adanty, Ali Khatib, Luc Champoux, among others. It has been a pleasure working alongside and learning from all of you. Thank you for the advice, encouragement, and most importantly, the laughter.

Last but not least, thank you to my family for supporting me along this journey. To my wife Kirsten, thank you for always being there and encouraging me when I needed it most. Thank you for putting up with me on stressful days and for always reminding me to take a break. It truly feels like we accomplished this together and I am very grateful for your support. Finally, thank you to my cats Marley and Teddy for their encouragement. Thank you for staying awake with me during all those late nights and for sitting on my keyboard while I was trying to type.

Abstract

Ice hockey helmets effectively mitigate the risk of skull fractures and focal traumatic brain injuries in professional ice hockey (PIH), but do not manage diffuse brain injuries such as concussion. This is due to current standard tests, which only represent one head impact event (a fall to the ice) and do not measure rotational head kinematics. It is important that helmets are evaluated using impact conditions that represent how players sustain concussions in ice hockey.

The objective of this study was to describe the relationship between three ice hockey helmet tests and reconstructions of three concussive injury events in PIH. A flat anvil drop test (representing head-to-ice impacts), angled anvil drop test (representing head-to-boards impacts at 30° and 45°) and pneumatic ram test (representing medium and high compliance shoulder-to-head impacts) were performed using parameters reflecting concussive injuries in PIH. Stepwise regressions identified the dynamic response variables producing the strongest relationships with MPS. For the flat anvil drop test, dominant linear acceleration had the strongest relationship with MPS (R^2 = 0.960), while there were no significant predictors of MPS from the PIH head-to-ice reconstructions. Rotational velocity had the strongest relationship for the 30° (R^2 = 0.978) and 45° Anvil Drop Tests (R^2 = 0.977), while rotational acceleration had the strongest relationship for the PIH head-to-boards reconstructions (R^2 = 0.649). Resultant rotational acceleration had the strongest relationship for the medium compliance ram test (R^2 = 0.671), the high compliance ram test (R^2 = 0.850) and the PIH shoulder-to-head reconstructions (R^2 = 0.763).

The flat anvil drop test results indicate that falls on a flat, rigid surface induce primarily linear acceleration of the head. Standards should continue using this type of test to ensure helmets prevent skull fracture and focal TBI. Ice hockey helmets should also be evaluated using an angled anvil drop test and a collision ram test, representing two unique head impact events known to cause concussive injuries. The 45° Anvil Drop Test provided a closer representation of concussive head-to-boards impacts in PIH, with rotational velocity producing the strongest relationship with MPS. For collision impacts, the Medium Compliance Ram Test yielded repeatable impact conditions while the High Compliance Ram Test provided a closer representation of real-world concussive shoulder-to-head impacts. For these pneumatic ram tests, rotational acceleration produced the strongest relationship with MPS. The information in this thesis may be used by standards organizations when designing future ice hockey helmet tests.

Table of Contents

Acknowledgements ii
Abstract iii
Table of Contents iv
List of Tables vii
List of Figures ix
List of Equations xii

Chapter 1: Introduction 1

Chapter 2: Literature Review 3
2.1 The Spectrum of Brain Trauma 3
2.2 Brain Trauma in Ice Hockey 4
2.3 Head Impact Events in Ice Hockey 5
2.4 Biomechanics of Brain Trauma 6
2.4.1 Linear Acceleration 7
2.4.2 Rotational Acceleration 7
2.4.3 Rotational Velocity 9
2.4.4 Resultant and Dominant Components of Dynamic Response 9
2.5 Brain Tissue Deformation 10
2.5.1 Finite Element Modelling 10
2.5.2 Maximum Principal Strain 10
2.6 Ice Hockey Helmet Test Methods 11
2.6.1 Standard Test Methods 11
2.6.2 Rotational Test Methods 12
2.7 Summary 13

Chapter 3: Research Design 14
3.1 Research Question 14
3.2 Objectives 14
3.3 Independent Variables 14
3.4 Dependent Variables 15

3.5 Null Hypotheses 15

Chapter 4: Methods 16

4.1 Test Equipment 16

4.1.1 Monorail Drop Rig 16

4.1.2 Pneumatic Linear Impactor 17

4.1.3 Hybrid III Headform 18

4.1.4 Unbiased Neckform 21

4.1.5 Ice Hockey Helmets 22

4.2 Helmet Test Methods 23

4.2.1 Flat Anvil Drop Test 23

4.2.2 Angled Anvil Drop Test 25

4.2.3 Pneumatic Ram Test 27

4.3 Finite Element Modeling 30

4.3.1 University College Dublin Brain Trauma Model 30

4.3.2 Calculation of Maximum Principal Strain 32

4.4 Professional Ice Hockey (PIH) Concussion Reconstruction Dataset 32

4.5 Statistical Analysis 34

4.5.1 Mann-Whitney *U* Tests 34

4.5.2 Stepwise Regressions 34

Chapter 5: Results 36

5.1 Mean Dynamic Response and MPS Comparisons (Mann-Whitney *U* Tests) 36

5.1.1 Flat Anvil Drop Test vs. PIH Head-to-Ice Concussion Reconstructions 36

5.1.2 Angled Anvil Drop Tests vs. PIH Head-to-Boards Concussion Reconstructions 37

5.1.3 Pneumatic Ram Impact Tests vs. PIH Shoulder-to-Head Concussion Reconstructions 40

5.2 Stepwise Regression Analysis 42

5.3 Limitations 45

5.3.1 Hybrid III Headform 45

5.3.2 Unbiased Neckform 46

5.3.3 UCDBTM 46

5.3.4 Helmets....46
5.3.5 Professional Ice Hockey Concussion Reconstruction Dataset....47
5.4 Delimitations....47
5.4.1 Generalizability of Findings....47

Chapter 6: Discussion....48
6.1 Flat Anvil Drop Test and PIH Head-to-Ice Concussion Reconstructions....48
6.2 Angled Anvil Drop Tests and PIH Head-to-Boards Concussion Reconstructions....49
6.3 Pneumatic Ram Tests and PIH Shoulder-to-Head Concussion Reconstructions....52
6.4 Comparison of Helmet Test Results to Concussive Injury Literature....55

Chapter 7: Conclusion....56

References....57

Appendix A....66
Appendix B....67
Appendix C....68
Appendix D....70
Appendix E....72
Appendix F....74
Appendix G....75
Appendix H....78
Appendix I....82
Appendix J....92

List of Tables

Table 1. Material properties of the UCDBTM

Table 2. Material characteristics of brain tissue represented in the UCDBTM

Table 3. Comparison of mean (±1 standard deviation) dynamic response and brain tissue deformation between the Flat Anvil Drop Test and the NHL head-to-ice concussion reconstructions (n = 4). Comparisons were made using the Mann-Whitney *U* Test ($\alpha = 0.007$).

Table 4. Comparison of mean (±1 standard deviation) dynamic response and brain tissue deformation between two Angled Anvil Drop Tests (30° and 45°) and NHL head-to-boards concussion reconstructions (n = 7). Comparisons were made using the Mann-Whitney *U* Test ($\alpha = 0.007$).

Table 5. Comparison of mean (±1 standard deviation) dynamic response and brain tissue deformation between the Medium Compliance Ram Test, High Compliance Ram Test, and NHL head-to-shoulder concussion reconstructions (n = 16). Comparisons were made using the Mann-Whitney *U* Test ($\alpha = 0.007$).

Table 6. Stepwise regression analysis examining the relationship between dynamic response and MPS for the Flat Anvil Drop Test and NHL head-to-ice concussion reconstructions.

Table 7. Stepwise regression analysis examining the relationship between dynamic response and MPS for the 30° Anvil Drop Test, 45° Anvil Drop Test, and NHL head-to-boards concussion reconstructions.

Table 8. Stepwise regression analysis examining the relationship between dynamic response and MPS for the Medium Compliance Ram Test, High Compliance Ram Test, and NHL shoulder-to-head concussion reconstructions.

Table A-1. Summary of test equipment, impact parameters, and pass/fail criteria for current ice hockey helmet standard tests

Table D-1. Calculated head impact angles for videos of head-to-boards concussions in the NHL.

Table E-1. Results of the tests for normality on all data used in this thesis, using $\alpha = 0.05$ to establish significance. *A p-value<0.05 indicates that the null hypothesis (H_o = data are normally distributed) should be rejected and the data are not normally distributed (indicated in red).

Table H-1. Impact duration range (ms) for each helmet test at low, medium, and high velocities.

Table H-2. Impact duration range (ms) for each head impact event in the NHL concussion reconstruction dataset.

Table I-1. Mean peak dynamic response and brain tissue deformation (±1 standard deviation) for the Flat Anvil Drop Test.

Table I-2. Mean peak dynamic response and brain tissue deformation (±1 standard deviation) for the 30^{o} Anvil Drop Test.

Table I-3. Mean peak dynamic response and brain tissue deformation (±1 standard deviation) for the 45^{o} Anvil Drop Test.

Table I-4. Mean peak dynamic response and brain tissue deformation (±1 standard deviation) for the Medium Compliance Ram Test.

Table I-5. Mean peak dynamic response and brain tissue deformation (±1 standard deviation) for the High Compliance Ram Test.

Table J-1. Average coefficients of variation for each dependent variable for each helmet test.

List of Figures

Figure 1. Head injury research paradigm, adapted from Ommaya et al., 1994. The framework for sport-related head impact research is outlined in red.

Figure 2. Monorail drop rig shown with vertical rail (A), motorized release system (B), drop carriage (C), steel anvil (D), time gate (E), and concrete base (F).

Figure X. Pneumatic linear impactor consisting of a steel frame (A), compressed air tank (B), piston chamber (C), impacting arm (D), time gate (E), striker cap (F), and sliding table (G).

Figure 4. The Hybrid III headform separated to reveal the interior steel structure (left) and external vinyl skin (right).

Figure 5. Posterior view of accelerometers inside the Hybrid III headform, placed in a 3-2-2-2 array. Two accelerometers are mounted at the top (A), front (B), and side (C), while 3 accelerometers are mounted at the centre of gravity of the headform (D).

Figure 6. Coordinate system of the headform defined by the right-hand rule. Arrows indicate the direction of positive rotation about each axis.

Figure 7. Hybrid III neckform (left) and unbiased neckform (right).

Figure 8. CCM Vector 08 helmet with 0.0094 m of black VN740 foam in the front and front boss locations (A) and 0.0094 m of black VN1000 foam in the side, rear boss, and rear locations (B). All black foam is covered with a 0.0031 m layer of beige VN600 foam.

Figure 9. Flat MEP anvil (black) attached to the support base (red).

Figure 10. Impact locations for the flat impact drop test: front boss (left) and rear boss (right).

Figure 11. Two steel anvils used for the angled impact tests: 30° steel anvil (left) and 45° steel anvil (right).

Figure 12. Impact locations for the angled drop test: side (left), rear boss (middle), and rear (right).

Figure 13. Medium compliance striker cap (left) and high compliance striker cap (right).

Figure 14. Impact locations and angles for the pneumatic ram impact test as viewed in the sagittal (first column), frontal (second column), and transverse (third column) planes. Red arrows indicate the impact vector through the headform (Walsh et al., 2012).

Figure 15. Comparison of mean peak resultant and dominant linear acceleration (A), rotational acceleration (B), rotational velocity (C), and MPS (D) between the Flat Anvil Drop Test and PIH head-to-ice concussion reconstructions. Error bars indicate ± one standard deviation. Significant differences indicated by an asterisk (*).

Figure 16. Comparison of mean peak resultant and dominant linear acceleration (A), rotational acceleration (B), rotational velocity (C), and MPS (D) between the 30° Anvil Drop Test, 45° Drop Test, and PIH head-to-boards concussion reconstructions. Error bars indicate ± one standard deviation. Significant differences indicated by an asterisk (*).

Figure 17. Comparison of mean peak resultant and dominant linear acceleration (A), rotational acceleration (B), rotational velocity (C), and MPS (D) between the Medium Compliance Ram Test, High Compliance Ram Test, and PIH shoulder-to-head concussion reconstructions. Error bars indicate ± one standard deviation. Significant differences indicated by an asterisk (*).

Figure 18. Examples of mean acceleration loading curve shapes from the 30° Anvil Drop Test, 45° Anvil Drop Test, and PIH head-to-boards concussion reconstructions. Dashed lines represent one standard deviation above and below the mean.

Figure 19. Examples of mean acceleration loading curve shapes from the Medium Compliance Ram Test, High Compliance Ram Test, and PIH shoulder-to-head concussion reconstructions. Dashed lines represent one standard deviation above and below the mean.

Figure B-1. Free body diagram of the moments acting on a helmeted headform during an angled impact drop test (Carnevale Lon, 2014).

Figure C-1. Spherical impactor instrumented with one uniaxial accelerometer.

Figure C-2. Monorail drop rig with spherical impactor, uniaxial accelerometer, and MEP pad.

Figure D-1. Head-to-boards impact angle calculation using Kinovea. Pictured above is the analysis of video number 7 (refer to Table D-1 for details).

Figure G-1. Dynamic response versus MPS for the Flat Anvil Drop Test and PIH head-to-ice concussion reconstructions.

Figure G-2. Dynamic response versus MPS for the 30° Anvil Drop Test, the 45° Anvil Drop Test, and the PIH head-to-boards concussion reconstructions.

Figure G-3. Dynamic response versus MPS for the Medium Compliance Ram Test, High Compliance Ram Test, and the PIH shoulder-to-head concussion reconstructions.

Figure H-1. Plot of rotational acceleration versus impact duration for the Flat Anvil Drop Test and PIH head-to-ice concussion reconstructions.

Figure H-2. Plot of rotational acceleration versus impact duration for the 30° Anvil Drop Test, 45° Anvil Drop Test, and PIH head-to-boards concussion reconstructions.

Figure H-3. Plot of rotational acceleration versus impact duration for the Medium Compliance Ram Test, High Compliance Ram Test, and PIH shoulder-to-head concussion reconstructions.

Figure I-1. Mean peak linear acceleration (A), rotational acceleration (B), rotational velocity (C), and MPS (D) for the Flat Anvil Drop Test, separated by impact velocity and location. Error bars indicate ± one standard deviation. FB = front boss; RB = rear boss.

Figure I-2. Mean peak linear acceleration (A), rotational acceleration (B), rotational velocity (C), and MPS (D) for the 30° Anvil Drop Test, separated by impact velocity and location. Error bars indicate ± one standard deviation. S = side; RB = rear boss; R = rear.

Figure I-3. Mean peak linear acceleration (A), rotational acceleration (B), rotational velocity (C), and MPS (D) for the 45° Anvil Drop Test, separated by impact velocity and location. Error bars indicate ± one standard deviation. S = side; RB = rear boss; R = rear.

Figure I-4. Mean peak linear acceleration (A), rotational acceleration (B), rotational velocity (C), and MPS (D) for the Medium Compliance Ram Test, separated by impact velocity and location. Error bars indicate ± one standard deviation. FBPA = front boss positive azimuth; S = side; RBNA = rear boss negative azimuth.

Figure I-5. Mean peak linear acceleration (A), rotational acceleration (B), rotational velocity (C), and MPS (D) for the High Compliance Ram Test, separated by impact velocity and location. Error bars indicate ± one standard deviation. FBPA = front boss positive azimuth; S = side; RBNA = rear boss negative azimuth.

List of Equations

Equation 1: Rotational acceleration of the headform about the x-axis

$$\overrightarrow{\alpha_x} = \frac{\overrightarrow{a_{zS}} - \overrightarrow{a_{zC}}}{2S} - \frac{\overrightarrow{\alpha_{yT}} - \overrightarrow{a_{yC}}}{2T}$$

Equation 2: Rotational acceleration of the headform about the y-axis

$$\overrightarrow{\alpha_y} = \frac{\overrightarrow{a_{xT}} - \overrightarrow{a_{xC}}}{2T} - \frac{\overrightarrow{\alpha_{zF}} - \overrightarrow{a_{zC}}}{2F}$$

Equation 3: Rotational acceleration of the headform about the z-axis

$$\overrightarrow{\alpha_z} = \frac{\overrightarrow{a_{yF}} - \overrightarrow{a_{yC}}}{2F} - \frac{\overrightarrow{\alpha_{xS}} - \overrightarrow{a_{xC}}}{2S}$$

Equation 4: Rotational velocity of the headform

$$\overrightarrow{\omega_i} = \int_0^T \overrightarrow{\alpha_i}\, dt + c_1$$

Equation 5: Shear characteristics of the viscoelastic behaviour of the brain

$$G(t) = G_\infty + (G_0 - G_\infty)e^{\beta t}$$

Equation 6: Hyperelastic Law

$$C_{10}(t) = 0.9C_{01}(t) = 620.5 + 1930e^{-\frac{t}{0.008}} + 1103e^{-\frac{t}{0.15}}(Pa)$$

Chapter 1: Introduction

Ice hockey is a fast-paced contact sport with more than 1.7 million participants worldwide (IIHF, 2017). Participation in ice hockey has been associated with a high risk of sustaining head injuries including concussion (CDCP, 2011; Cusimano et al., 2013; McFaull et al., 2016). To protect athletes, all ice hockey helmets must meet performance criteria established by standards organizations. Currently, standard tests drop a rigidly fixed helmeted headform on a flat surface and use linear acceleration-based performance criteria. These standard tests are primarily designed to ensure helmets prevent skull fractures and focal traumatic brain injuries (TBI), which have been associated with high magnitudes of linear acceleration (Kleiven, 2013; Ommaya and Hirsch, 1971). However, standards do not measure rotational acceleration, which has been reported to be more influential in the production of diffuse brain injuries such as concussion (Adams et al., 1981; Gennarelli et al., 1972, 1971). Furthermore, standard tests only represent one head impact event (a fall to the ice), yet concussions have been reported to result from multiple other events including head-to-boards and shoulder-to-head impacts (Hutchison et al., 2015, 2013). Developing standard helmet tests that use rotational performance criteria and represent different head impact events may increase the protective capacity of helmets and reduce the incidence of brain injuries in ice hockey.

Several rotation-inducing impact tests have been used in laboratory settings to evaluate helmet performance and risk of injury. A proposed European Committee for Standardization (CEN) impact test for cycling and equestrian helmets drops a helmeted headform on a 45° steel anvil to elicit rotation (CEN, 2015). This type of helmet test can be used to represent head-to-boards impacts in ice hockey. Additionally, non-centric pneumatic ram tests have been used to evaluate helmet performance in sports such as football and ice hockey (Clark et al., 2016; De

Grau, 2017; Post et al., 2013). A pneumatic ram test can be used to represent shoulder-to-head impacts in ice hockey. These two impact tests generate rotational responses of the head and may better reflect the mechanism of concussive injury compared to standard flat anvil drop tests. Determining how these tests relate to real-world concussive injuries is an important step in standard test development.

This thesis will examine a Flat Anvil Drop Test (representing head-to-ice impacts), an Angled Anvil Drop Test (representing head-to-boards impacts at 30^{o} and 45^{o}), and a Pneumatic Ram Test (representing medium and high compliance shoulder-to-head impacts). The results of each helmet test will be compared to reconstructions of concussive injury events in professional ice hockey (PIH). The relationship between dynamic response and brain tissue strain will be evaluated to identify the variables producing the strongest relationship with MPS for each helmet test and each concussive head impact event in PIH. The results of this thesis will determine whether the 30^{o} or 45^{o} Anvil Drop Test provides a closer representation of concussive head-to-boards impacts in professional ice hockey. Additionally, this thesis will discuss whether a medium or high compliance pneumatic ram test should be used to represent concussive shoulder-to-head impacts in professional ice hockey.

This study will inform the development of rotational standard ice hockey helmet tests that better address the risks associated with concussive injury. In response to a rotational standard test, ice hockey manufacturers would be required to address rotational head kinematics. This would increase helmet performance and reduce the incidence of brain injuries in ice hockey.

Chapter 2: Literature Review

2.1 The Spectrum of Brain Trauma

Brain trauma has been defined as a "consequence, direct or indirect, of the movements, forces, and deformations at each point in the brain" (Holbourn et al., 1943). Brain injuries can be broadly categorized as either mild traumatic brain injuries (mTBI) or as more severe traumatic brain injuries (TBI). Brain trauma can also be classified as either focal or diffuse, representing two unique mechanisms of injury (Biasca and Simmen, 2004).

Focal brain injuries result from forces associated with blunt trauma to the head, compressing tissues underneath the site of impact (coup) or opposite to the site of impact (contrecoup) (Andriessen et al., 2010). Deformation of the skull can produce coup contusions, in which small blood vessels in the brain are damaged or ruptured. Additionally, movement of the brain against the rough interior surface of the skull can produce contrecoup contusions (Viano et al., 1989). Whereas contusions are analogous to bruising, more severe focal injuries involve brain bleeding (called hematomas). The bleeding associated with epidural (between the skull and dura), subdural (between the dura and brain), and intracerebral (within the brain) hematomas may all lead to fatal levels of intracranial pressure (Adams et al., 1980). These injuries represent the severe end of the brain trauma spectrum and are classified as TBIs. In sports, focal injuries may be induced by falls resulting in the head striking a stiff surface, such as a bare head striking the ice surface in hockey (Hoshizaki et al., 2013).

While focal brain injuries only encompass localized neural damage, diffuse injuries affect larger volumes of the brain and are caused by the inertial effect of a head impact (Holbourn et al., 1943; Biasca and Simmen, 2004). Researchers have identified an association between diffuse brain injuries and rotation of the head, which induces shearing of neural tissue (Biasca and

Simmen, 2004; Gennarelli et al., 1982; Holbourn et al., 1943). The severity of injury depends on the volume of damaged neural tissue and the magnitude of strain (Ommaya and Gennarelli, 1974). At the severe end of the spectrum, diffuse axonal injury (DAI) involves extensive shearing of neural tissue and is a form of TBI (Hoshizaki and Brien, 2004). Mild traumatic brain injuries (commonly referred to as concussions) represent a less severe form of diffuse injury (Biasca and Simmen, 2004). Concussions are highly prevalent in contact sports such as ice hockey, football, and lacrosse (Cantu, 1996; Casson et al., 2010; Delaney et al., 2002).

2.2 Brain Trauma in Ice Hockey

Ice hockey has been identified as the sport with the highest incidence rate of concussive injury (Cusimano et al., 2013; Koh et al., 2003). In Canada, ice hockey is the primary cause of sport and recreation-related head injuries, accounting for up to 21% of head injuries presenting in Canadian emergency departments (Kelly et al., 2001). High concussion incidence rates have been documented in both amateur and professional levels of the sport (McFaull et al., 2016; Roberts et al., 1999; Wennberg and Tator, 2003). Wennberg and Tator (2003) examined the media reported rate of concussions in a North American professional ice hockey league between the 1986-87 and 2001-02 seasons. The authors reported an average of 6.4 concussions per 1000 games during the first 10 seasons, followed by an average of 24.7 concussions per 1000 games during the latter 6 seasons. The increase in concussion incidence rate over time was attributed to larger, faster athletes and increased injury reporting (Wennberg and Tator, 2003). In recent years, high rates of concussions in professional ice hockey remain a concern that has not been effectively managed (Wennberg and Tator, 2008). To improve the safety of ice hockey, it is important to understand the types of head impact events contributing to concussive injuries.

2.3 Head Impact Events in Ice Hockey

Ice hockey is a fast-paced sport played on a hard surface (ice) enclosed by rigid boundaries (boards and glass). This setting, combined with the increasing speed and size of athletes, creates a high-risk environment in which the head may impact a variety of surfaces. Head injuries can be caused by falls (impacting the ice, boards, or glass), collisions (impacting a shoulder, elbow, glove, or other protective equipment), and projectiles (impact from a puck) (Post et al., 2019). At younger levels, youth ice hockey players are still developing their balance and coordination skills. This leads to younger athletes frequently falling and impacting their heads on the ice. In contrast, adult and professional athletes are typically less prone to falling, unless due to an impact with another player. Head impacts to the boards and glass occur more frequently than impacts to the ice (Goodman et al., 2001). Additionally, the use of body checking to separate opponents from the puck yields frequent collisions between players. Research examining concussive events in professional ice hockey reported that collisions accounted for 88% of concussions, of which more than 40% involved shoulder-to-head contact (Hutchison et al., 2015, 2013). Furthermore, 37% of total concussions involved head contact with the boards or glass, while 7% of concussions were due to a fall or trip (Hutchison et al., 2015, 2013).

Each head impact event in ice hockey can be characterized by unique impact parameters. The impact velocity, location, and compliance interact to influence the nature of energy transfer to the head (Oeur, 2018). This affects the head dynamic response and subsequent degree of brain injury (Post et al., 2017a). To better understand the mechanics of brain injuries, a variety of cadaver, animal, and computational models have been used (Gennarelli et al., 1982; Löwenhielm, 1974; Nahum et al., 1977; Ommaya and Hirsch, 1971; Willinger and Baumgartner,

2003; Zhang et al., 2001). The following section will discuss how researchers have used these models to study the relationship between head dynamic response and brain trauma.

2.4 Biomechanics of Brain Trauma

During a head impact, brain trauma is caused by forces acting on the neural tissue. The head injury research paradigm proposed by Ommaya et al. (1994) (Figure 1) serves as a guide for understanding how mechanical loading induces dynamic response of the head, ultimately producing focal and diffuse damage to neural tissue. The effects of linear (often called translational) and rotational acceleration on brain injury have been extensively researched.

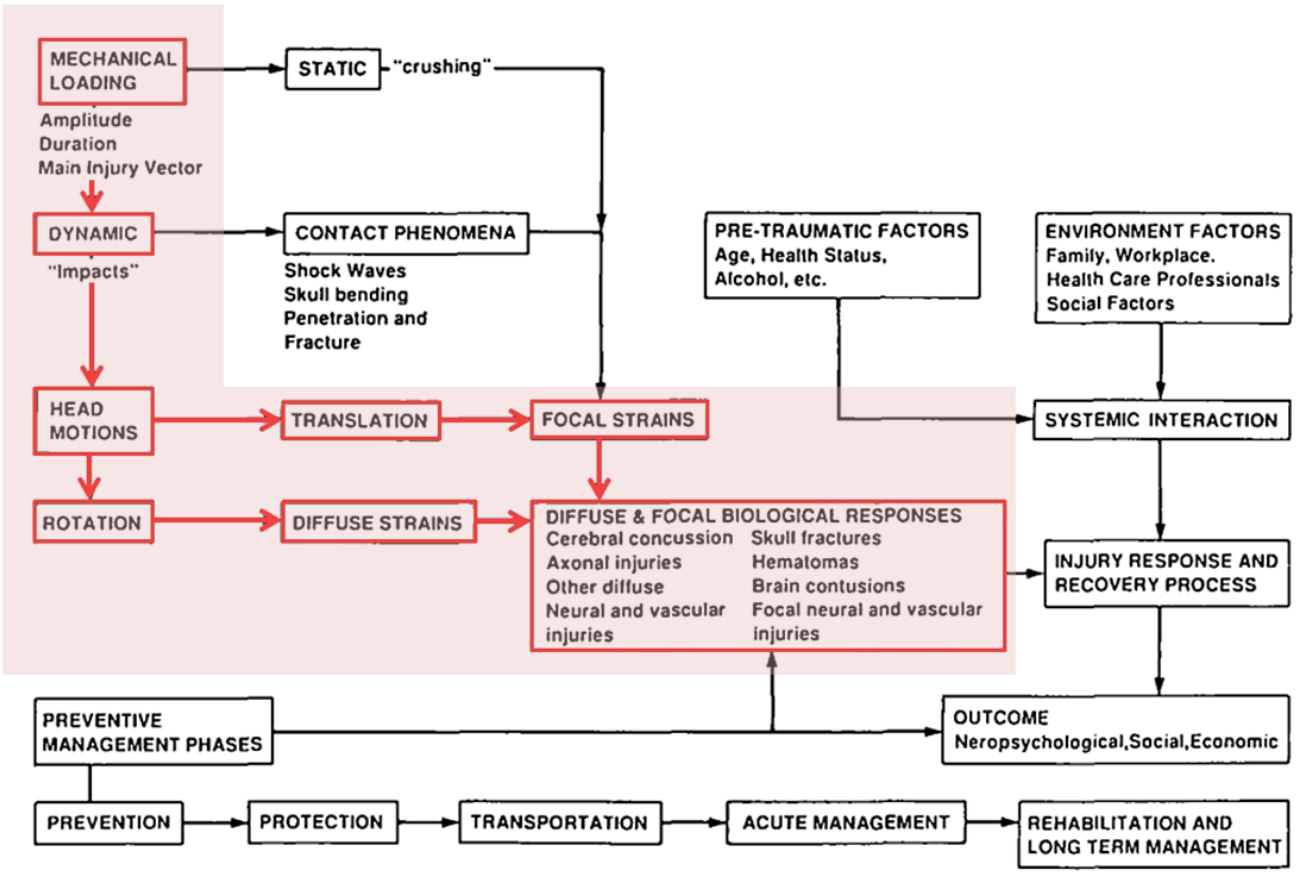

Figure 1. Head injury research paradigm, adapted from Ommaya et al., 1994. The framework for sport-related head impact research is outlined in red.

2.4.1 Linear Acceleration

Linear acceleration has been used to predict the risk of focal head injury and is typically reported in units of gravity, g (where 1 g = 9.81 m/s^2). Early research by Gurdjian and colleagues studied anesthetized dogs and associated linear acceleration of an impact with increased intracranial pressure and skull fracture (Gurdjian et al., 1953). The same research group also demonstrated that concussive outcomes in dogs were directly associated with the severity and duration of an applied pressure pulse (Gurdjian et al., 1955). Haddad et al. (1955) discovered a similar relationship between acceleration and cerebral concussion and produced "moderate" or "severe" concussive outcomes in 13 of 34 animals following impacts to the head. Future work continued to confirm that head impacts could induce visible skull fractures and intracranial pressure gradients (Gurdjian, 1966; Thomas et al., 1966).

Using data from cadaveric and animal model frontal impacts, Gurdjian and colleagues developed the Wayne State Tolerance Curve (WSTC) defining a threshold for skull fracture based on linear acceleration and impact duration (Gurdjian, 1966). Following the publication of this work, several measures of head injury severity were developed using weighted integrations of the linear acceleration-time curve: the Gadd Severity Index (GSI) (Gadd, 1966) and Head Injury Criterion (HIC) (Versace, 1970). These measures have been widely implemented as criteria for safety standards in automotive crash tests and sport helmet impact testing.

2.4.2 *Rotational Acceleration*

Rotational acceleration is defined as the change in rotational velocity, measured in units of rad/s^2. The association between rotational acceleration and concussive brain injury was first presented by Holbourn, a physicist in Oxford (1943, 1945). It was theorized that, due to the brain's extreme incompressibility (high bulk modulus) and low modulus of rigidity (low shear

modulus), neural tissue was more susceptible to shear-strains than compression or rarefaction (Holbourn et al., 1943). Holbourn supported this concept using gelatin models of the human brain. He demonstrated the relative weakness of the gelatin when exposed to shearing loads, as compared to compressive loads (Holbourn et al., 1943).

Researchers have supported this notion by producing brain injuries in animals through the application of controlled, non-impact rotational acceleration (Unterharnscheidt & Higgins, 1969). Studying primates (squirrel monkeys), Gennarelli and colleagues (1972) observed that rotational acceleration contributed more to concussive injury than linear acceleration. Concussive injuries were observed in all primates subjected to rotational acceleration, while concussion was not attainable in 12 of 25 primates subjected to pure linear acceleration (Gennarelli et al., 1972). In another study, rotation of primate heads in the sagittal plane induced a range of injuries including concussion, subdural hematoma, and death (Adams et al., 1981). Similarly, Gennarelli and colleagues (1982) subjected primates to controlled rotational acceleration in three planes, producing concussion and DAI. Finite element analysis has demonstrated that brain tissue strain is more influenced by rotational acceleration than linear acceleration (Zhang et al., 2006).

The injurious effect of rotational acceleration has been attributed to the inhomogeneous densities across different areas of the brain, resulting in uneven movement and shearing when stressed (Ommaya and Gennarelli, 1974). Additionally, the brain's inability to freely rotate within the skull contributes to rotation-induced injury (Hardy et al., 1994). As rotational acceleration is a primary contributor to concussive injury, it will be examined in this thesis.

2.4.3 Rotational Velocity

While the role of rotational acceleration has been extensively investigated in brain injury biomechanics, rotational velocity has also been presented as a measure of brain injury risk. Holbourn (1943) theorized that the severity of shear-strains in the brain were directly related to the change in rotational velocity. Rotational velocity has been reported to correlate with MPS (Takhounts et al., 2013) and has been used to distinguish between concussive and non-concussive sporting head impacts (McIntosh et al., 2014).

2.4.4 Resultant and Dominant Components of Dynamic Response

Linear acceleration, rotational acceleration, and rotational velocity are typically reported as peak resultant magnitudes. Resultant dynamic response describes the overall magnitude of head motion and correlates well with brain injury. Researchers have also examined the orthogonal coordinate components of dynamic response (x, y, and z) which account for the direction of head motion. Mcintosh and colleagues (2014) identified significant differences in coordinate components of linear and rotational acceleration between concussive and non-concussive impacts in Australian rules football. Recent research using American football helmets investigated the relationship between coordinate components of dynamic response and brain tissue strain (Taylor, 2018). The author identified strong correlations between both resultant and dominant components of dynamic response with brain tissue strain. The dominant component, which is the coordinate component experiencing the highest magnitude of response, accounts for the primary direction of head motion (Taylor, 2018). As such, the dominant component of dynamic response has been suggested to be an appropriate variable for helmet performance evaluation (Taylor, 2018). Both the resultant and dominant magnitudes of dynamic response will be evaluated in this thesis.

2.5 Brain Tissue Deformation

2.5.1 Finite Element Modelling

Advancements in computerized three-dimensional finite element (FE) models have permitted researchers to model the human skull and brain analytically. FE models can be used to evaluate the magnitude, location, and distribution of neural tissue strain, from which injury risk can be predicted (Horgan and Gilchrist, 2003; Kleiven, 2007; Willinger and Baumgartner, 2003; Zhang et al., 2001). In a FE model, the human skull and brain are decomposed into thousands of small elements. Each element is assigned material properties corresponding to the neural tissue it represents, in order to accurately predict the biomechanical response of the brain (Tse et al., 2014). Linear and rotational acceleration-time loading curves recorded during laboratory testing can be used as input for finite element models. While numerous measures of tissue strain can be extracted from finite element models, maximum principal strain will be used in this thesis.

2.5.2 Maximum Principal Strain

Mechanically, maximum principal strain (MPS) refers to the maximum elongation of neural tissue, in one of the primary axes, relative to the tissue's original length (Tse et al., 2014). Studies investigating the relationship between elongating neural tissue and brain injury have typically been conducted using *in vitro* cellular models. Thibault and colleagues (1974) stretched sciatic nerve bundles of a frog and evaluated the compound action potential as a measure of neuronal function. Small stretches produced temporary changes to the signal, while large stretches resulted in irreversible changes to neuronal function (Thibault et al., 1974). In another study, uniaxial loading of isolated giant squid axons resulted in a graded depolarization response (Galbraith et al., 1988; 1993). The responses ranged from mild reversible injury at strains equal

to or less than 10%, permanent disruption of function at strains of 20%, and structural failure at strains of 25% (Galbraith et al., 1988; 1993).

The results of *in vitro* studies have helped researchers understand how the biomechanics of tissue deformation at the microscopic level can influence brain injury at the macroscopic level (Ommaya et al., 1994). Importantly, these studies have demonstrated that strained neurons can experience alterations in function without structural damage. This is similar to concussive injuries, in which strained neural tissue experiences alterations in function without any change to the gross structure of the tissue. This is supported by the fact that conventional imaging methods, such as magnetic resonance imaging (MRI) and computed tomography (CT), do not reveal structural changes to the brain in patients with concussive injuries (Shin et al., 2017).

The magnitude of MPS experienced by neural tissue during a head impact is an effective indicator of injury risk. MPS has been used as a predictor of concussive outcomes in sporting impacts, demonstrating that it is an appropriate metric to represent brain tissue deformation (Kleiven, 2007; Patton et al., 2015; Zhang et al., 2004). While FE modelling allows researchers to represent injury at the tissue level, its application is limited by long computational times. Thus it is impractical for use in helmet standard tests. Standards typically measure simple head kinematics to predict risk of injury and helmet performance.

2.6 Ice Hockey Helmet Test Methods

2.6.1 Standard Test Methods

Numerous standards organizations publish safety standard tests for ice hockey helmets (refer to Appendix A, Table 1 for a complete summary). A drop system guiding the acceleration of a helmeted headform is widely used to evaluate helmet performance (Hoshizaki and Brien, 2004). Currently, ice hockey standard tests drop a helmeted headform on a stiff, flat modular

elastomer programmer (MEP) anvil using either a monorail drop tower (ASTM F1045-16; CSA Z262.1-15) or a twin-wire guided drop rig (NOCSAE DOC 030-11m16). This primarily represents an individual falling and impacting their head on the ice. In all current ice hockey helmet standard tests, a headform is rigidly attached to the drop system which only permits linear acceleration to occur. Additionally, all standard organizations use peak linear acceleration or linear acceleration-based injury metrics as performance criteria for certifying ice hockey helmets. These criteria were established to primarily prevent traumatic injuries. In response, helmets have been designed to protect against falling impacts and have essentially eliminated skull fractures and TBIs from ice hockey (Hoshizaki and Brien, 2004). However, standards only represent one head impact event (a fall on the ice) and do not measure rotational kinematics of the head. As a result, helmets are not adequately designed to protect against rotation-induced diffuse injuries such as concussion. It would be beneficial to evaluate helmets using rotational tests that represent head impact events known to cause concussions in ice hockey.

2.6.2 Rotational Test Methods

Several rotation-inducing impact tests have been used in laboratory settings to evaluate helmet performance and risk of injury. The European Committee for Standardization (CEN) has proposed an impact test for cycling and equestrian helmets which drops a helmeted headform on a 45° steel anvil to elicit rotation (Appendix B) (CEN, 2015). Researchers have also used pneumatic linear impact test protocols, involving centric and non-centric head impacts, to evaluate helmet performance in contact sports such as football and ice hockey (Clark et al., 2016; De Grau, 2017; Post et al., 2013). Walsh and colleagues (2011) investigated 20 impact conditions using a linear impactor (five locations and four angles) and identified eight conditions which produced a 80% risk of concussion based on dynamic response. From these results, five

impact conditions were selected to create the University of Ottawa Testing Protocol (uOTP). This impact test protocol incorporated non-centric impacts to the head. Currently, the NOCSAE pneumatic ram impact test for football helmets is the only standard rotational helmet test (NOCSAE DOC 002-17m17a). This test includes centric and non-centric impacts and applies a rotational acceleration criterion. Thus, American football helmet manufacturers are required to meet rotational acceleration standards for the head during impact.

While there is no current standard rotational ice hockey helmet test, an angled anvil drop test can be used to represent head-to-boards impacts in ice hockey. Additionally, a pneumatic ram test can be used to represent shoulder-to-head collision impacts. It is important that these tests evaluate helmets using impact parameters known to produce concussive injuries in ice hockey. Understanding the relationship between these helmet tests and real-world concussive injuries would provide important information to standards organizations.

2.7 Summary

The high incidence of concussions in ice hockey highlights the importance of assessing helmet testing methods. Current standard tests only evaluate ice hockey helmets under one condition and use performance criteria intended to prevent skull fracture and focal TBI. Consequently, helmets are not specifically designed to protect against diffuse brain injuries such as concussion, which have been associated with rotational kinematics of the head. Evaluating ice hockey helmets using rotational impact tests may better reflect the mechanism of concussive injury. This thesis will investigate how different helmet tests relate to concussive injuries in professional ice hockey, based on the relationships between dynamic response and MPS. This information will inform ice hockey helmet standard test development.

Chapter 3: Research Design

3.1 Research Question

How do three ice hockey helmet tests relate to reconstructions of concussive injuries in professional ice hockey, based on relationships between dynamic response and brain tissue deformation?

3.2 Objectives

1) Describe the relationship between a Flat Anvil Drop Test and professional ice hockey head-to-ice concussion reconstructions.
2) Describe the relationship between an Angled Anvil Drop Test and professional ice hockey head-to-boards concussion reconstructions.
3) Describe the relationship between a Pneumatic Ram Test and professional ice hockey shoulder-to-head concussion reconstructions.

3.3 Independent Variables

- Helmet Test
  - Flat Anvil Drop Test
  - Angled Anvil Drop Test (30^{o} and 45^{o})
  - Pneumatic Ram Test (medium and high compliance)
- Impact Location
  - Two locations for the Flat Anvil Drop Test (refer to section 4.2.1)
  - Three locations for the Angled Anvil Drop Test (refer to section 4.2.2)
  - Three locations for the Pneumatic Ram Test (refer to section 4.2.3)
- Impact Velocity
  - Three impact velocities for each test (refer to section 4.2)

3.4 Dependent Variables

- Dynamic Response (resultant, dominant)
    - Peak linear acceleration (g)
    - Peak rotational acceleration (rad/s^2)
    - Peak rotational velocity (rad/s)

- Brain Tissue Deformation
    - Maximum principal strain ($\frac{\text{elongated length of tissue}}{\text{original length of tissue}}$)

3.5 Null Hypotheses

1) There will be no significant relationships (R^2) between linear acceleration/rotational acceleration/rotational velocity and MPS for the Flat Anvil Drop Test.
2) There will be no significant relationships (R^2) between linear acceleration/rotational acceleration/rotational velocity and MPS for the head-to-ice concussion reconstructions.
3) There will be no significant relationships (R^2) between linear acceleration/rotational acceleration/rotational velocity and MPS for the 30^o Anvil Drop Test.
4) There will be no significant relationships (R^2) between linear acceleration/rotational acceleration/rotational velocity and MPS for the 45^o Anvil Drop Test.
5) There will be no significant relationships (R^2) between linear acceleration/rotational acceleration/rotational velocity and MPS for head-to-boards concussion reconstructions.
6) There will be no significant relationships (R^2) between linear acceleration/rotational acceleration/rotational velocity and MPS for the Medium Compliance Pneumatic Ram Test.
7) There will be no significant relationships (R^2) between linear acceleration/rotational acceleration/rotational velocity and MPS for the High Compliance Pneumatic Ram Test.
8) There will be no significant relationships (R^2) between linear acceleration/rotational acceleration/rotational velocity and MPS for shoulder-to-head concussion reconstructions.

Chapter 4: Methods

4.1 Test Equipment

4.1.1 Monorail Drop Rig

The monorail drop rig is a guided free-fall impact apparatus commonly used for evaluating ice hockey helmet performance (ASTM F1045-16; CSA Z262.1-15). It consists of a vertical rail (h = 4.7 m) secured to the wall and attached to a concrete base. A motorized release system raises the drop carriage and headform up the rail and a pneumatic piston initiates its release, allowing the headform to fall down the frictionless rail. The headform impacts an anvil at the base of the rail, which can be substituted to simulate different impact surfaces and angles. To minimize vibrations in the system, the base of the anvil is securely fixed to the floor using six concrete bolts. The monorail drop rig is connected to a computer with Cadex Impact Data Acquisition Software (Cadex Inc., Saint-Jean-sur-Richilieu, QC) which is used to input the impact velocity. A photoelectric time gate is positioned 0.02 m above the anvil to calculate the velocity for each impact (Figure 2).

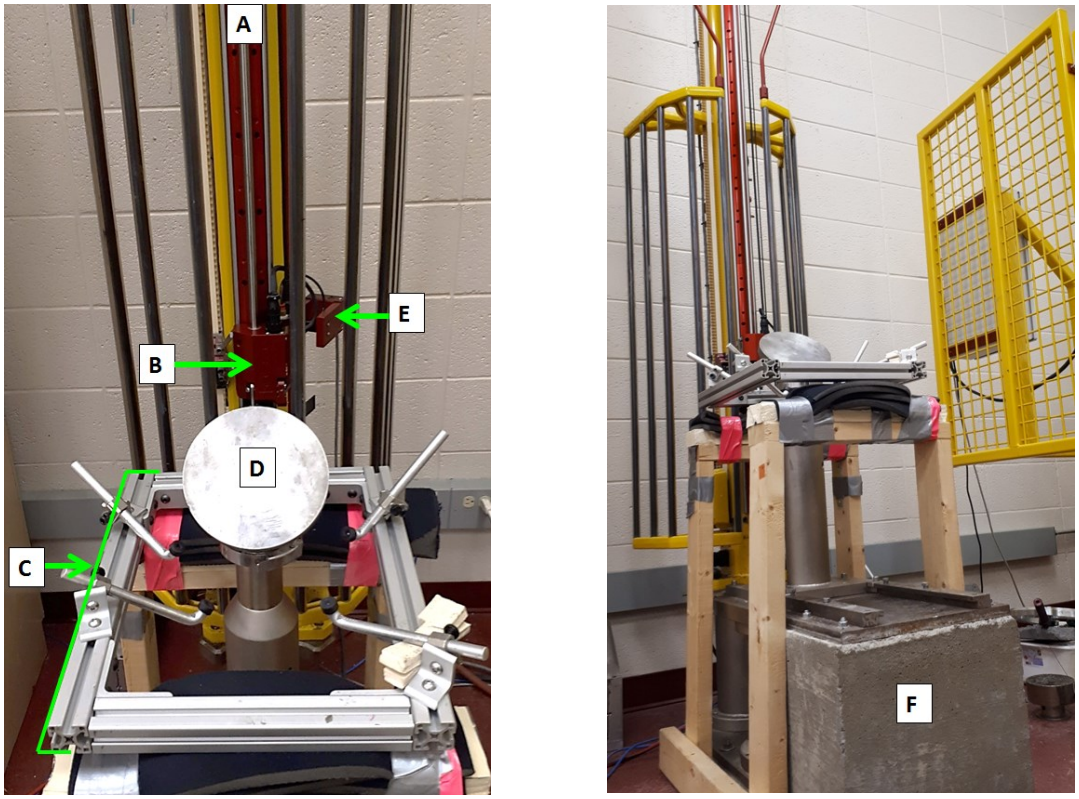

Figure 2. Monorail drop rig with vertical rail (A), motorized release system (B), drop carriage (C), steel anvil (D), time gate (E), and concrete base (F).

4.1.2 Pneumatic Linear Impactor

The pneumatic linear impactor is a system used to simulate collision impacts to the head and can be used to evaluate helmet performance (NOCSAE (ND) 081-18m18). It consists of a compressed air tank connected to a piston chamber, supported by a large steel frame. The release of compressed air forces the piston forward which thrusts the impacting arm (m = 13.1 ± 0.1 kg) towards the headform. A striker cap is attached to the end of the impacting arm and can be substituted to simulate different surface compliances. A flag on the impacting arm passes through a photoelectric time gate immediately prior to impact to calculate the inbound velocity. The desired velocity is achieved by adjusting the pressure within the compressed air tank (air tank pressure is measured in Psi, where $1\ Psi = 6.90 \times 10^3\ Pa$). The position of the headform

can be freely manipulated and is attached to a sliding table (m = 12.78 ± 0.01 kg). This table slides on low-friction rails permitting post-impact translation of 0.33 ± 0.01 m. The headform and sliding table are attached to a larger motorized table that can be raised or lowered to achieve the desired impact location (Figure 3).

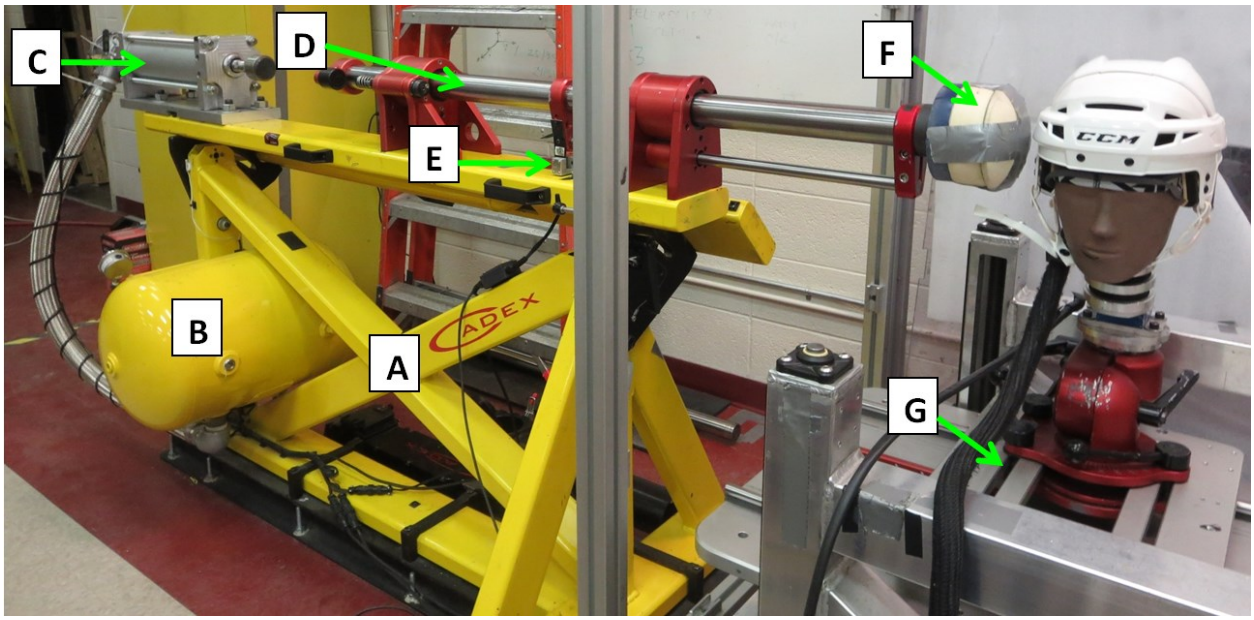

Figure 3. Pneumatic linear impactor consisting of a steel frame (A), compressed air tank (B), piston chamber (C), impacting arm (D), time gate (E), striker cap (F), and sliding table (G).

4.1.3 Hybrid III Headform

A Hybrid III 50th percentile adult headform (m = 4.54 ± 0.01 kg) was used throughout this thesis, as described in the CEN proposed test method (CEN, 2015). This headform was originally developed as part of a General Motors project as a human head surrogate for automotive crash testing (Hubbard and McLeod, 1974). During development, the headform yielded acceleration data within the ranges observed in cadaveric drop tests. The headform consists of a steel interior covered with a vinyl skin and is intended to sustain repeated high-energy impacts without structural failure (Figure 4).

Figure 4. The Hybrid III headform separated to reveal the interior steel structure (left) and external vinyl skin (right).

Nine single-axis Endevco 7264C-2KTZ-2-300 piezoresistive accelerometers (Endevco, San Juan Capistrano, CA, USA) were mounted inside the headform using a 3-2-2-2 array (Padgaonkar et al., 1975). This array was developed to measure three-dimensional rotational acceleration during an impact using single-axis linear accelerometers (Padgaonkar et al., 1975). Three accelerometers were mounted at the centre of gravity of the headform, while two accelerometers were mounted at each the top, front, and side of the headform (Figure 5). Accelerometer data was sampled at 20 kHz, collected by a TDAS Pro Lab System (DTS, Seal Beach, CA, USA) and filtered with a CFC 1000 filter in accordance with SAE J211, 8.4.1.

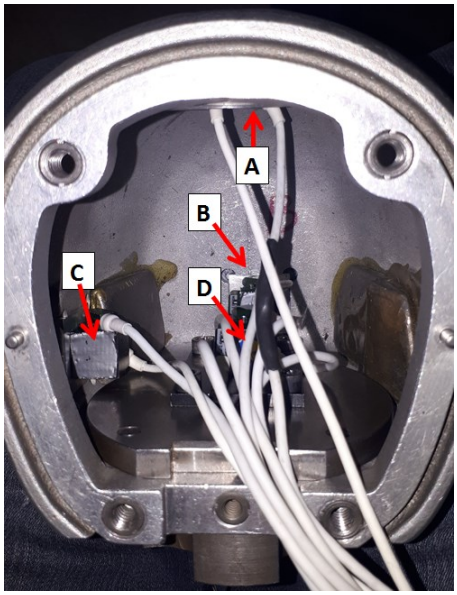

Figure 5. Posterior view of accelerometers inside the Hybrid III headform, placed in a 3-2-2-2 array. Two accelerometers are mounted at the top (A), front (B), and side (C), while 3 accelerometers are mounted at the centre of gravity of the headform (D).

The following equations were used to calculate rotational acceleration:

$$\overrightarrow{\alpha_x} = \frac{\overrightarrow{a_{zS}} - \overrightarrow{a_{zC}}}{2S} - \frac{\overrightarrow{\alpha_{yT}} - \overrightarrow{a_{yC}}}{2T} \quad [1]$$

$$\overrightarrow{\alpha_y} = \frac{\overrightarrow{a_{xT}} - \overrightarrow{a_{xC}}}{2T} - \frac{\overrightarrow{\alpha_{zF}} - \overrightarrow{a_{zC}}}{2F} \quad [2]$$

$$\overrightarrow{\alpha_z} = \frac{\overrightarrow{a_{yF}} - \overrightarrow{a_{yC}}}{2F} - \frac{\overrightarrow{\alpha_{xS}} - \overrightarrow{a_{xC}}}{2S} \quad [3]$$

Where α_i represents rotational acceleration for component $i\,(x, y, z)$, a_{ij} represents linear acceleration for component i along the orthogonal arm $j\,(F\,(front),\ S(side), T\,(top))$ (Padgaonkar et al., 1975). The right-hand rule was used to define a coordinate system for the headform, with positive x, y, and z axes directed anteriorly, towards the left ear, and caudally, respectively (Figure 6).

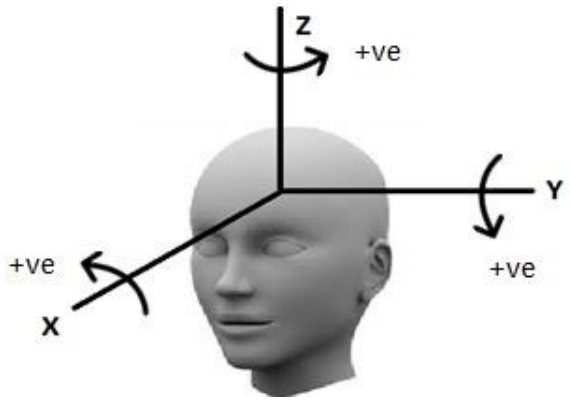

Figure 6. Coordinate system of the headform defined by the right-hand rule. Arrows indicate the direction of positive rotation about each axis.

Rotational velocity was determined by integrating the rotational acceleration about each of the three axes, using Equation 4:

$$\overrightarrow{\omega_i} = \int_0^T \overrightarrow{\alpha_i}\, dt + c_1 \qquad [4]$$

where w_i represents rotational velocity for component i (x, y, z), α_i represents rotational acceleration about component i (x, y, z), and T is the time interval.

4.1.4 Unbiased Neckform

While the Hybrid III neckform is often used in helmet standard tests (such as the NOCSAE pneumatic ram impact test), its asymmetric design may bias the headform response. The Hybrid III neckform was developed for use in non-impact automotive crash testing, in which head motion primarily occurs in the anterior-posterior direction. Consequently, the Hybrid III neckform is biased towards movement in the sagittal plane and resists motion in the other two anatomical planes (Foreman and Hoshizaki, 2011). To eliminate this potential bias, researchers at the University of Ottawa developed an unbiased neckform which responds similarly to impacts in all directions (Walsh et al., 2018). The unbiased neckform consists of four centred and

unarticulated rubber butyl disks (r = 0.068 ± 0.001 m, h = 0.022 ± 0.001 m) recessed inside aluminum disks (r = 0.086 ± 0.001 m, h = 0.013 ± 0.001 m) (Figure 7). The neckform is held together using a braided steel cable passing through the centre of the disks and torqued to $1.10\,N \cdot m$ (Walsh et al., 2018). The unbiased neckform was used for the pneumatic ram test in this thesis. No neckform was used for the flat or angled anvil drop tests, isolating the kinematics of the headform (Halldin, 2015).

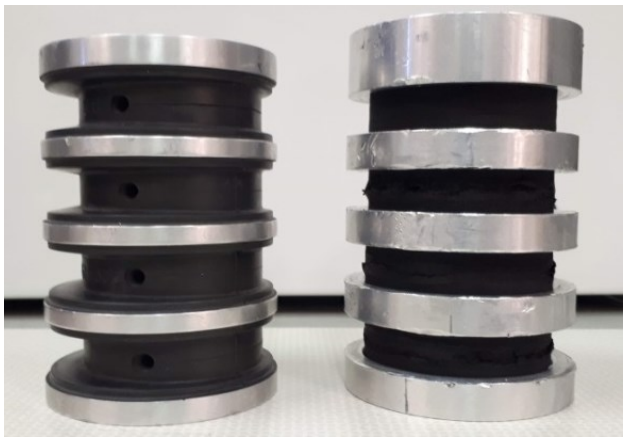

Figure 7. Hybrid III neckform (left) and unbiased neckform (right).

4.1.5 Ice Hockey Helmets

A medium CCM Vector 08 ice hockey helmet was used for all tests in thesis. The Vector 08 is a CSA-certified helmet that contains a vinyl nitrile (VN) foam liner. The liner consists of 0.0094 m of VN740 foam (medium density) in the front and front boss locations and 0.0094 m of VN1000 foam (high density) in the side, rear boss, and rear locations. All foam is covered with 0.0031 m of VN600 (low density) comfort foam (Figure 8). Each location on the helmet was impacted a maximum of three times. A total of 8 helmets were used to complete this thesis.

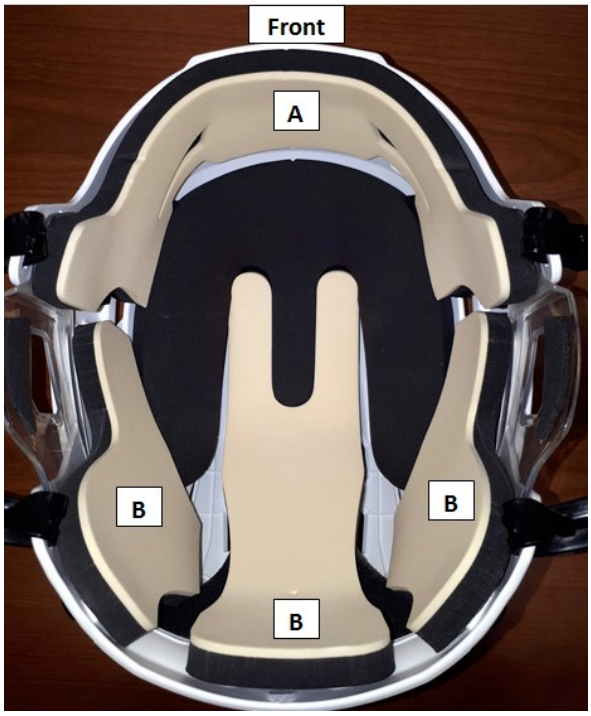

Figure 8. CCM Vector 08 helmet with 0.0094 m of black VN740 foam in the front and front boss locations (A) and 0.0094 m of black VN1000 foam in the side, rear boss, and rear locations (B). All black foam is covered with a 0.0031 m layer of beige VN600 foam.

4.2 Helmet Test Methods

4.2.1 Flat Anvil Drop Test

A head impacting the ice surface can lead to severe outcomes such as skull fractures or focal TBIs. To ensure helmets are capable of preventing these catastrophic injuries, standard tests evaluate ice hockey helmets by simulating a player falling and impacting their head on the ice. The flat anvil drop test in this thesis is similar to standard tests and was also designed to represent head-to-ice impacts. Similar to the CSA and ISO standard ice hockey helmet test methods, the flat anvil drop test used a monorail drop rig (CSA Z262.1-15; ISO 10256-2:2016). However, while standard tests rigidly attach a headform to the monorail drop rig (prohibiting rotation), the flat anvil drop test in this thesis used a free-falling headform. This allowed the headform to respond in an unrestricted manner upon impact.

To produce a free-falling condition, the helmeted headform was positioned on a rectangular drop carriage. The drop carriage used four adjustable arms to support the headform. These support arms were locked in place to ensure repeatable impact conditions. Once the helmeted headform was positioned, the drop carriage was raised up the monorail drop rig. Upon release, the headform and carriage fell to the base of the frictionless rail. The headform impacted a flat anvil while the drop carriage passed around the anvil and landed on a braking system, permitting the headform to respond freely.

The flat anvil drop test used a flat steel anvil covered with a cylindrical MEP pad (height = 0.025 ± 0.001 m, diameter = 0.152 ± 0.001 m) with a durometer of (60 ± 2) Shore A (Figure 9). The MEP pad created a very low compliance impact condition, representative of the stiff ice surface. The MEP pad was calibrated following the methods described in the document ASTM F1045-16 (refer to Appendix C for detailed calibration method).

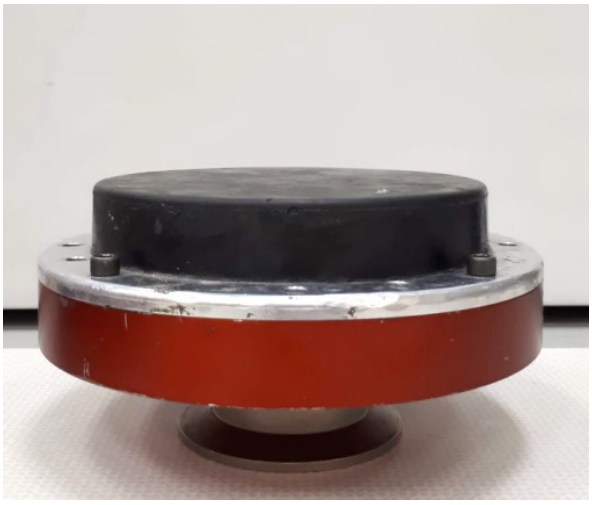

Figure 9. Flat MEP anvil (black) attached to the support base (red).

A dataset of professional ice hockey concussion reconstructions was analyzed to identify the most common concussive head-to-ice impact locations (Post et al., 2019). From this dataset, two impact locations were identified and used for the flat anvil drop test: front boss and rear boss

(Figure 10). Furthermore, the professional ice hockey injury dataset reported a mean (SD) impact velocity of 4.5 (0.7) m/s for concussive head-to-ice impacts (Post et al., 2019). In order to represent the range of real-world concussive head-to-ice impact velocities, the flat anvil drop test was performed at 3.0 m/s, 4.0 m/s, and 5.0 m/s.

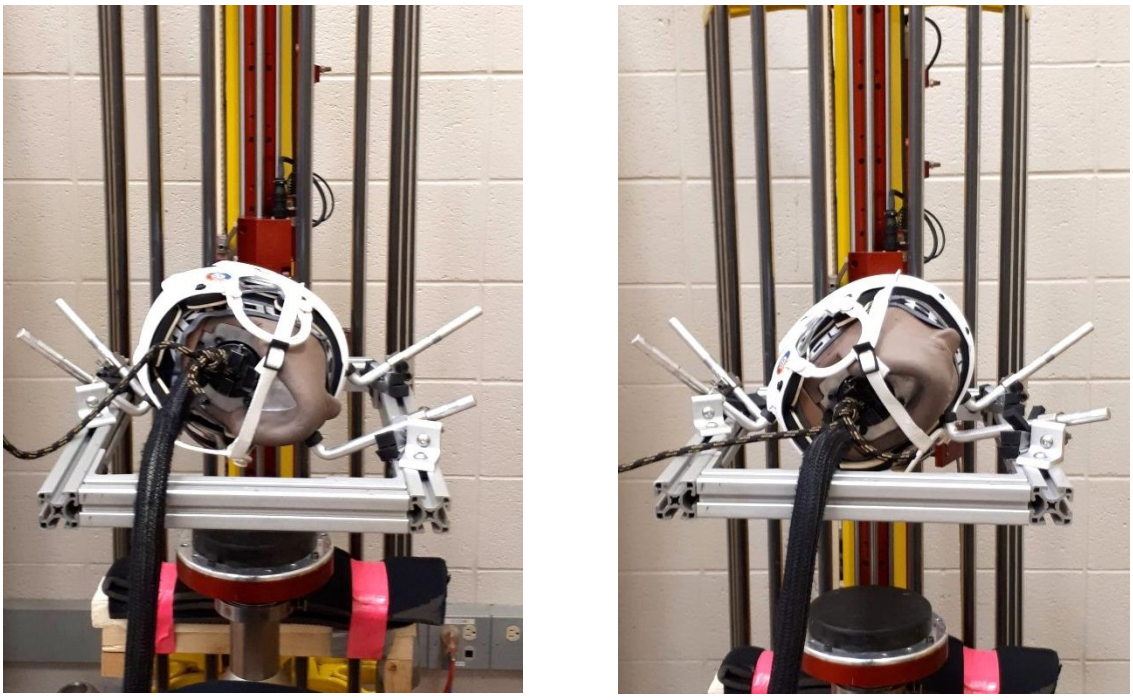

Figure 10. Impact locations for the flat anvil drop test: front boss (left) and rear boss (right).

4.2.2 Angled Anvil Drop Test

To represent head-to-boards impacts in ice hockey, this thesis used the angled anvil drop test. This test was adapted from the CEN proposed test method for cycling and equestrian helmet evaluation (CEN, 2015). The CEN proposed test method uses a monorail drop rig to impact a free-falling helmeted headform on a 45° steel anvil layered with sandpaper. An angled anvil is used to induce rotation of the headform. In place of sandpaper, a bare steel anvil was used in this

thesis to simulate the low friction surface of ice hockey boards. Additionally, a rectangular drop carriage was used to pass around the anvil and achieve a free-falling impact condition.

Video analysis of concussive head-to-boards impacts from a dataset of professional ice hockey concussion reconstructions (Post et al., 2019) identified that players fall into the boards with head impact angles ranging from 38° to 49.9°, with an average impact angle of 44° (refer to Appendix D for a description of the video analysis method). To represent two angles of concussive head-to-boards impacts in professional ice hockey, the angled drop test was performed on two steel anvils: 30° and 45°, each with the same dimensions (height = 0.021 ± 0.001 m, diameter = 0.180 ± 0.001 m) (Figure 11). Impact angle was adjusted by substituting the anvil base and confirmed using a Smart Tool Digital Inclinometer (Level Developments Ltd., Chicago, IL, USA).

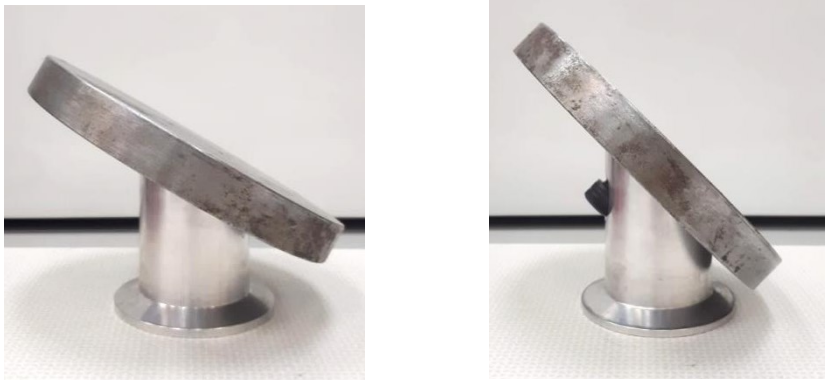

Figure 11. Steel anvils used for the angled drop tests: 30° (left) and 45° (right).

A dataset of professional ice hockey concussion reconstructions was analyzed to identify the most common concussive head-to-boards impact locations (Post et al., 2019). From this dataset, three impact locations were identified and used for the angled anvil drop test: side, rear boss, and rear (Figure 12). Additionally, this injury dataset reported a mean (SD) impact velocity of 4.5 (1.5) m/s for concussive impacts to the boards in professional ice hockey (Post et al.,

2019). To represent the range of concussive head-to-boards impact velocities in professional ice hockey, the angled anvil drop test was performed at 3.0 m/s, 4.5 m/s, and 6.0 m/s.

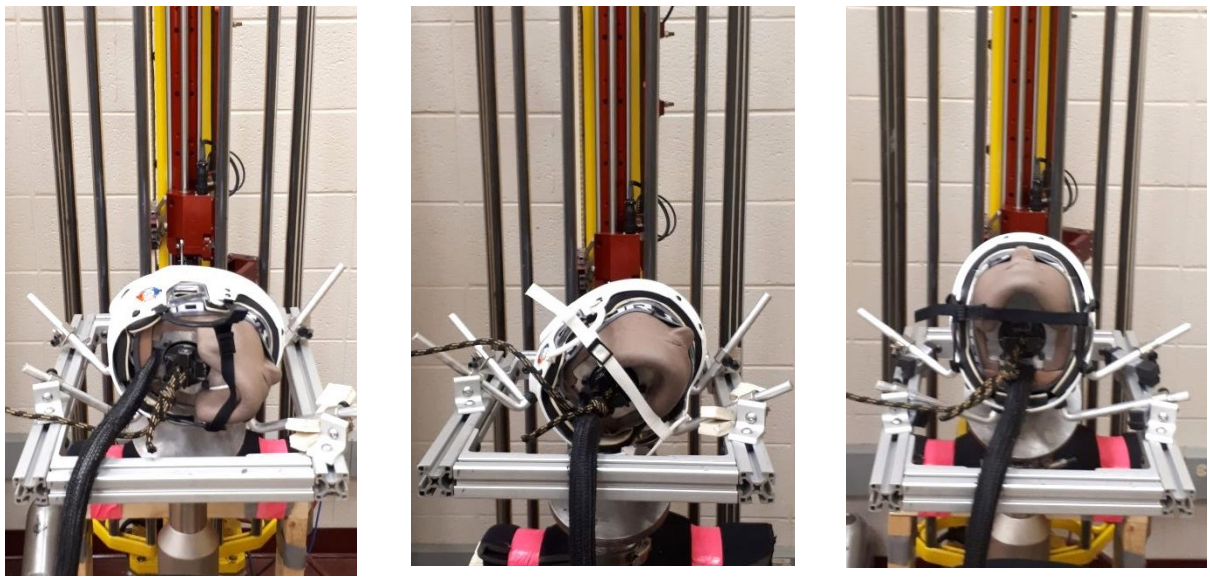

Figure 12. Impact locations for the angled drop test:
side (left), rear boss (middle), and rear (right).

4.2.3 Pneumatic Ram Test

Shoulder-to-head collision impacts have been reported to account for more than 35% of all concussions in professional ice hockey (Hutchison et al., 2015, 2013). However, ice hockey helmet standard tests do not currently evaluate helmets under compliant collision impact conditions. The pneumatic ram test in this thesis was designed to represent shoulder-to-head impacts and used a pneumatic linear impactor, described in section 4.1.2.

A human shoulder protected with ice hockey shoulder pads is a compliant system. It has been reported that shoulder-to-head impacts in ice hockey produce an average impact duration of 25 milliseconds (ms), which can be represented in a laboratory setting using a high compliance striker cap (Rousseau, 2014). However, the range of concussive shoulder-to-head impact

durations has been reported to vary from 18 to 32 ms (Rousseau, 2014). This indicates that the duration of a shoulder-to-head impact may differ depending on impact parameters, such as velocity and location. To represent two levels of compliance, the pneumatic ram test in this thesis used a medium and a high compliance striker cap.

The medium compliance striker (mass = 0.368 ± 0.001 kg) consisted of a 0.041 ± 0.001 m thick layer of VN foam covered with a 0.037 ± 0.001 m tall rounded VN cap. This striker was designed to produce an average impact duration of 15 ms. The high compliance striker (mass = 0.463 ± 0.001 kg) consisted of a 0.111 ± 0.001 m thick layer of 405S DER-TEX foam (DER-TEX Corp., Saco, ME, USA) covered with a 0.037 ± 0.001 m tall rounded VN cap (Figure 13). This striker was designed to produce an average impact duration of 25 ms. The striker caps created for this thesis only represent two distinct levels of compliance. Therefore, it is possible that a compliance level in between the medium and high striker caps may also provide an effective representation of shoulder-to-head impacts in ice hockey.

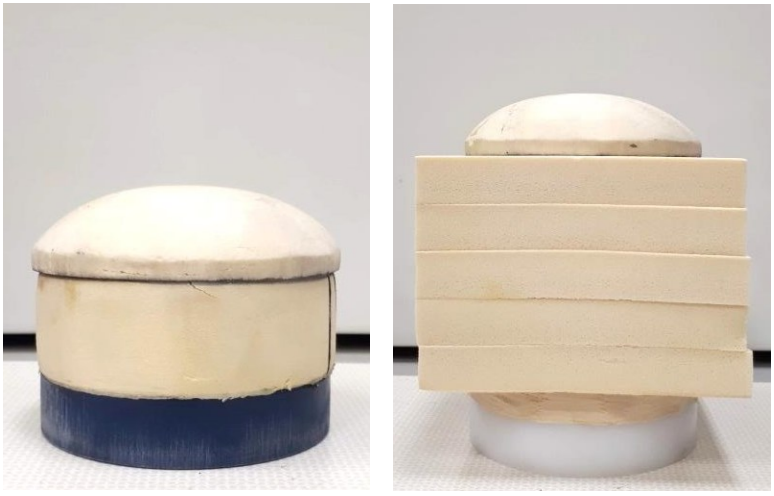

Figure 13. Medium compliance striker cap (left) and high compliance striker cap (right).

A dataset of professional ice hockey concussion reconstructions was analyzed to identify the most frequent shoulder-to-head concussive impact locations (Post et al., 2019). From this

dataset, three impact locations were identified and used for the pneumatic ram impact test: front boss positive azimuth (FBPA), side (S), and rear boss negative azimuth (RBNA) (Figure 14). The impact locations are consistent with those prescribed by NOCSAE, with front boss and rear boss impact angles modified to produce non-centric impacts (Walsh et al., 2012). This professional ice hockey concussion reconstruction dataset reported a mean (SD) impact velocity of 7.5 (1.5) m/s for shoulder-to-head impacts (Post et al., 2019). To represent the range of concussive shoulder-to-head impact velocities, the medium and high compliance pneumatic ram tests were conducted at 6.0 m/s, 7.5 m/s, and 9.0 m/s.

Figure 14. Impact locations and angles for the pneumatic ram impact test as viewed in the sagittal (first column), frontal (second column), and transverse (third column) planes. Arrows indicate the impact vectors (adapted from Walsh et al., 2012).

4.3 Finite Element Modeling

4.3.1 University College Dublin Brain Trauma Model

The linear and rotational acceleration-time data from each impact were applied to the University College Dublin Brain Trauma Model (UCDBTM) at the center of gravity (Horgan and Gilchrist, 2003). The head impact simulations were performed using ABAQUS software (Dassault Systèmes, Waltham, MA, USA).

The UCDBTM is a three-dimensional model of the skull and brain that was constructed using computed tomography (CT) and magnetic resonance imaging (MRI) scans of a male human cadaver (Horgan and Gilchrist, 2003). It is composed of 26,000 hexahedral elements and includes the scalp, 3-layered skull (outer and inner tables, diploe), dura, cerebrospinal fluid (CSF), pia, falx, tentorium, cerebral hemispheres, cerebellum, and brain stem (Horgan and Gilchrist, 2003). Material properties of the model were sourced from Ruan (1994), Willinger et al. (1995), Zhou et al. (1995), and Kleiven and von Holst (2002) and detailed in Tables 1 and 2.

Table 1. Material properties of the UCDBTM

Material	Young's modulus (MPa)	Poisson's Ratio	Density (kg/m^3)
Scalp	16.7	0.42	1000
Cortical Bone	15000	0.22	2000
Trabecular Bone	1000	0.24	1300
Dura	31.5	0.45	1130
Pia	11.5	0.45	1130
Falx	31.5	0.45	1140
Tentorium	31.5	0.45	1140
CSF	-	0.50	1000
Grey Matter	Hyperelastic	0.49	1060
White Matter	Hyperelastic	0.49	1060

Table 2. Material characteristics of brain tissue represented in the UCDBTM.

Material	G_0	G_∞	Decay Constant (Gpa)	Bulk Modulus (s^{-1})
Cerebellum	10	2	80	2.19
Brain Stem	22.5	4.5	80	2.19
White Matter	12.5	2.5	80	2.19
Grey Matter	10	2	80	2.19

Brain tissue in the UCDBTM was modeled using a linearly viscoelastic model combined with a large-deformation theory. This material was characterized as viscoelastic in shear with a deviatoric stress rate dependent on the shear relaxation modulus (Horgan and Gilchrist, 2003). The compressive behaviour of the brain tissue was characterized as elastic. Equation 5 expresses the shear characteristics and viscoelastic behaviour of the brain tissue:

$$G(t) = G_\infty + (G_0 - G_\infty)e^{\beta t} \quad [5]$$

where G_∞ is the long-term shear modulus, G_0 is the short-term shear modulus, and β is the decay factor (Horgan and Gilchrist, 2003). In between the skull and brain, the CSF layer was modelled as solid elements with a low shear modulus and high bulk modulus. This resulted in the CSF acting as a nearly incompressible material such as water. The interaction at the CSF-pia interface was assigned no separation with a friction coefficient of 0.2 (Miller et al., 2010). A hyperelastic material law was applied to the brain tissue, expressed in Equation 6:

$$C_{10}(t) = 0.9C_{01}(t) = 620.5 + 1930e^{-\frac{t}{0.008}} + 1103e^{-\frac{t}{0.15}}(Pa) \quad [6]$$

where C_{10} and C_{01} are temperature-dependent material parameters, and t is time in seconds. The UCDBTM was validated using cadaver head impact pressure data from Nahum et al. (1977) and

cadaver head motion data from Hardy et al. (2001). The model was also later validated using reconstructions of real-world TBI events (Doorly and Gilchrist, 2006).

Newer finite element models of the brain with more refinement have been developed in recent years. However, the UCDBTM was selected for this thesis because it has been used to model the largest dataset of injured and non-injured sporting head impacts, allowing the results of this thesis to be evaluated in the context of prior research (Clark et al., 2018; Hoshizaki et al., 2016; Oeur et al., 2015; Post et al., 2019, 2017c).

4.3.2 Calculation of Maximum Principal Strain

The ABAQUS simulations calculated the magnitude of strain experienced by each element over 50 points in time. Using 50 time points was determined to produce an acceptable number of data points without sacrificing the integrity of the data. After the simulations were completed, the results of each head impact were analyzed individually. The three elements experiencing the highest strain at each point in time were isolated. The peak strain magnitude from each of these three elements was then averaged to obtain MPS for the head impact.

4.4 Professional Ice Hockey (PIH) Concussion Reconstruction Dataset

Each helmet test in this thesis was compared to professional ice hockey concussion reconstructions, previously performed by Post and colleagues (2019). The flat anvil drop test was compared against head-to-ice concussion reconstructions, the angled anvil drop test was compared against head-to-boards concussion reconstructions, and the pneumatic ram test was compared against shoulder-to-head concussion reconstructions.

Post and colleagues (2019) analyzed every regular season game of professional North American ice hockey from 2007 to the end of the 2014 season, identifying all concussive head impacts. Concussive outcomes were confirmed using publicly available medical reports and

communications on the league or individual team websites. Each concussive head impact was cropped and further analyzed to determine the impact event, location, and velocity (Post et al., 2019). Impact velocity was calculated with Kinovea video analysis software (www.kinovea.org, open source) by using known markings and distances on the ice to generate a calibrated reference grid. The velocity of impact was calculated by tracking the motion of the player for 5 frames prior to impact and calculating the distance travelled ($velocity = distance/time$) (Post et al., 2018).

Using the parameters obtained from video analysis, each concussive head impact was reconstructed on a Hybrid III headform. For head-to-ice reconstructions, the headform was attached to a monorail drop rig using an unbiased neckform and dropped on an anvil made of ice. Head impact locations varied for each case and impact velocities ranged from 3.1 to 4.7 m/s. To reconstruct head-to-boards concussive impacts, the headform was attached to a monorail drop rig using an unbiased neckform and dropped on a sheet of high-density polyethylene. Head impact locations varied for each case and impact velocities ranged from 2.0 to 6.2 m/s. For shoulder-to-head reconstructions, the headform was impacted using a linear impactor equipped with a high compliance striking cap producing an average impact duration of 23.9 ms (Rousseau, 2014). Head impact locations varied for each case and impact velocities ranged from 5.5 to 11.5 m/s. The dynamic response data from each reconstruction was used to calculate MPS using the UCDBTM.

For this thesis, reconstructions were only analyzed if the principal point of contact was the player's helmet (impacts to the face or visor were excluded from the analysis). Using this criteria, reconstructions of concussive impacts to the ice (n = 4, average impact velocity 4.5 m/s),

boards (n = 7, average impact velocity 4.5 m/s), and shoulder (n = 16, average impact velocity 7.5 m/s) were included in this thesis.

4.5 Statistical Analysis

4.5.1 Mann-Whitney U Tests

Mean resultant and dominant linear acceleration, rotational acceleration, rotational velocity, and MPS were compared between each test method (averaged across all velocities and locations) and the corresponding concussion reconstruction events. These comparisons were performed using a series of Mann-Whitney *U* tests. The following comparisons were made: Flat Anvil Drop Test vs. head-to-ice concussion reconstructions; 30° Anvil Drop Test vs. head-to-boards concussion reconstructions; 45° Anvil Drop Test vs. head-to-boards concussion reconstructions; Medium Compliance Ram Test vs. shoulder-to-head concussion reconstructions; and High Compliance Ram Test vs. shoulder-to-head concussion reconstructions. To reduce the likelihood of identifying differences due to comparing multiple variables (type I error), a Bonferroni corrected alpha level of 0.007 (α = 0.05/7 comparisons) was used to establish significance.

4.5.2 Stepwise Regressions

Next, for each impact test, a forward stepwise linear regression was conducted between dynamic response (peak resultant linear acceleration, peak dominant linear acceleration, peak resultant rotational acceleration, peak dominant rotational acceleration, peak resultant rotational velocity, and peak dominant rotational velocity) and MPS. The same forward stepwise linear regression was performed on the results of each concussion reconstruction event (head-to-ice, head to-boards, and shoulder-to-head). The stepwise regression analysis used a probability of F = 0.05 to enter variables into the model, and a probability of F = 0.10 to remove variables from the

model. Each regression yielded a statistical model identifying the dynamic response variables with the strongest association to MPS, indicated by the coefficient of determination (R^2). In this thesis, R^2 values are described as very weak (0.0-0.19), weak (0.20-0.39), moderate (0.40-0.59), strong (0.60-0.79), or very strong (0.80-1.0). Each model also indicates whether the addition of subsequent independent variables into the model significantly increased the R^2 value (p <0.05).

The stepwise linear regression models were compared between the flat anvil drop test and the PIH head-to-ice concussion reconstructions. Next, the stepwise linear regression models were compared between the two angled anvil drop tests (30^o and 45^o) and the PIH head-to-boards concussion reconstructions. Lastly, the stepwise linear regression models were compared between the two pneumatic ram tests (medium and high compliance) and the PIH shoulder-to-head concussion reconstructions. All statistical analyses were performed using IBM SPSS Statistics 19 for Windows (IBM Inc., Armonk, NY, USA).

Chapter 5: Results

All data was tested for normality using the Shapiro-Wilk test (Appendix E). As not all the data follows a normal distribution, non-parametric statistical tests were used in this thesis.

5.1 Mean Dynamic Response and MPS Comparisons (Mann-Whitney *U* Tests)

All data satisfied the assumptions of the Mann-Whitney *U* Test (Appendix F).

5.1.1 Flat Anvil Drop Test vs. PIH Head-to-Ice Concussion Reconstructions

Mean linear acceleration, rotational acceleration, rotational velocity, and MPS were compared between the Flat Anvil Drop Test (average impact velocity 4.0 m/s) and the PIH head-to-ice concussion reconstructions (average impact velocity 4.5 m/s) (Table 3).

Table 3. Comparison of overall mean (± 1 standard deviation) dynamic response and brain tissue deformation between the Flat Anvil Drop Test and the PIH head-to-ice concussion reconstructions (n = 4). Comparisons were made using the Mann-Whitney *U* Test (α = 0.007).

	Dynamic Response						*Brain Tissue Deformation*
	Linear Acceleration (g)		**Rotational Acceleration (rad/s^2)**		**Rotational Velocity (rad/s)**		**MPS (%)**
	Res.	**Dom.**	**Res.**	**Dom.**	**Res.**	**Dom.**	
Flat Anvil Drop Test	97.2 (29.5)	78.3 (23.5)	5986.3 (2646.6)	5237.9 (2288.7)	21.0 (6.9)	18.4 (5.9)	0.339 (0.108)
PIH Head-to-Ice Concussions	95.4 (26.3)	89.2 (23.7)	7377.2 (2178.4)	6119.8 (1775.2)	34.6 (4.2)	28.4 (6.7)	0.423 (0.078)
Flat Drop vs. PIH (p-value)	0.755	0.249	0.146	0.249	<0.001*	0.001*	0.148

Res. = Resultant; Dom. = Dominant
* = significant difference (p<0.007)

The results of the Flat Anvil Drop Test were significantly lower than the PIH head-to-ice concussion reconstructions in terms of resultant rotational velocity ($U = 13.5$, $p < 0.001$) and dominant rotational velocity ($U = 30$, $p = 0.001$) (Figure 15).

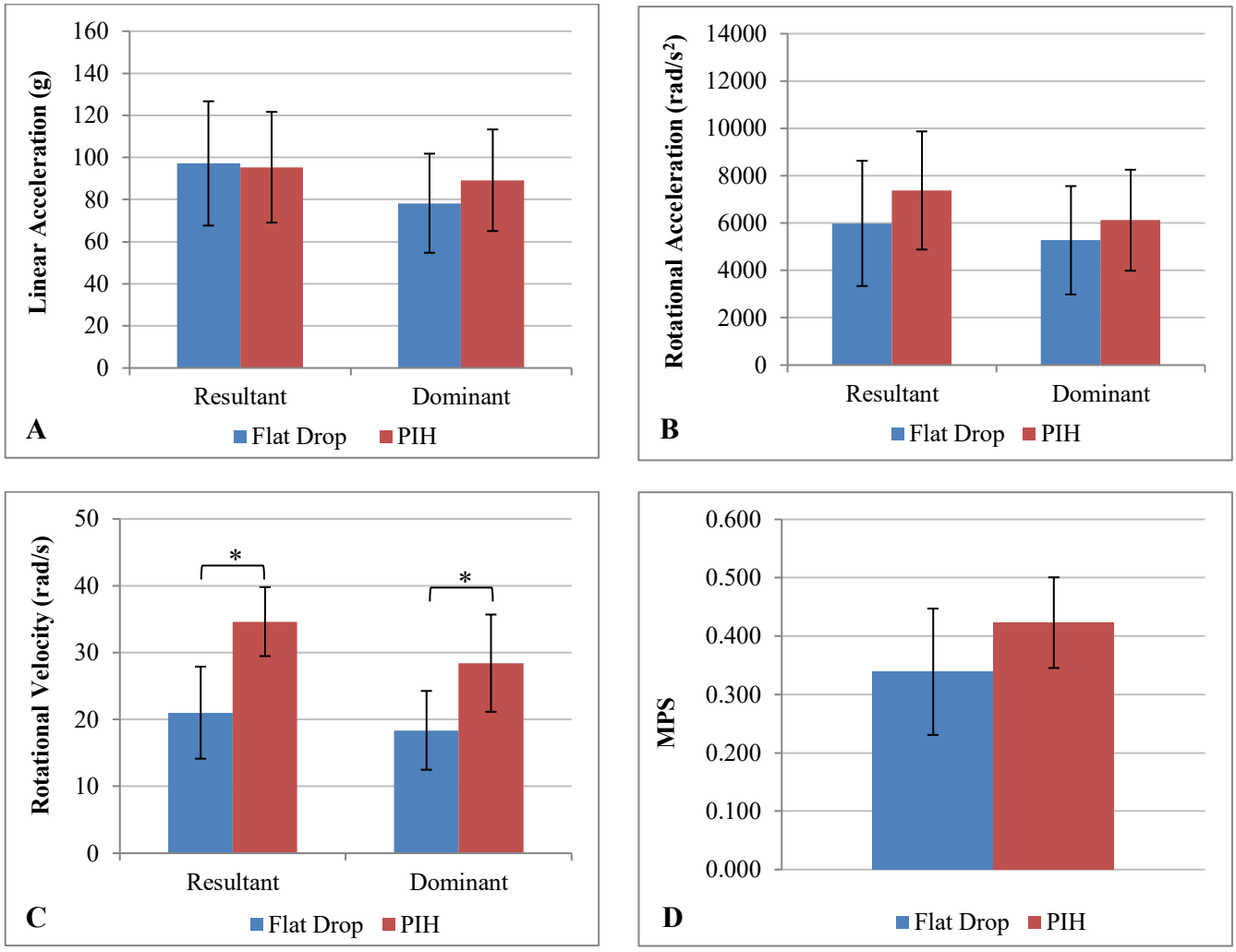

Figure 15. Comparison of mean peak resultant and dominant linear acceleration (A), rotational acceleration (B), rotational velocity (C), and MPS (D) between the Flat Anvil Drop Test and the PIH head-to-ice concussion reconstructions. Error bars indicate ± one standard deviation. Significant differences indicated by an asterisk (*).

5.1.2 Angled Anvil Drop Tests vs. PIH Head-to-Boards Concussion Reconstructions

Mean linear acceleration, rotational acceleration, rotational velocity, and MPS were compared between the 30° Anvil Drop Test (average velocity 4.5 m/s) and the PIH head-to-

boards concussion reconstructions (average velocity 4.5 m/s). The same comparisons were made between the 45° Anvil Drop Test (average velocity 4.5 m/s) and the PIH head-to-boards concussion reconstructions (Table 4).

Table 4. Comparison of mean (± 1 standard deviation) dynamic response and brain tissue deformation between two Angled Anvil Drop Tests (30° and 45°) and PIH head-to-boards concussion reconstructions (n = 7). Comparisons were made using the Mann-Whitney *U* Test (α = 0.007).

	Dynamic Response						*Brain Tissue Deformation*
	Linear Acceleration (g)		**Rotational Acceleration (rad/s^2)**		**Rotational Velocity (rad/s)**		**MPS (%)**
	Res.	**Dom.**	**Res.**	**Dom.**	**Res.**	**Dom.**	
30° Anvil Drop Test	97.1 (45.0)	80.7 (37.6)	7622.5 (3980.0)	6448.8 (3363.7)	28.0 (10.2)	23.9 (8.8)	0.411 (0.156)
45° Anvil Drop Test	70.0 (38.2)	56.6 (33.8)	5886.9 (2746.8)	5244.1 (2596.4)	27.5 (10.0)	24.7 (8.9)	0.388 (0.142)
PIH Boards Concussions	49.7 (23.2)	45.4 (23.1)	3393.7 (1255.0)	2906.6 (1139.7)	27.6 (9.5)	23.2 (8.3)	0.277 (0.097)
30° vs. PIH (p value)	<0.001*	<0.001*	<0.001*	<0.001*	0.724	0.811	0.032
45° vs. PIH (p value)	0.044	0.184	0.001*	<0.001*	0.903	0.219	0.025

Res. = Resultant; Dom. = Dominant
* = significant difference (p<0.007)

The results of the 30° Anvil Drop Test were significantly higher than the PIH head-to-boards concussion reconstructions in terms of resultant linear acceleration ($U = 52$, $p < 0.001$),

dominant linear acceleration ($U = 71$, $p < 0.001$), resultant rotational acceleration ($U = 30$, $p < 0.001$), and dominant rotational acceleration ($U = 58$, $p < 0.001$). The results of the 45° Anvil Drop Test were significantly higher than the PIH head-to-boards concussion reconstructions in terms of resultant rotational acceleration ($U = 112$, $p = 0.001$) and dominant rotational acceleration ($U = 105$, $p = 0.001$) (Figure 16).

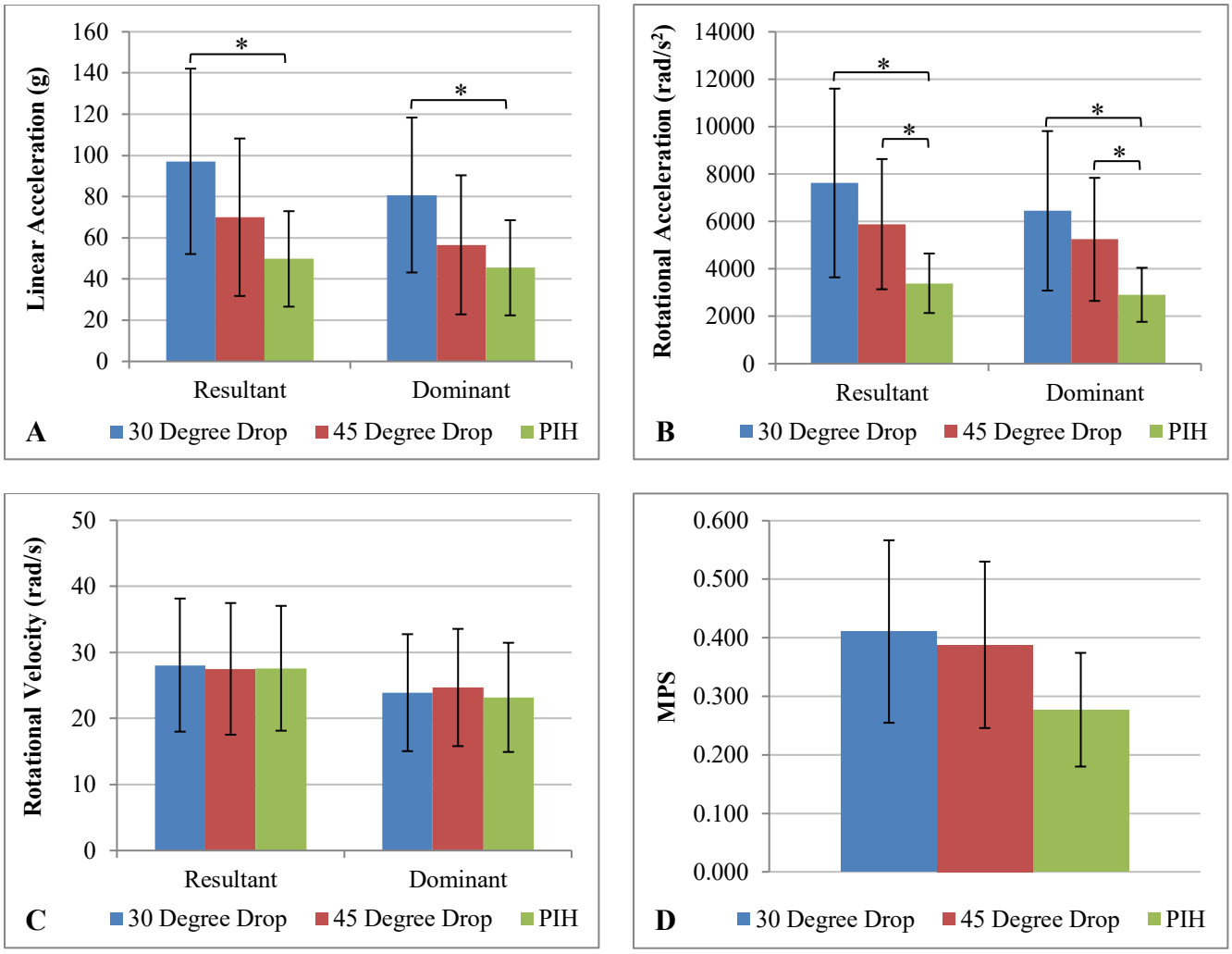

Figure 16. Comparison of mean peak resultant and dominant linear acceleration (A), rotational acceleration (B), rotational velocity (C), and MPS (D) between the 30° Anvil Drop Test, 45° Anvil Drop Test, and PIH head-to-boards concussion reconstructions. Error bars indicate ± one standard deviation. Significant differences indicated by an asterisk (*).

5.1.3 Pneumatic Ram Impact Tests vs. PIH Shoulder-to-Head Concussion Reconstructions

Mean linear acceleration, rotational acceleration, rotational velocity, and MPS were compared between the Medium Compliance Ram Test (average velocity 7.5 m/s) and the PIH shoulder-to-head concussion reconstructions (average velocity 7.5 m/s). The same comparisons were made between the High Compliance Ram Test (average velocity 7.5 m/s) and the PIH shoulder-to-head concussion reconstructions (Table 5).

Table 5. Comparison of mean (± 1 standard deviation) dynamic response and brain tissue deformation between the Medium Compliance Ram Test, High Compliance Ram Test, and PIH head-to-shoulder concussion reconstructions (n = 16). Comparisons were made using the Mann-Whitney *U* Test ($\alpha = 0.007$).

	Dynamic Response						*Brain Tissue Deformation*
	Linear Acceleration (g)		**Rotational Acceleration (rad/s^2)**		**Rotational Velocity (rad/s)**		**MPS (%)**
	Res.	**Dom.**	**Res.**	**Dom.**	**Res.**	**Dom.**	
Ram, Med. Compliance	50.4 (13.4)	49.9 (13.5)	4472.5 (1415.4)	3904.2 (1178.4)	31.5 (4.9)	27.5 (3.9)	0.383 (0.088)
Ram, High Compliance	18.6 (3.4)	18.5 (3.4)	1959.9 (511.3)	1677.6 (427.1)	19.5 (4.0)	16.0 (2.9)	0.196 (0.036)
PIH Shoulder Concussions	29.2 (8.0)	27.8 (7.8)	2683.6 (776.2)	2400.1 (757)	28.1 (5.8)	24.3 (5.1)	0.255 (0.070)
Med. Compliance vs. PIH (p value)	<0.001*	<0.001*	<0.001*	<0.001*	0.058	0.010	<0.001*
High Compliance vs. PIH (p value)	<0.001*	<0.001*	<0.001*	<0.001*	<0.001*	<0.001*	0.001*

Res. = Resultant; Dom. = Dominant

* = significant difference ($p<0.007$)

The results of the Medium Compliance Ram Test were significantly higher than the PIH shoulder-to-head concussion reconstructions in terms of resultant linear acceleration ($U = 99.0$, $p < 0.001$), dominant linear acceleration ($U = 81.5$, $p < 0.001$), resultant rotational acceleration ($U = 173.0$, $p < 0.001$), dominant rotational acceleration ($U = 194.0$, $p < 0.001$), and MPS ($U = 36.0$, $p < 0.001$). The results of the High Compliance Ram Test were significantly lower than the PIH shoulder-to-head concussion reconstructions in terms of resultant linear acceleration ($U = 89.0$, $p < 0.001$), dominant linear acceleration ($U = 148.5$, $p < 0.001$), resultant rotational acceleration ($U = 277.0$, $p < 0.001$), dominant rotational acceleration ($U = 275.0$, $p < 0.001$), resultant rotational velocity ($U = 154.0$, $p < 0.001$), dominant rotational velocity ($U = 104.5$, $p < 0.001$), and MPS ($U = 83.0$, $p = 0.001$) (Figure 17).

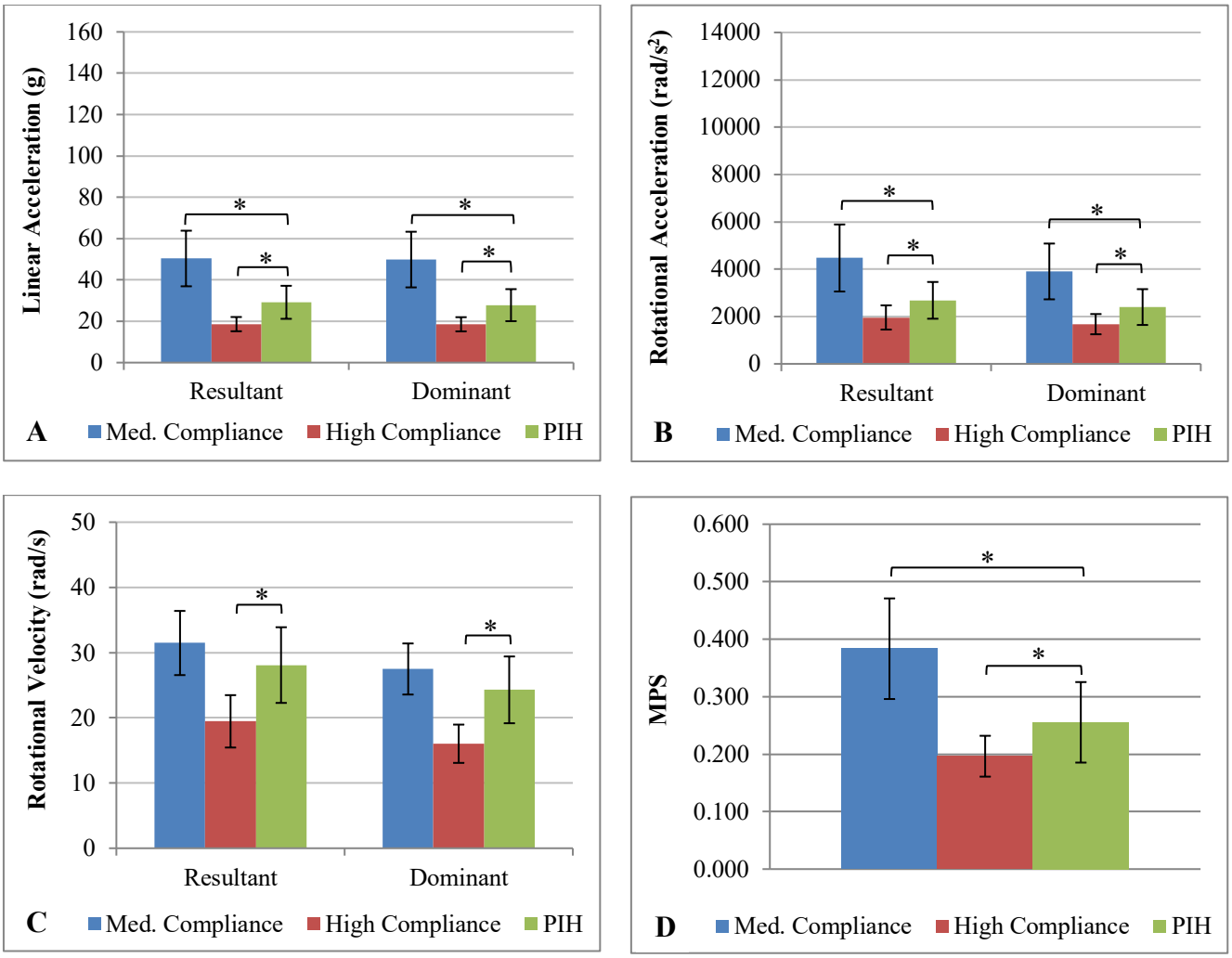

Figure 17. Comparison of mean peak resultant and dominant linear acceleration (A), rotational acceleration (B), rotational velocity (C), and MPS (D) between the Medium Compliance Ram Test, High Compliance Ram Test, and PIH shoulder-to-head concussion reconstructions. Error bars indicate ± one standard deviation. Significant differences indicated by an asterisk (*).

5.2 Stepwise Regression Analysis

Stepwise linear regressions were conducted to identify the dynamic response variables that demonstrated the strongest relationship with MPS. For each regression analysis, all models that achieved a statistically significant relationship with MPS are presented. For the Flat Anvil Drop Test, dominant linear acceleration had the strongest relationship with MPS ($R^2 = 0.960$, $p = 0.001$). No other variables significantly increased the strength of the model. In the stepwise

regression analysis of the PIH head-to-ice concussion reconstructions, no dynamic response variables had a significant relationship with MPS (Table 6).

Table 6. Stepwise regression analysis examining the relationship between dynamic response and MPS for the Flat Anvil Drop Test and PIH head-to-ice concussion reconstructions.

	Model Number	**Variables Included**	R^2	R^2 **Change**	p **value**
Flat Anvil Drop Test	1	Dom. Linear Acceleration	0.960	---	0.001
PIH Head-to-Ice Concussion Reconstructions	1	No variables were entered into the equation	---	---	---

Dom. = Dominant

For the 30º Anvil Drop Test, resultant rotational velocity had the strongest relationship with MPS (R^2 = 0.978, p < 0.001). The addition of dominant rotational acceleration slightly increased the coefficient of determination (R^2 = 0.998, p < 0.001). For the 45º Anvil Drop Test, dominant rotational velocity had the strongest relationship with MPS (R^2 = 0.977, p < 0.001). The addition of resultant rotational velocity slightly increased the coefficient of determination (R^2 = 0.991, p = 0.022). For the PIH head-to-boards concussion reconstructions, resultant rotational acceleration had the strongest relationship with MPS (R^2 = 0.649, p = 0.029). The addition of dominant rotational acceleration into the model produced a very strong coefficient of determination (R^2 = 0.897, p = 0.036) (Table 7).

Table 7. Stepwise regression analysis examining the relationship between dynamic response and MPS for the 30º Anvil Drop Test, 45º Anvil Drop Test, and PIH head-to-boards concussion reconstructions.

	Model Number	Variables Included	R^2	R^2 Change	*p* value
30º Anvil Drop Test	1	Res. Rotational Velocity	0.978	---	<0.001
	2	Res. Rotational Velocity Dom. Rotational Velocity	0.998	0.019	<0.001
45º Anvil Drop Test	1	Dom. Rotational Velocity	0.977	---	<0.001
	2	Dom. Rotational Velocity Res. Rotational Velocity	0.991	0.014	0.022
PIH Head-to-Boards Concussion Reconstructions	1	Res. Rotational Acceleration	0.649	---	0.029
	2	Res. Rotational Acceleration Dom. Rotational Acceleration	0.897	0.248	0.036

Res. = Resultant; Dom. = Dominant

For the Medium Compliance Ram Test, resultant rotational acceleration had the strongest relationship with MPS (R^2 = 0.671, p = 0.007). The addition of dominant rotational acceleration produced a very strong coefficient of determination (R^2 = 0.854, p = 0.033). Adding resultant linear acceleration into the model further increased the R^2 value to 0.989 (p = 0.001). For the High Compliance Ram Test, resultant rotational acceleration also had the strongest relationship with MPS (R^2 = 0.850, p < 0.001). The addition of dominant rotational acceleration increased the R^2 value to 0.976 (p = 0.001). Consistent with the two pneumatic ram tests, resultant rotational acceleration also had the strongest relationship with MPS for the PIH shoulder-to-head concussion reconstructions (R^2 = 0.763, p < 0.001). No further dynamic response variables were entered into the model (Table 8).

Table 8. Stepwise regression analysis examining the relationship between dynamic response and MPS for the Medium Compliance Ram Test, High Compliance Ram Test, and PIH shoulder-to-head concussion reconstructions.

	Model Number	Variables Included	R^2	R^2 Change	*p* value
Medium Compliance Ram Test	1	Res. Rotational Acceleration	0.671	---	0.007
	2	Res. Rotational Acceleration Dom. Rotational Acceleration	0.854	0.184	0.033
	3	Res. Rotational Acceleration Dom. Rotational Acceleration Res. Linear Acceleration	0.989	0.135	0.001
High Compliance Ram Test	1	Res. Rotational Acceleration	0.850	---	<0.001
	2	Res. Rotational Acceleration Dom. Rotational Acceleration	0.976	0.126	0.001
PIH Shoulder-to-Head Concussion Reconstructions	1	Res. Rotational Acceleration	0.763	---	<0.001

Res. = Resultant; Dom. = Dominant

5.3 Limitations

5.3.1 Hybrid III Headform

The Hybrid III 50th percentile headform was originally developed as part of a General Motors project to be a human head surrogate for automotive crash testing (Hubbard and McLeod, 1974). It was determined that the headform yielded acceleration data within the ranges observed in cadaveric drop tests. The headform design, a steel interior covered with a vinyl skin, was intended to sustain repeated high-energy impacts without structural failure. However, these material characteristics may cause the Hybrid III 50th percentile headform to respond differently compared to a living human head. While not completely biofidelic, the assumption was made

that the Hybrid III 50th percentile headform is a reasonable representation of an adult human head for biomechanical impact testing.

5.3.2 Unbiased Neckform

A Hybrid III neckform is often suggested for use in helmet testing settings. This neckform was developed for use in non-impact automotive crash testing, in which head motion primarily occurs in the anterior-posterior direction. Consequently, the Hybrid III neckform is biased towards movement in the sagittal plane and resists motion in the other two anatomical planes (Foreman and Hoshizaki, 2011). To eliminate this bias, researchers at the University of Ottawa developed an unbiased neckform designed to respond similarly to impacts in all directions (Walsh et al., 2018). The assumption was made that the unbiased neckform serves as an effective representation of a human neck.

5.3.3 UCDBTM

The output of a finite element model is highly dependent on the material properties assigned to the model's neural tissue. The tissue mechanical properties utilized by the UCDBTM were derived from cadaver testing, as evaluating tissue response *in vivo* is not feasible (Horgan and Gilchrist, 2003). This model has been validated against cadaveric head impact experiments (Nahum et al., 1977; Hardy et al., 2001) and reconstructions of traumatic brain injuries (Doorly and Gilchrist, 2006). The assumption was made the strain outputs of the UCDBTM are representative of a human brain.

5.3.4 Helmets

Only one model of a CSA-certified ice hockey helmet was used in this thesis. This decision was made in order to eliminate the effect of helmet shell geometry and liner materials

on the response of the headform. Using a different helmet model may produce different magnitudes of dynamic response and MPS.

5.3.5 Professional Ice Hockey Concussion Reconstruction Dataset

The professional ice hockey concussion reconstruction dataset contained laboratory reconstructions of concussive impacts to the ice (n = 4), boards (n = 7), and shoulder (n = 16). A limitation of this dataset is the low number of reconstructions to the ice and boards. However, this also reflects the frequency of these concussive head impact events in professional ice hockey. Additionally, the reference dataset only included concussive head impact events that could be reconstructed in a laboratory setting. The total number of concussive impacts, including those that could not be reconstructed, was not reported (Post et al., 2019). Nevertheless, the relative distribution of head impact events in the dataset aligns with the professional ice hockey concussion data reported by Hutchison et al. (2015, 2013). Despite these limitations, the assumption was made that the concussion reconstruction dataset provides a reasonable representation of concussive head impact events in professional ice hockey.

5.4 Delimitations

5.4.1 Generalizability of Findings

The reference dataset from Post et al. (2019), containing reconstructions of concussive injuries in professional ice hockey, was used to inform the impact parameters in each of the three helmet tests. Therefore, the three helmet tests used impact parameters that reflect a risk of concussive injury in professional ice hockey. The results of this thesis are not intended to represent all ages and skill levels of ice hockey.

Chapter 6: Discussion

This thesis investigated how three ice hockey helmet tests relate to reconstructions of concussive injuries in professional ice hockey, based on relationships between dynamic response and brain tissue deformation. The following sections will discuss the helmet tests in this thesis and how each test compares to the concussive injury event they were designed to represent.

6.1 Flat Anvil Drop Test and PIH Head-to-Ice Concussion Reconstructions

The Flat Anvil Drop Test in this thesis is similar to current ice hockey helmet standard tests involving a helmeted headform dropped on a stiff, flat surface to simulate a fall to the ice. Standard tests rigidly attach a helmeted headform to a monorail drop rig and only measure linear acceleration of the impact. These standard tests were initially designed to prevent traumatic brain injuries and skull fractures, which are known to result from high magnitudes of linear acceleration (Gurdjian, 1966; Gurdjian et al., 1953; Thomas et al., 1966). In this thesis, the Flat Anvil Drop Test used a free-falling headform that was permitted to respond without any restrictions upon impact. Compared to current standard tests, a free-falling headform provides a closer representation of a human head striking the ice (CEN, 2015).

The additional degrees of freedom allowed the headform to rotate, however dominant linear acceleration was identified as the dynamic response with the strongest relationship to MPS (R^2 = 0.960). This can be in part explained by the range of impact velocities used in the test. Increasing the impact velocity produced increases in both linear acceleration and MPS, strengthening the relationship between these variables (Appendix G, Figure G-1). The very strong relationship between linear acceleration and MPS reflects the high magnitudes of linear acceleration experienced at center of gravity of the headform under flat anvil impact conditions.

This is consistent with prior research that also identified a strong correlation between linear acceleration and MPS for ice hockey falls on a hard surface (R^2 = 0.967) (Clark et al., 2015).

When examining the stepwise regression for the PIH head-to-ice concussion reconstructions, no dynamic response variables had a significant relationship with MPS. This is likely a result of the small dataset of reconstructions for this event (n = 4) and due to variations in impact parameters between the head-to-ice concussion reconstructions. While the small dataset is a limitation, it reflects the incidence of this type of head impact event in professional ice hockey. Hutchison and colleagues (2013) reported that only 7% of concussions in professional ice hockey are the result of players falling or tripping on the ice. This may be due to the strong skating and balance skills that professional ice hockey players possess. Therefore, while head-to-ice impacts are dangerous, they do not account for many concussions in professional ice hockey.

6.2 Angled Anvil Drop Tests and PIH Head-to-Boards Concussion Reconstructions

The two angled anvil drop tests in this thesis (30° and 45°) evaluated ice hockey helmets under rotation-inducing impact conditions. The tests represented two angles at which a player may fall and impact their head against the boards. Under these impact conditions, rotational velocity was identified to have the strongest relationship with MPS for both angled drop tests. The very strong R^2 values for the 30° Anvil Drop Test (resultant rotational velocity R^2 = 0.978) and the 45° Anvil Drop Test (dominant rotational velocity R^2 = 0.977) are in part attributed to the range of impact velocities used in each test. As impact velocity increased, the headform experienced higher magnitudes of rotational dynamic response and higher MPS, re-enforcing the relationship between these variables (Appendix G, Figure G-2).

While rotational velocity had the strongest relationship with MPS for the two angled drop tests, rotational acceleration had the strongest relationship with MPS for the PIH head-to-boards concussion reconstructions. This difference is due to variations in laboratory methods used between the angled anvil drop tests and the head-to-boards concussion reconstructions. In the angled anvil drop tests, a free-falling headform impacted a stiff steel anvil and produced very reliable impact conditions. Impact durations were consistently 12.6 to 20.9 ms for the 30° Anvil Drop Test and 14.2 to 23.9 ms for the 45° Anvil Drop Test (Appendix H, Table H-1). The acceleration loading curves were very smooth and had consistent shapes from one impact to the next (Figure 18). Rotational velocity was a more stable measure under these controlled testing conditions, and therefore a stronger predictor of MPS. In contrast, for the PIH head-to-boards concussion reconstructions, the headform was attached to a monorail drop rig (using a neckform) and dropped on a compliant sheet of high-density polyethylene. The use of a neckform and a higher compliance impact surface produced more variable conditions with longer impact durations ranging from 25.0 to 37.8 ms (Appendix H, Table H-2). Furthermore, impact velocity and location varied between each of the head-to-boards concussion reconstructions, producing variation within the dataset. Under these more variable impact conditions, rotational velocity was a less stable measure (Appendix G, Figure G-2). This explains why rotational acceleration was a stronger predictor of MPS for the PIH head-to-boards concussion reconstructions.

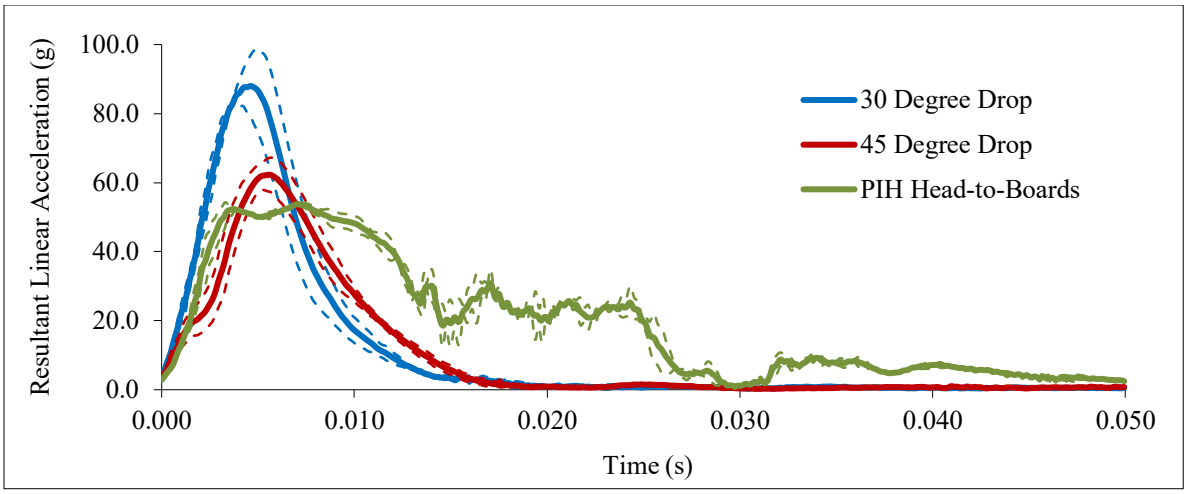

Figure 18. Examples of mean acceleration loading curve shapes from the 30° Anvil Drop Test, 45° Anvil Drop Test, and PIH head-to-boards concussion reconstructions. Dashed lines represent one standard deviation above and below the mean.

When comparing the two angled drop tests, the 30° Anvil Drop Test produced higher magnitudes of linear and rotational acceleration than the 45° Anvil Drop Test. Despite higher dynamic response, the overall mean MPS values were nearly identical between tests (mean MPS of 0.41 and 0.38 for the 30° and 45° Anvil Drop Tests, respectively). This similarity persisted even after the results of the two angled drop tests were separated by impact velocity and location (Appendix I, Tables I-2 and I-3). For any given impact condition, the magnitudes of MPS in the two drop tests differed by less than 0.05. These results suggest that both a drop test using a 30° anvil and a drop test on a 45° anvil capture a similar risk of brain injury, as indicated by MPS.

Since both angled drop tests captured a similar risk of injury, it would be useful to identify the test that provides a closer representation of concussive head-to-boards impacts in professional ice hockey. As described in Methods section 4.2.2, video analysis of the PIH head-to-boards concussive impacts revealed a mean impact angle of 44°. Therefore, based on the video analysis results, it is more appropriate to use the 45° Anvil Drop Test to evaluate ice hockey helmets. It is also important that the test evaluates helmets within energy ranges that players are

exposed to on the ice. Impacts at 6.0 m/s in this thesis generated very high magnitudes of dynamic response and MPS that were not representative of the PIH head-to-boards concussion reconstructions. Although head-to-boards impacts of this magnitude were not observed in the dataset of concussion reconstructions, they may still occur in professional ice hockey. On the other hand, low and medium impact velocities (3.0 m/s and 4.5 m/s) produced dynamic response and MPS magnitudes that more closely reflect the PIH head-to-boards concussion reconstructions. The 45° Anvil Drop Test at 3.0 m/s and 4.5 m/s would best represent concussive head-to-boards impacts in professional ice hockey, based on the PIH dataset in this thesis.

This information should be used by standards organizations to develop an angled anvil drop test for ice hockey helmets that captures the risk of concussive injury better than current flat anvil drop tests. The angled anvil drop tests in this thesis support the use of rotational velocity as a predictor of concussion for future standard helmet tests. Rotational velocity can also be used as a target variable for helmet innovation when evaluating helmets with an angled anvil drop test.

6.3 Pneumatic Ram Tests and PIH Shoulder-to-Head Concussion Reconstructions

The pneumatic ram tests in this thesis were designed to represent shoulder-to-head collision impacts, which account for the highest incidence of concussions in professional ice hockey (Hutchison et al., 2015, 2013). The three impact locations were selected to represent the most frequent locations observed in the PIH shoulder-to-head concussion reconstruction dataset. Impacts to these three locations on the head have been reported to induce high magnitudes of rotational acceleration (Walsh et al., 2011). In this thesis, both pneumatic ram tests identified resultant rotational acceleration as the dynamic response variable most predictive of MPS. Resultant rotational acceleration was also identified as most predictive of MPS for the PIH shoulder-to-head concussion reconstructions. These relationships are demonstrated by plotting

dynamic response versus MPS for the two pneumatic ram tests and for the shoulder-to-head concussion reconstructions (Appendix G, Figure G-3). While linear acceleration moderately associates with MPS, rotational acceleration displays a stronger relationship with MPS. These findings are consistent with previous work that examined compliant ice hockey collision impacts and identified strong correlations between rotational acceleration and MPS (Post et al., 2011). Furthermore, these findings indicate that both the medium and high compliance ram tests induce high magnitudes of rotational dynamic response, consistent with concussive shoulder-to-head impacts in professional ice hockey.

While resultant rotational acceleration was most predictive of MPS for both the medium compliance (R^2 = 0.671) and high compliance (R^2 = 0.850) ram tests, there were some differences that should be noted. Firstly, the High Compliance Ram Test impacts were longer in duration than the Medium Compliance Ram Test (Appendix H, Table H-1). Additionally, the softer striker cap used for the High Compliance Ram Test induced lower magnitudes of dynamic response and MPS. This is consistent with recent research reporting that higher striking compliance was associated with lower dynamic response over longer impact durations (De Grau, 2017). Based on similarities in impact duration and rotational acceleration, the High Compliance Ram Test provides a closer representation of the PIH shoulder-to-head concussion reconstructions (Appendix G, Figure G-3). These similarities may be attributed to the methods used for the concussion reconstructions, which were also performed using a high compliance striker cap (Rousseau, 2014, Post et al., 2019). Several higher magnitude PIH shoulder-to-head concussion reconstructions were not represented by the High Compliance Ram Test. In contrast, the Medium Compliance Ram Test results did not overlap with the PIH shoulder-to-head concussion reconstructions in terms of impact duration and rotational acceleration (Appendix G,

Figure G-3). The optimal compliance for representing the PIH shoulder-to-head concussion reconstructions may exist in between the medium and high levels of compliance.

While the High Compliance Ram Test provided a closer representation of concussive shoulder-to-head impacts, it produced varying acceleration loading curve shapes for some impact conditions. Dual peaks were observed in the acceleration-time curves, resulting from the multiple materials in the striker deforming upon impact and interacting with external geometry on the helmet. This interaction can influence the transfer of energy to the headform and introduce variability from one impact to the next. In contrast, when the medium compliance striker cap was used to impact the helmeted headform, consistent acceleration loading curve shapes (with single peaks) were observed between impacts (Figure 19). The stiffer impactor interacts less with the helmet geometry and provides a consistent transfer of energy during each impact. Furthermore, a stiffer impactor may better identify performance differences between different ice hockey helmets. The medium compliance ram test may be a more reliable and repeatable ice hockey helmet test (Appendix J), but less representative of real-world injury events.

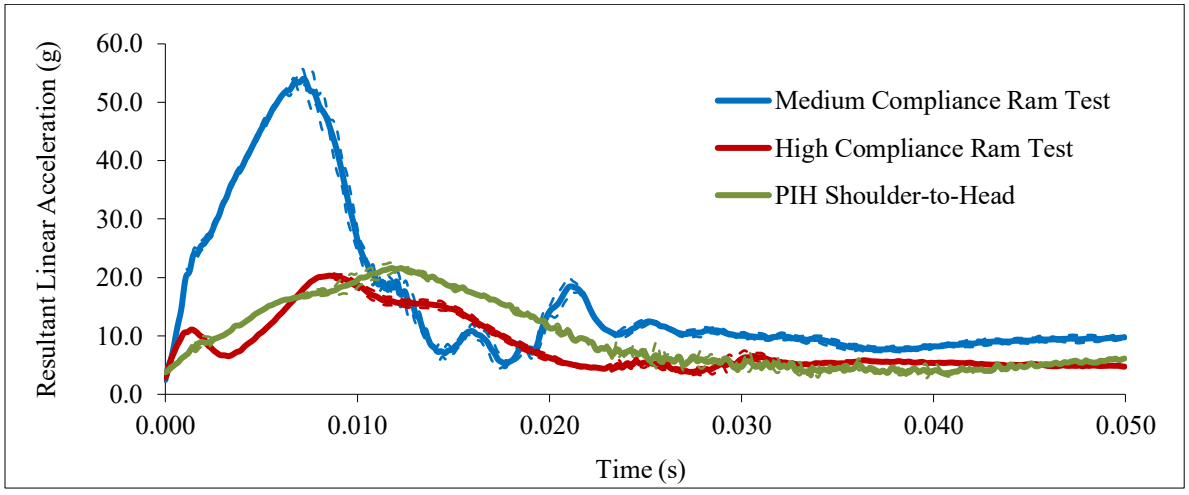

Figure 19. Examples of mean acceleration loading curve shapes from the Medium Compliance Ram Test, High Compliance Ram Test, and PIH shoulder-to-head concussion reconstructions. Dashed lines represent one standard deviation above and below the mean.

Overall, the Medium Compliance Ram Test provided more repeatable impact conditions. However, the High Compliance Ram Test provide a closer representation of concussive shoulder-to-head impacts in professional ice hockey. This information is important for standards organizations to consider when developing a pneumatic ram helmet test. Additionally, future research should be performed to determine the sensitivity of these two pneumatic ram tests. It would be beneficial to evaluate the ability of each test to identify performance differences between different types of helmets. Regardless of whether the Medium or High Compliance Ram Test is used, the results in this thesis support the use of rotational acceleration as a predictor of concussive injury. Rotational acceleration can also be used as a target variable for helmet innovation under medium or high compliance impact conditions.

6.4 Comparison of Helmet Test Results to Concussive Injury Literature

Each helmet test in this thesis was designed using information from the PIH concussion reconstruction dataset. Therefore, it is expected that test should evaluate helmet performance within the range of concussive injury. To identify magnitudes of dynamic response and brain tissue strain associated with a risk of concussive injury, researchers have used reconstructions of sporting impacts such as American football helmet-to-helmet impacts (Kleiven, 2007; Newman et al., 2000; Pellman et al., 2003; Zhang et al., 2004), rugby collision impacts (Fréchède and McIntosh, 2009), and ice hockey collision impacts (Rousseau, 2014). Using this literature as a point of comparison, the Flat Anvil Drop Test, 30^{o} Anvil Drop Test, and 45^{o} Anvil Drop Test elicited responses representing a 25 to 50% risk of concussive injury. The Medium and High Compliance Ram Tests both elicited responses exceeding a 50% risk of concussive injury. In summary, all helmet tests used in this thesis elicited magnitudes of dynamic response and MPS associated with a 25 to 50% risk of concussive injury.

Chapter 7: Conclusion

The objective of this thesis was to describe how three ice hockey helmet tests relate to three concussive injury events in professional ice hockey, based on relationships between dynamic response and MPS. This thesis demonstrated that a Flat Anvil Drop Test, representing a fall on the ice, produces a strong relationship between linear acceleration and MPS. However, using this helmet test in isolation neglects other more common head impact events that are known to cause concussive injuries. In professional ice hockey, head-to-boards and shoulder-to-head impacts occur more frequently than impacts to the ice and are leading causes of concussive injuries. Therefore, it is important that helmets are assessed under impact conditions that reflect how players sustain injuries on the ice.

For the 30^{o} and 45^{o} Anvil Drop Tests, resultant and dominant rotational velocity produced the strongest relationships with MPS, respectively. While both angled anvil drop tests captured a similar risk of injury, the 45^{o} Anvil Drop Test provided a closer representation of concussive head-to-boards impacts, based on video analysis of head-to-boards concussions in professional ice hockey. This thesis also demonstrated that for the pneumatic ram tests, resultant rotational acceleration produced the strongest relationship with MPS. The Medium Compliance Ram Test provided reliable impact conditions, while the High Compliance Ram Test provided a closer representation of concussive shoulder-to-head impacts in professional ice hockey.

In the future, ice hockey helmets should be evaluated using both an angled anvil drop test and a pneumatic ram test, representing two unique head impact events that are not represented in current standard tests. The information in this thesis will inform the development of rotational standard ice hockey helmet tests that better address the risks associated with concussive injury in professional ice hockey.

References

Adams, J.H., Graham, D.I., Scott, G., Parkert, L.S., Doyle, D., 1980. Brain damage in fatal non-missile head injury. J. Clin. Pathol. 33, 1132–1145.

Adams, L., Graham, D.I., Gennarellp, T.A., 1981. Acceleration induced head injury in the monkey. ll. Neuropathology. Acta Neuropathol 26–28.

Andriessen, T.M.J.C., Jacobs, B., Vos, P.E., 2010. Clinical characteristics and pathophysiological mechanisms of focal and diffuse traumatic brain injury 14, 2381–2392. https://doi.org/10.1111/j.1582-4934.2010.01164.x

Biasca, N., Simmen, H.-P., 2004. Minor Traumatic Brain Injury "mTBI" in Ice Hockey and Other Contact Sports: Injury Mechanisms at the Macro and Histological Levels and Prevention Strategies, Safety in Ice Hockey: Fourth Volume, ASTM STP 1446. West Conshohocken, PA. https://doi.org/10.1520/stp1446-eb

Cantu, R.C., 1996. Head injuries in sport. Br JSports Med 30, 289–296.

Carnevale Lon, S.C., 2014. A new helmet testing method to assess potential damages in the brain and the head due to rotational energy. KTH.

Casson, I.R., Viano, D.C., Powell, J.W., Pellman, E.J., 2010. Twelve years of National Football League concussion data. Sports Health 2, 471–483. https://doi.org/10.1177/1941738110383963

CDCP, 2011. Nonfatal traumatic brain injuries related to sports and recreation activities among persons aged ≤19 years--United States, 2001-2009. MMWR. Morb. Mortal. Wkly. Rep. 60, 1337–42. https://doi.org/mm6039a1 [pii]

Clark, J.M., Post, A., Hoshizaki, T.B., Gilchrist, M.D., 2016. Protective capacity of ice hockey helmets against different impact events. Ann. Biomed. Eng. 44, 3693–3704. https://doi.org/10.1007/s10439-016-1686-3

Clark, M., Taylor, K., Post, A., Hoshizaki, T.B., Gilchrist, M.D., 2018. Comparison of Ice Hockey Goaltender Helmets for Concussion Type Impacts. Ann. Biomed. Eng.

https://doi.org/10.1007/s10439-018-2017-7

Clark, Post, A., Hoshizaki, T.B., Gilchrist, M.D., 2015. Determining the relationship between linear and rotational acceleration and MPS for different magnitudes of classified brain injury risk in ice hockey, in: IRCOBI Conference. pp. 168–179.

Cusimano, M.D., Cho, N., Amin, K., Shirazi, M., McFaull, S.R., Do, M.T., Wong, M.C., Russell, K., 2013. Mechanisms of team-sport-related brain injuries in children 5 to 19 years old: Opportunities for prevention. PLoS One 8, 1–8. https://doi.org/10.1371/journal.pone.0058868

De Grau, S., 2017. Effects of striker compliance on dynamic response and brain tissue strain for helmeted ice hockey impacts. University of Ottawa.

Delaney, J.S., Lacroix, V.J., Leclerc, S., Johnston, K.M., 2002. Concussions among university football and soccer players. Clin J Sport Med 12, 331–338.

Doorly, M.C., Gilchrist, M.D., 2006. The use of accident reconstruction for the analysis of traumatic brain injury due to head impacts arising from falls. Comput. Methods Biomech. Biomed. Engin. 9, 371–377. https://doi.org/10.1080/10255840601003551

Emery, C., Meeuwisse, W.H., 2006. Injury rates, risk factors, and mechanisms of injury in minor hockey. Am. J. Sports Med. 34, 1960–1969. https://doi.org/10.1177/0363546506290061

Foreman, S., Hoshizaki, T.B., 2011. The Influence of Headform Geometry on the Dynamic Impact Response of a Hybrid III Headform, in: ISB. Brussels, pp. 2–3.

Fréchède, B., McIntosh, A.S., 2009. Numerical reconstruction of real-life concussive football impacts. Med. Sci. Sports Exerc. https://doi.org/10.1249/MSS.0b013e318186b1c5

Galbraith, J.A., Thibault, L.E., Matteson, D.R., 1993. Mechanical and Electrical Responses of the Squid Giant Axon to Simple Elongation. J. Biomech. Eng. 115, 13. https://doi.org/10.1115/1.2895464

Gennarelli, T.A., Thibault, L.E., Adams, J.H., Graham, D.I., Thompson, C.J., Marcincin, R.P., 1982. Diffuse axonal injury and traumatic coma in the primate. Ann. Neurol. 12, 564–574.

https://doi.org/10.1002/ana.410120611

Gennarelli, T.A., Thibault, L.E., Ommaya, A.K., 1972. Pathophysiological responses to rotational and translational accelerations of the head, SAE Paper No. 720970, in: 16th Stapp Car Crash Conference. SAE International, pp. 296–308. https://doi.org/10.4271/720970

Gennarelli, T.A., Thibault, L.E., Ommaya, A.K., 1971. Comparison of translational and rotational head motions in experimental cerebral concussion, in: 15th Stapp Car Crash Conference. Proceedings, SAE, New York, pp. 797–803.

Goodman, D., Gaetz, M., Meichenbaum, D., 2001. Concussions in hockey: there is cause for concern. Med. Sci. Sport. Exerc. 33, 2004–2009.

Gurdjian, E.S., 1966. Tolerance curves of acceleration and intracranial pressure and protective index in experimental head injury. J. Trauma Inj. Infect. Crit. Care 6, 600–604.

Gurdjian, E.S., Lissner, H.R., Latimer, F.R., Haddad, B.F., Webster, J.E., 1953. Quantitative determination of acceleration and intracranial pressure in experimental head injury - Preliminary report. Neurology 3, 417–423.

Gurdjian, E.S., Lissner, H.R., Webster, J.E., 1955. Observations on the mechanism of brain concussion, contusion, and laceration. Surgery, Gynecol. Obstet. 680–690.

Haddad, B.F., Lissner, H.R., Webster, J.E., Gurdjian, E.S., 1955. Experimental concussion: relation of acceleration to physiologic effect. Neurology 5, 798–800.

Halldin, P., 2015. Proposal for a new test method measuring the head kinematics in angled helmeted impacts, in: IRCOBI-NOCSAE-Snell-PDB TBI Workshop. Lyon.

Hardy, W.N., Foster, C.D., Mason, M.J., Yang, K.H., King, A.I., Tashman, S., 2001. Investigation of Head Injury Mechanisms Using Neutral Density Technology and High-Speed Biplanar X-ray. Stapp Car Crash J. 45, 337–68.

Hardy, W.N., Khalil, T.B., King, A.I., 1994. Literature review of head injury biomechanics. Int. J. Impact Eng. 15, 561–568. https://doi.org/10.1016/0734-743X(94)80034-7

Holbourn, A.H.S., 1945. The mechanics of brain injuries. Br. Med. Bull. 3, 147–149.

Holbourn, A.H.S., Edin, M., Oxfd, D.P., 1943. Mechanics of head injuries. Lancet 242, 438–441.

Horgan, T.J., Gilchrist, M.D., 2003. The creation of three-dimensional finite element models for simulating head impact biomechanics. Int. J. Crashworthiness 8, 353–366. https://doi.org/10.1533/ijcr.2003.0243

Hoshizaki, T.B., Brien, S.E., 2004. The science and design of head protection in sport. Neurosurgery 55. https://doi.org/10.1227/01.NEU.0000137275.50246.0B

Hoshizaki, T.B., Post, A., Kendall, M., Cournoyer, J., Rousseau, P., Gilchrist, M.D., Brien, S., Cusimano, M., Marshall, S., 2016. The development of a threshold curve for the understanding of concussion in sport. Trauma (United Kingdom) 19, 196–206. https://doi.org/10.1177/1460408616676503

Hoshizaki, T.B., Post, A., Kendall, M., Karton, C., Brien, S., 2013. The relationship between head impact and brain trauma. J Neurol Neurophysiol 5. https://doi.org/10.4172/2155-9562.1000181

Hutchison, M.G., Comper, P., Meeuwisse, W.H., Echemendia, R.J., 2013. A systematic video analysis of National Hockey League (NHL) concussions, part I: who, when, where and what? Br. J. Sports Med. 00, 1–5. https://doi.org/10.1136/bjsports-2013-092234

Hutchison, M.G., Comper, P., Meeuwisse, W.H., Echemendia, R.J., Hutchison, M., Macintosh, D.L., 2015. A systematic video analysis of National Hockey League (NHL) concussions, part II: how concussions occur in the NHL. Br. J. Sports Med. 49, 552–555. https://doi.org/10.1136/bjsports-2013-092235

IIHF, 2017. Annual Report July 2016 - June 2017.

Kelly, K.D., Lissel, H.L., Rowe, B.H., Vincenten, J.A., Voaklander, D.C., 2001. Sport and recreation-related head injuries treated in the emergency department. Clin. J. Sport Med. 11, 77–81. https://doi.org/10.1097/00042752-200104000-00003

Kleiven, S., 2013. Why most traumatic brain injuries are not caused by linear acceleration but skull fractures are. Front. Bioeng. Biotechnol. 1, 1–5. https://doi.org/10.3389/fbioe.2013.00015

Kleiven, S., 2007. Predictors for traumatic brain injuries evaluated through accident reconstructions. Stapp Car Crash J. 51, 81–114.

Koh, J.O., Cassidy, J.D., Watkinson, E.J., 2003. Incidence of concussion in contact sports: A systematic review of the evidence. Brain Inj. 17, 901–917. https://doi.org/10.1080/0269905031000088869

Löwenhielm, P., 1974. Dynamic Properties of the Parasagittal Bridging Veins. Z Rechtsmedizin 74, 55–62.

McFaull, S., Subaskaran, J., Branchard, B., Thompson, W., 2016. Emergency department surveillance of injuries and head injuries associated with baseball, football, soccer and ice hockey, children and youth, ages 5 to 18 years, 2004 to 2014. Heal. Promot. Chronic Dis. Prev. Canada 36, 13–14.

McIntosh, A.S., Patton, D.A., Fréchède, B., Pierré, P.-A., Ferry, E., Barthels, T., 2014. The biomechanics of concussion in unhelmeted football players in Australia: a case–control study. BMJ Open 4, e005078. https://doi.org/10.1136/bmjopen-2014-005078

Miller, R.T., Margulies, S.S., Leoni, M., Nonaka, M., Chen, X., Smith, D.H., Meaney, D.F., 2010. Finite Element Modeling Approaches for Predicting Injury in an Experimental Model of Severe Diffuse Axonal Injury. SAE Tech. Pap. Ser. 1. https://doi.org/10.4271/983154

Nahum, A., Smith, R., Ward, C., 1977. Intracranial Pressure Dynamics During Head Impact, SAE Technical Paper 770922. https://doi.org/https://doi.org/10.4271/770922

Newman, J., Barr, C., Beusenberg, M., Fournier, E., Shewchenko, N., Welbourne, E., Withnall, C., 2000. A new biomehcanical assessment of mild traumatic brain injury part 2 - Results and conclusions, in: IRCOBI Conference. pp. 223–233.

NOCSAE, 2017. NOCSAE DOC (ND) 027- 12m14 - Standard Performance Specification for Newly Manufactured Football Helmets. Overland Park, Kansas, USA.

Oeur, R.A., 2018. The Effects of Reconstructed Head Impact Event Parameters on Risk of Sport Related Concussions. University of Ottawa.

Oeur, R.A., Karton, C., Post, A., Rousseau, P., Hoshizaki, T.B., Marshall, S., Brien, S., Smith, A., Cusimano, M., Gilchrist, M.D., 2015. A Comparison of head dynamic response and brain tissue stress and strain using accident reconstructions for concussion, concussion with persistent postconcussive symptoms, and subdural hematoma. J Neurosurg 1–8.

Ommaya, A.K., Gennarelli, T.A., 1974. Cerebral concussion and traumatic unconsciousness. Correlation of experimental and clinical observations of blunt head injuries. Brain 97, 633–654.

Ommaya, A.K., Hirsch, A.E., 1971. Tolerances for cerebral concussion from head impact and whiplash in primates. J. Biomech. 4, 13–21.

Ommaya, A.K., Thibault, L., Bandak, F.A., 1994. Mechanisms of impact head injury. Int. J. Impact Eng. 15, 535–560. https://doi.org/10.1016/0734-743X(94)80033-6

Padgaonkar, A.J., Krieger, K.W., King, A.I., 1975. Measurement of Angular Acceleration of a Rigid Body Using Linear Accelerometers. J. Appl. Mech.

Patton, D.A., McIntosh, A.S., Kleiven, S., 2015. The biomechanical determinants of concussion: Finite element simulations to investigate tissue-level predictors of injury during sporting impacts to the unprotected head. J. Appl. Biomech. 31, 264–268. https://doi.org/10.1123/jab.2014-0223

Pellman, E.J., Viano, D.C., Tucker, A.M., Casson, I.R., Waeckerle, J.F., Maroon, J.C., Lovell, M.R., Collins, M.W., Kelly, D.F., Valadka, A.B., Cantu, R.C., Bailes, J.E., Levy, M.L., 2003. Concussion in professional football: Reconstruction of game impacts and injuries. Neurosurgery 53, 799–814. https://doi.org/10.1227/01.NEU.0000083559.68424.3F

Post, A., Hoshizaki, T.B., Gilchrist, M.D., Cusimano, M.D., 2017a. Peak linear and rotational acceleration magnitude and duration effects on maximum principal strain in the corpus callosum for sport impacts. J. Biomech. 61, 183–192. https://doi.org/10.1016/j.jbiomech.2017.07.013

Post, A., Hoshizaki, T.B., Karton, C., Clark, J.M., Cournoyer, J., Taylor, K., Oeur, R.A., Gilchrist, M.D., Cusimano, M.D., Post, A., Hoshizaki, T.B., Karton, C., Clark, J.M.,

Cournoyer, J., Taylor, K., Oeur, R.A., Gilchrist, M.D., 2019. The biomechanics of concussion for ice hockey head impact events. Comput. Methods Biomech. Biomed. Engin. 22, 631–643. https://doi.org/10.1080/10255842.2019.1577827

Post, A., Hoshizaki, T.B., Karton, C., Clark, J.M., Dawson, L., Taylor, K., Oeur, R.A., Gilchrist, M.D., Cusimano, M.D., 2017b. The Biomechanics of Concussion for Ice Hockey Head Impact Events. Submitt. to Comput. Methods Biomech. Biomed. Eng.

Post, A., Hoshizaki, T.B., Zemek, R., Gilchrist, M.D., Koncan, D., Dawson, L., Chen, W., Ledoux, A., 2017c. Pediatric concussion: biomechanical differences between outcomes of transient and persistent (> 4 weeks) postconcussion symptoms. J Neurosurg Pediatr 19, 641–651. https://doi.org/10.3171/2016.11.PEDS16383.

Post, Andrew, Kendall, M., Cournoyer, J., Karton, C., Oeur, R.A., Dawson, L., Hoshizaki, T.B., 2018. Brain tissue analysis of impacts to American football helmets. Comput. Methods Biomech. Biomed. Engin. 1–14. https://doi.org/10.1080/10255842.2018.1445229

Post, A., Koncan, D., Kendall, M., Cournoyer, J., Michio Clark, J., Kosziwka, G., Chen, W., de Grau Amezcua, S., Blaine Hoshizaki, T., 2018. Analysis of speed accuracy using video analysis software. Sport. Eng. https://doi.org/10.1007/s12283-018-0263-4

Post, A., Oeur, A., Hoshizaki, B., Gilchrist, M.D., 2011. Examination of the relationship between peak linear and angular accelerations to brain deformation metrics in hockey helmet impacts. Comput. Methods Biomech. Biomed. Engin. iFirst art, 1–9. https://doi.org/10.1080/10255842.2011.627559

Post, A., Oeur, A., Walsh, E., Hoshizaki, B., Gilchrist, M.D., 2013. A centric/non-centric impact protocol and finite element model methodology for the evaluation of American football helmets to evaluate risk of concussion. Comput. Methods Biomech. Biomed. Engin. https://doi.org/10.1080/10255842.2013.766724

Roberts, W.O., Brust, J.D., Leonard, B., 1999. Youth ice hockey tournament injuries: rates and patterns compared to season play. Med. Sci. Sports Exerc. 31, 46–51. https://doi.org/10.1097/00005768-199901000-00009

Rousseau, P., 2014. Analysis of Concussion Metrics of Real-World Concussive and Non-Injurious Elbow and Shoulder to Head Collisions in Ice Hockey. University of Ottawa.

Shin, S.S., Bales, J.W., Edward Dixon, C., Hwang, M., 2017. Structural imaging of mild traumatic brain injury may not be enough: overview of functional and metabolic imaging of mild traumatic brain injury. Brain Imaging Behav. 11, 591–610. https://doi.org/10.1007/s11682-017-9684-0

Takhounts, E.G., Craig, M.J., Moorhouse, K., McFadden, J., Hasija, V., 2013. Development of brain injury criteria (BrIC). Stapp Car Crash J. 57, 243.

Taylor, K., 2018. The Use of Decoupling Structures in Helmet Liners to Reduce Maximum Principal Brain Tissue Strain for Head Impacts Acknowledgment. University of Ottawa.

Thomas, L.M., Roberts, V.L., Gurdjian, E.S., 1966. Experimental intracranial pressure gradients in the human skull. J. Neurol. Neurosurgery. Psychiatry 29, 404.

Tse, K.M., Lim, S.P., Tan, V.C., Lee, H.P., 2014. A Review of Head Injury and Finite Element Head Models A review of head injury and finite element head models 1, 28–52.

Unterharnscheidt, F., Higgins Ls, 1969. Traumatic lesions of brain and spinal cord due to nondeforming angular acceleration of the head. Texas Reports Biol. Med. 27, 127–66.

Viano, D.C., King, A.I., Melvin, J.W., Weber, K., 1989. Injury biomechanics research: An essential element in the prevention of trauma. J. Biomech. 22, 403–417. https://doi.org/10.1016/0021-9290(89)90201-7

Walsh, E., Post, A., Rousseau, P., Kendall, M., Karton, C., Oeur, A., Foreman, S., Hoshizaki, T.B., 2012. Dynamic impact response characteristics of a helmeted Hybrid III headform using a centric and non-centric impact protocol. Proc. Inst. Mech. Eng. Part P J. Sport. Eng. Technol. 0, 1–6. https://doi.org/10.1177/1754337112442299

Walsh, E., Rousseau, P., Hoshizaki, T.B., 2011. The influence of impact location and angle on the dynamic impact response of a Hybrid III headform. Sport. Eng. https://doi.org/10.1007/s12283-011-0060-9

Walsh, E.S., Kendall, M., Post, A., Meehan, A., Hoshizaki, T.B., 2018. Comparative analysis of Hybrid III neckform and an unbiased neckform. Sport. Eng. https://doi.org/10.1007/s12283-018-0286-x

Wennberg, R.A., Tator, C.H., 2008. Concussion incidence and time lost from play in the NHL during the past ten years. Can. J. Neurol. Sci. 35, 647–651.

Wennberg, R.A., Tator, C.H., 2003. National Hockey League reported concussions, 1986-87 to 2001-02. Can. J. Neurol. Sci. 30, 206–209.

Willinger, R., Baumgartner, D., 2003. Human head tolerance limits to specific injury mechanisms. I J Crash 8, 605–617.

Zhang, J., Yoganandan, N., Pintar, F.A., Gennarelli, T.A., 2006. Role of Translational and Rotational Accelerations on Brain Strain in Lateral Head Impact. Biomed. Sci. Instrum. 42, 501–506.

Zhang, L, Yang, K.H., Dwarampudi, R., Omori, K., Li, T., Chang, K., Hardy, W.N., Khalil, T.B., King, A.I., 2001. Recent Advances in Brain Injury Research : A New Human Head Model Development and Validation. Stapp Car Crash J. 45, 1–25. https://doi.org/2001-22-0017 [pii]

Zhang, L., Yang, K.H., King, A.I., 2004. A Proposed Injury Threshold for Mild Traumatic Brain Injury. Am. Soc. Mech. Eng. 126. https://doi.org/10.1115/1.1691446

Zhang, Liying, Yang, K.H., King, A.I., 2001. Comparison of brain responses between frontal and lateral impacts by finite element modeling. J. Neurotrauma 18, 21–30.

Appendix A

Summary of current ice hockey helmet standard tests

Table A-1. Summary of test equipment, impact parameters, and pass/fail criteria for current ice hockey helmet standard tests

	CSA Z262.1-15	NOCSAE DOC 030-11m16	ASTM F1045-16	ISO 10256-2:2016
Equipment	Monorail	Twin-wire	Monorail or Twin-wire	Monorail or Twin-wire
Headform	CEN EN 960 magnesium headform, uniaxial accelerometer	NOCSAE-certified headform, triaxial accelerometer	CEN EN 960 magnesium headform, uniaxial accelerometer	CEN EN 960 magnesium headform, uniaxial (monorail drop) or triaxial (twin-wire drop) accelerometer
Velocity	4.5 m/s	3.46 m/s 4.88 m/s 5.46 m/s	4.5 m/s	4.5 m/s
Anvil	25 mm 60 ± 5 Shore A MEP Pad	12.5 mm Test MEP Pad (durometer unspecified)	25 mm 60 ± 5 Shore A MEP Pad	25 mm 60 ± 5 Shore A MEP Pad
Locations	Crown, Front, Front Boss, Side, Rear Boss, Rear	Crown, Front, Front Boss, Side, Rear Boss, Rear	Crown, Front, Front Boss, Side, Rear Boss, Rear	Crown, Front, Front Boss, Side, Rear Boss, Rear
Pass/Fail Criteria	275 g	1200 SI	275 g	275 g

Note: The CEN standard uses ISO 10256-2:2016

Appendix B

Forces and Moments During an Angled Drop Test

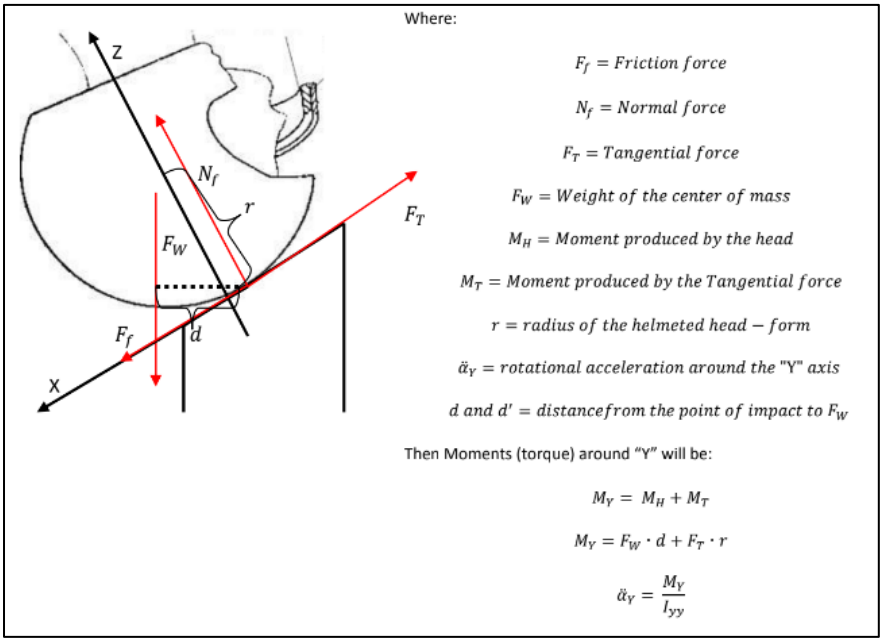

Figure B-1. Free body diagram of the moments acting on a helmeted headform during an angled impact drop test (Carnevale Lon, 2014).

Appendix C

Calibration of MEP Pad

Prior to performing the Flat Anvil Drop Test, the MEP pad was calibrated following the methods described in the standard documents ASTM F1045-16 and ISO 10256-2:2016. A spherical magnesium impactor (mass = 4.0 ± 0.1 kg) instrumented with a uniaxial accelerometer (Figure C-1) was dropped onto the MEP pad at an impact velocity of 5.44 ± 0.11 m/s (Figure C-2). The mass of the drop assembly (impactor and supporting assembly) was 5.0 ± 0.1 kg. Three impacts were performed and peak linear acceleration (g) was recorded for each impact. In order to pass calibration, the peak acceleration magnitudes were required to be 389 ± 8 g. The results of the calibration impacts are displayed below:

Impact 1: Velocity = 5.40 m/s; Peak linear acceleration = 396.9g

Impact 2: Velocity = 5.45 m/s; Peak linear acceleration = 383.7g

Impact 3: Velocity = 5.45 m/s; Peak linear acceleration = 388.2g

The MEP pad passed calibration and the Flat Anvil Drop Test was performed.

Figure C-1. Spherical impactor instrumented with one uniaxial accelerometer.

Figure C-2. Monorail drop rig with spherical impactor, uniaxial accelerometer, and MEP pad.

Appendix D

Head-to-Boards Impact Angle Calculation

Videos of the seven head-to-boards concussive impacts were analyzed using Kinovea video analysis software (www.kinovea.org, open source). Of the seven videos, three were excluded due to poor video quality, poor camera angle, or because the injured player was falling away from the broadcast camera. First, an angle in the environment was calculated using fixed distances within the playing surface. In the example below (Figure D-1), the height of the boards (h = 3.51 m) and distance across the blue line to the faceoff dot (d = 6.25 m) created a right triangle. The calculated environmental angle in Kinovea was 64º, while the actual environmental angle was determined to be 60º. Thus, this method resulted in an error of +4º using Kinovea. Next, the angle of head impact was calculated using Kinovea, and then adjusted using the calculated error. In the example below, the head impact angle was calculated in Kinovea to be 42º. Adjusting for an error of +4º yields an estimated head impact angle of 38º. From the four videos analyzed, the mean head impact angle was 44º.

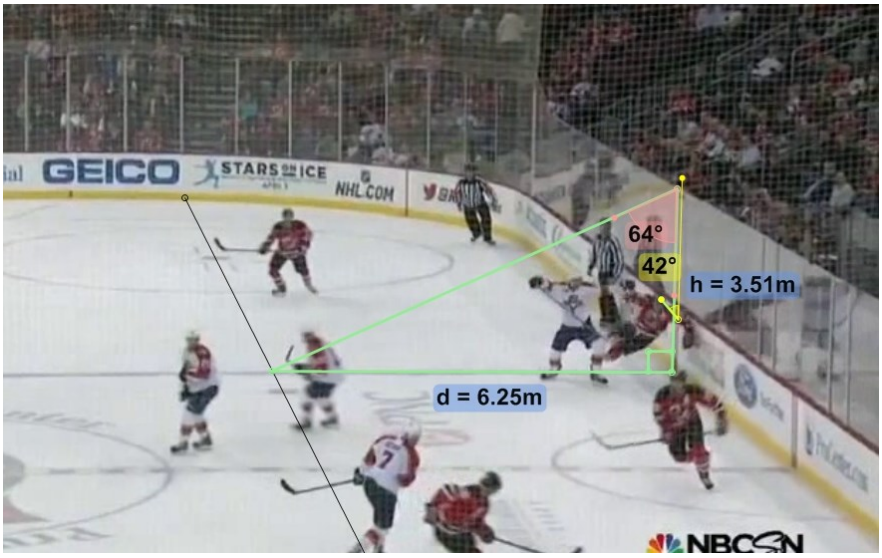

Figure D-1. Head-to-boards impact angle calculation using Kinovea. Pictured above is the analysis of video number 7 (refer to Table D-1 for details).

Table D-1. Calculated head impact angles for videos of head-to-boards concussions in the PIH dataset.

Video Number	Calculated Angle in Environment	Actual Angle in Environment	Error	Calculated Angle of Head Impact	Adjusted Angle of Head Impact
1					Excluded
2	55º	72.7º	-17.7º	32º	49.9º
3	61º	72.7º	-11.7º	31º	42.8º
4					Excluded
5	68º	70.0º	-2º	45º	47º
6					Excluded
7	64º	60º	+4º	42º	38º
Mean					44º

Appendix E

Shapiro-Wilk Tests for Normality

Table E-1. Results of the tests for normality on all data used in this thesis, using $\alpha = 0.05$ to establish significance. *A p-value<0.05 indicates that the null hypothesis (H_o = data are normally distributed) should be rejected and the data are not normally distributed (indicated in red).

Data Source	Dependent Variable	Statistic	df	Sig.
30° Anvil Drop Test	LA, Resultant	.901	25	.020
	LA, Dominant	.947	25	.212
	RA, Resultant	.892	25	.012
	RA, Dominant	.887	25	.009
	RV, Resultant	.955	25	.327
	RV, Dominant	.957	25	.359
	MPS	.957	25	.770
45° Anvil Drop Test	LA, Resultant	.924	26	.054
	LA, Dominant	.891	26	.010
	RA, Resultant	.939	26	.127
	RA, Dominant	.900	26	.016
	RV, Resultant	.963	26	.460
	RV, Dominant	.970	26	.631
	MPS	.981	26	.889
Medium Compliance Pneumatic Ram Test	LA, Resultant	.922	27	.044
	LA, Dominant	.919	27	.038
	RA, Resultant	.936	27	.097
	RA, Dominant	.903	27	.015
	RV, Resultant	.920	27	.038
	RV, Dominant	.871	27	.003
	MPS	.897	27	.011
High Compliance Pneumatic Ram Test	LA, Resultant	.931	27	.073
	LA, Dominant	.932	27	.078
	RA, Resultant	.932	27	.079
	RA, Dominant	.937	27	.103
	RV, Resultant	.937	27	.103
	RV, Dominant	.920	27	.039

	MPS	.912	27	.026
Flat Anvil Drop Test	LA, Resultant	.872	18	.019
	LA, Dominant	.955	18	.513
	RA, Resultant	.927	18	.172
	RA, Dominant	.920	18	.127
	RV, Resultant	.955	18	.514
	RV, Dominant	.954	18	.498
	MPS	.938	18	.270
PIH head-to-boards concussion reconstructions	LA, Resultant	.907	20	.056
	LA, Dominant	.914	20	.078
	RA, Resultant	.963	20	.600
	RA, Dominant	.909	20	.060
	RV, Resultant	.964	20	.628
	RV, Dominant	.893	20	.031
	MPS	.885	20	.252
PIH shoulder-to-head concussion reconstructions	LA, Resultant	.936	124	.000
	LA, Dominant	.935	124	.000
	RA, Resultant	.967	124	.004
	RA, Dominant	.948	124	.000
	RV, Resultant	.983	124	.129
	RV, Dominant	.978	124	.038
	MPS	.988	124	.940
PIH head-to-ice concussion reconstructions	LA, Resultant	.983	12	.993
	LA, Dominant	.977	12	.968
	RA, Resultant	.843	12	.030
	RA, Dominant	.854	12	.042
	RV, Resultant	.939	12	.490
	RV, Dominant	.878	12	.082
	MPS	.915	12	.512

* LA = linear acceleration; RA = rotational acceleration; RV = rotational velocity.

Appendix F

Assumptions of the Mann-Whitney U Test

1) The dependent variable should be measured at the continuous level.
    a. All data in this thesis are continuous ratio (zero indicates none of the variable).
2) The independent variable should consist of categorical, independent groups.
    a. All data are categorical (LAR, LAD, RAR, RAD, RVR, RVD, MPS). The results of each test method are independent of the PIH injury data.
3) There should be independence of observations.
    a. This condition is satisfied by the thesis data.
4) The data are not normally distributed.
    a. This was confirmed using the Shapiro-Wilk Test for Normality.

Appendix G

Scatterplots of Dynamic Response versus MPS

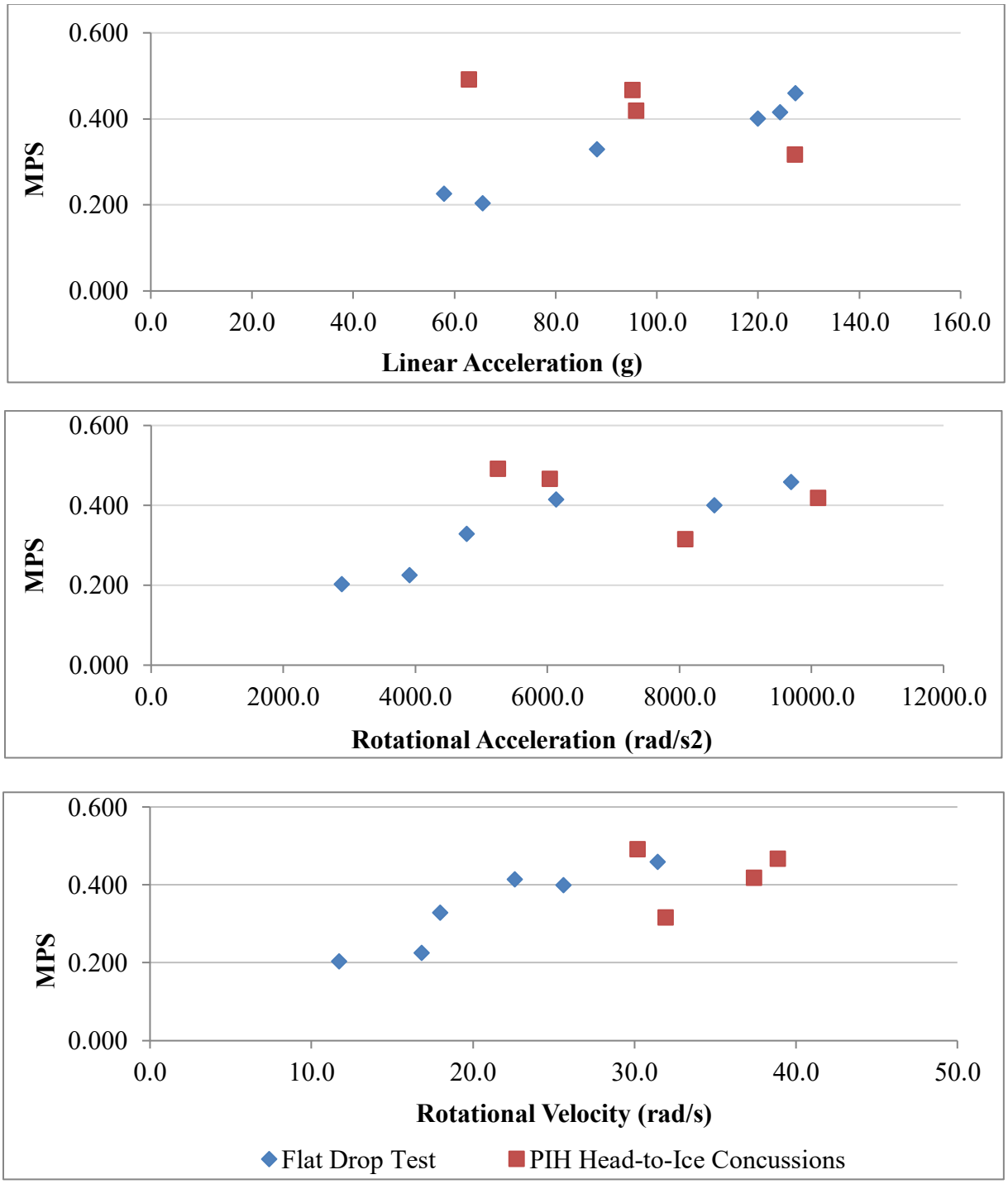

Figure G-1. Dynamic response versus MPS for the Flat Anvil Drop Test and PIH head-to-ice concussion reconstructions.

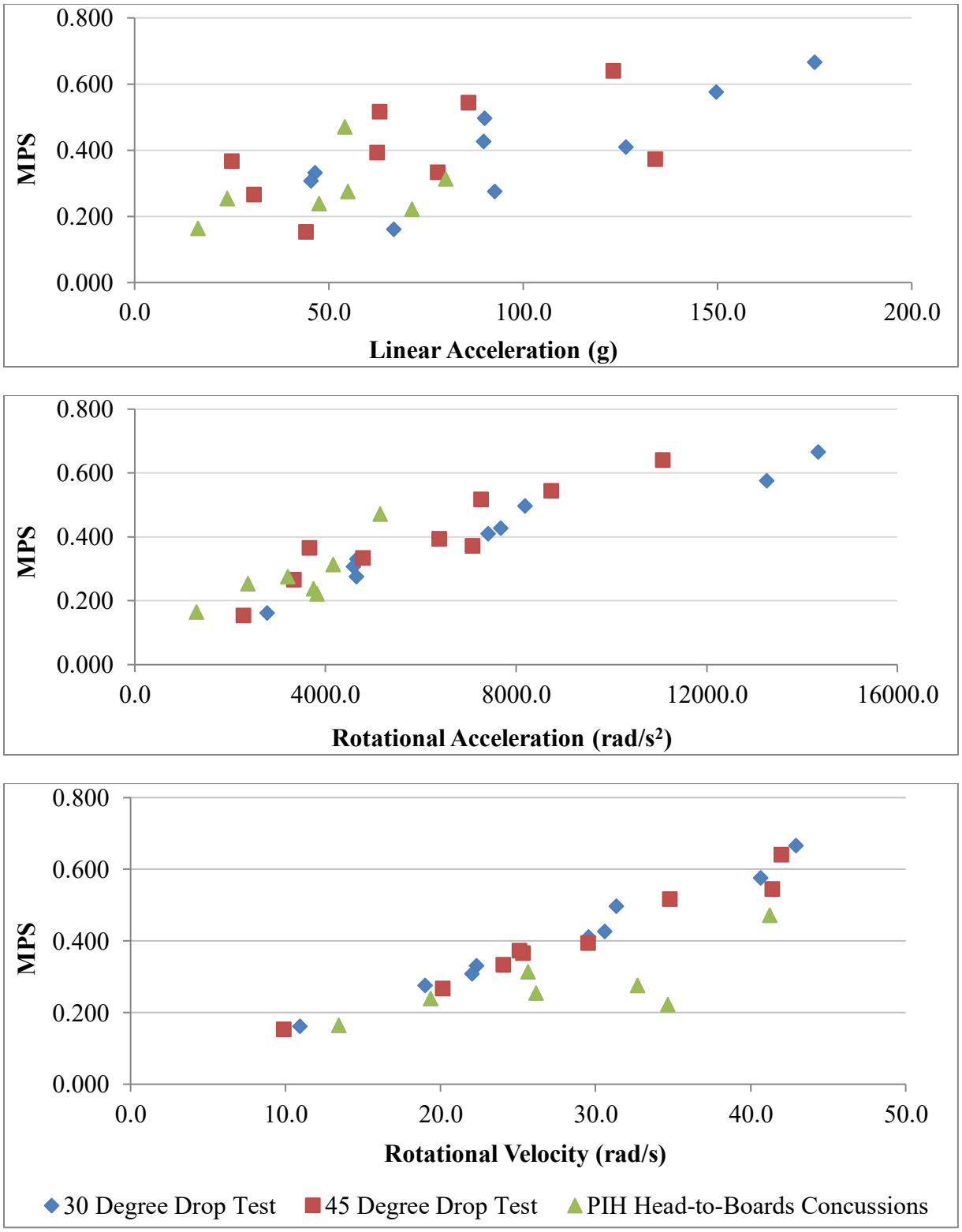

Figure G-2. Dynamic response versus MPS for the 30° Anvil Drop Test, the 45° Anvil Drop Test, and the PIH head-to-boards concussion reconstructions.

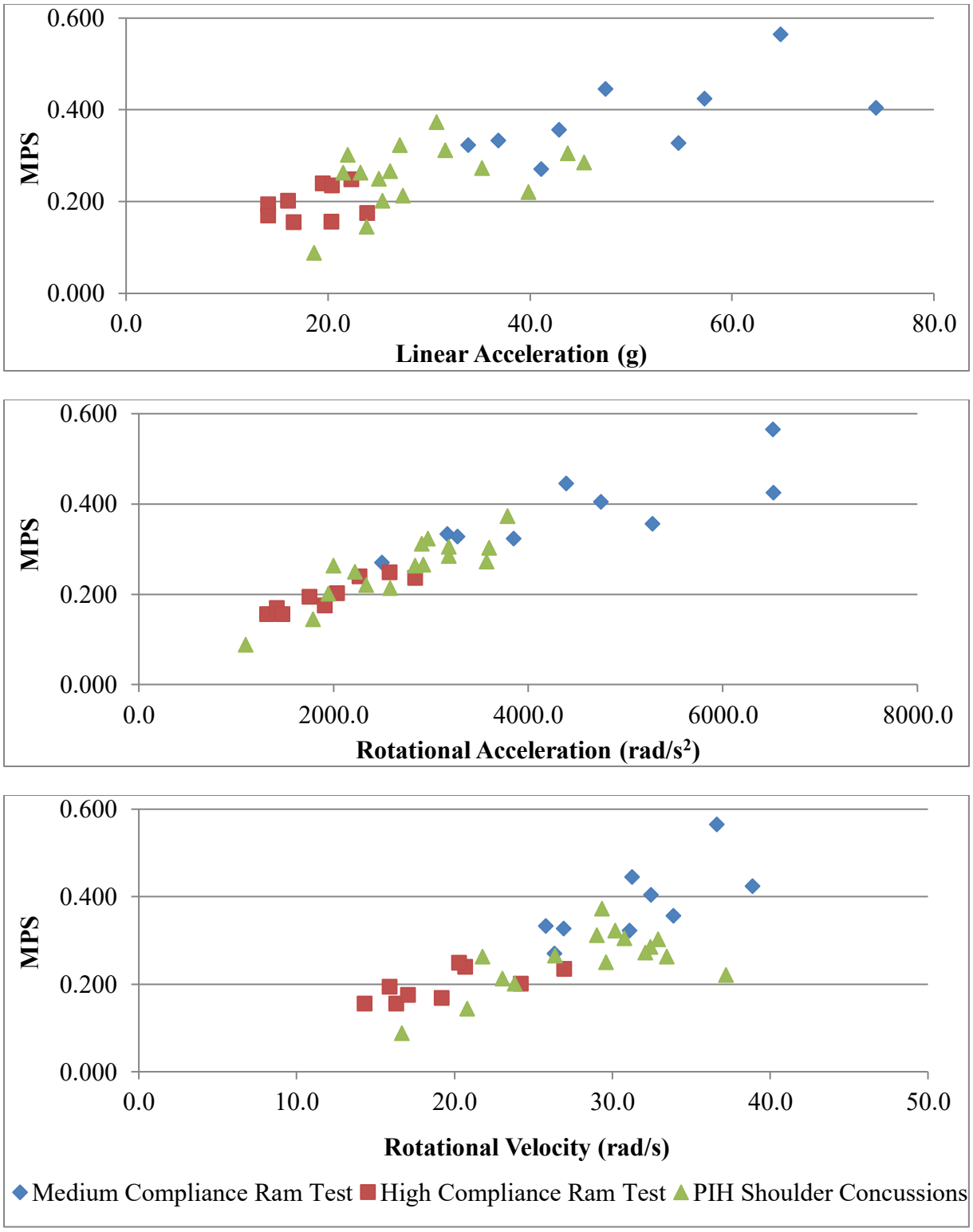

Figure G-3. Dynamic response versus MPS for the Medium Compliance Ram Test, High Compliance Ram Test, and the PIH shoulder-to-head concussion reconstructions.

Appendix H

Impact Duration Comparisons

Across all impact velocities, the Flat Anvil Drop Test yielded impact durations ranging from 13.0 to 22.7 ms. The 30º Anvil Drop Test yielded impact durations ranging from 13.2 to 20.9 ms, while the 45º Anvil Drop Test yielded impact durations ranging from 14.2 to 23.9 ms. The Medium Compliance Ram Test yielded impact durations ranging from 15.0 to 19.4 ms, while the High Compliance Ram Test yielded impact durations ranging from 21.0 to 27.5 ms. A breakdown of impact durations from each helmet test is displayed in Table I-1.

Table H-1. Impact duration range (ms) for each helmet test at low, medium, and high velocities.

	Impact Duration Range (ms)		
	Low Velocity	Medium Velocity	High Velocity
Flat Anvil Drop Test	15.4 – 20.0	13.0 – 22.7	13.0 – 19.8
30º Anvil Drop Test	15.7 – 18.5	12.6 – 20.9	13.2 – 20.6
45º Anvil Drop Test	15.0 – 23.9	14.3 – 21.9	14.2 – 20.2
Pneumatic Ram, Medium Compliance	16.5 – 19.4	15.0 – 18.0	15.0 – 17.7
Pneumatic Ram, High Compliance	24.1 – 27.5	23.0 – 25.8	21.0 – 23.9

An analysis of the PIH concussion reconstructions revealed impact duration ranges of 25.0 to 37.8 for head-to-boards concussions, 13.9 to 36.3 for shoulder-to-head concussions, and 11.4 to 19.0 for head-to- ice concussions. A summary of these impact durations can be found in Table I-2.

Table H-2. Impact duration range (ms) for each head impact event in the PIH concussion reconstruction dataset.

Impact Event	Impact Duration Range (ms)
Head-to-Ice	11.4 – 19.0
Head-to-Boards	25.0 – 37.8
Shoulder-to-Head	13.9 – 36.3

A graphical comparison of impact durations between the Flat Anvil Drop Test and PIH head-to-ice concussion reconstructions is presented in Figure I-1.

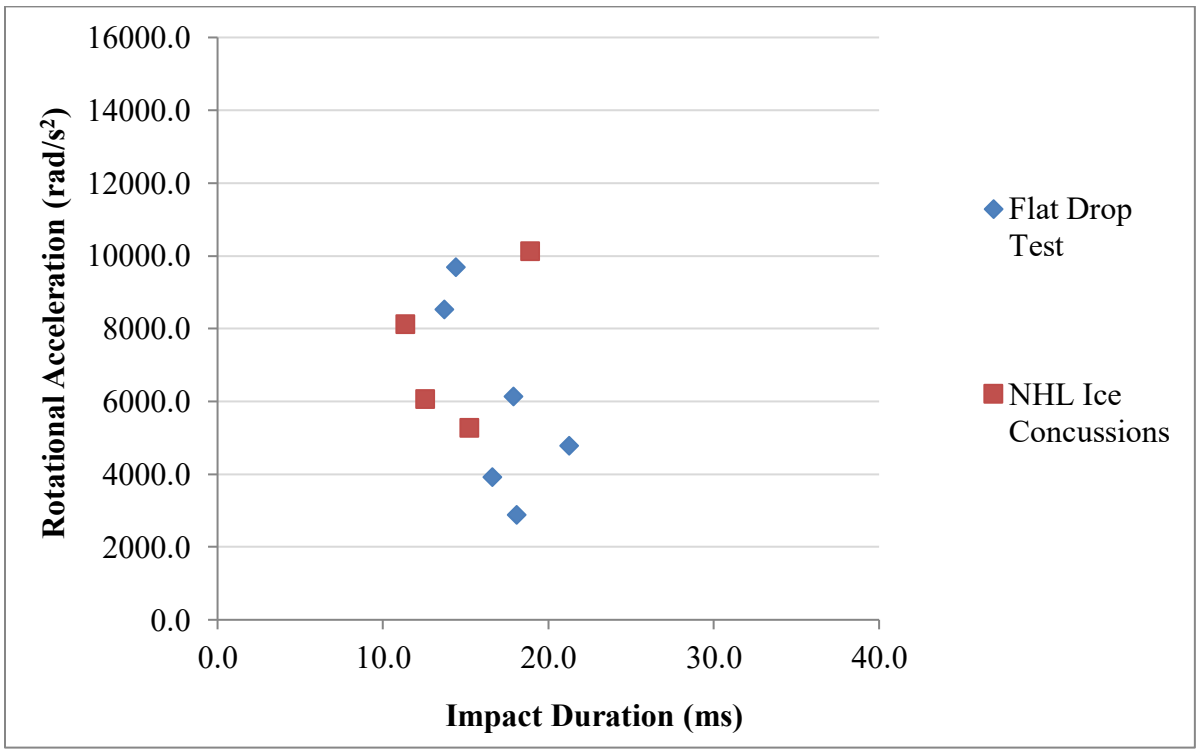

Figure H-1. Plot of rotational acceleration versus impact duration for the Flat Anvil Drop Test and PIH head-to-ice concussion reconstructions.

A graphical comparison of impact durations between the 30° Anvil Drop Test, 45° Anvil Drop Test, and PIH head-to-boards concussion reconstructions is presented in Figure I-2.

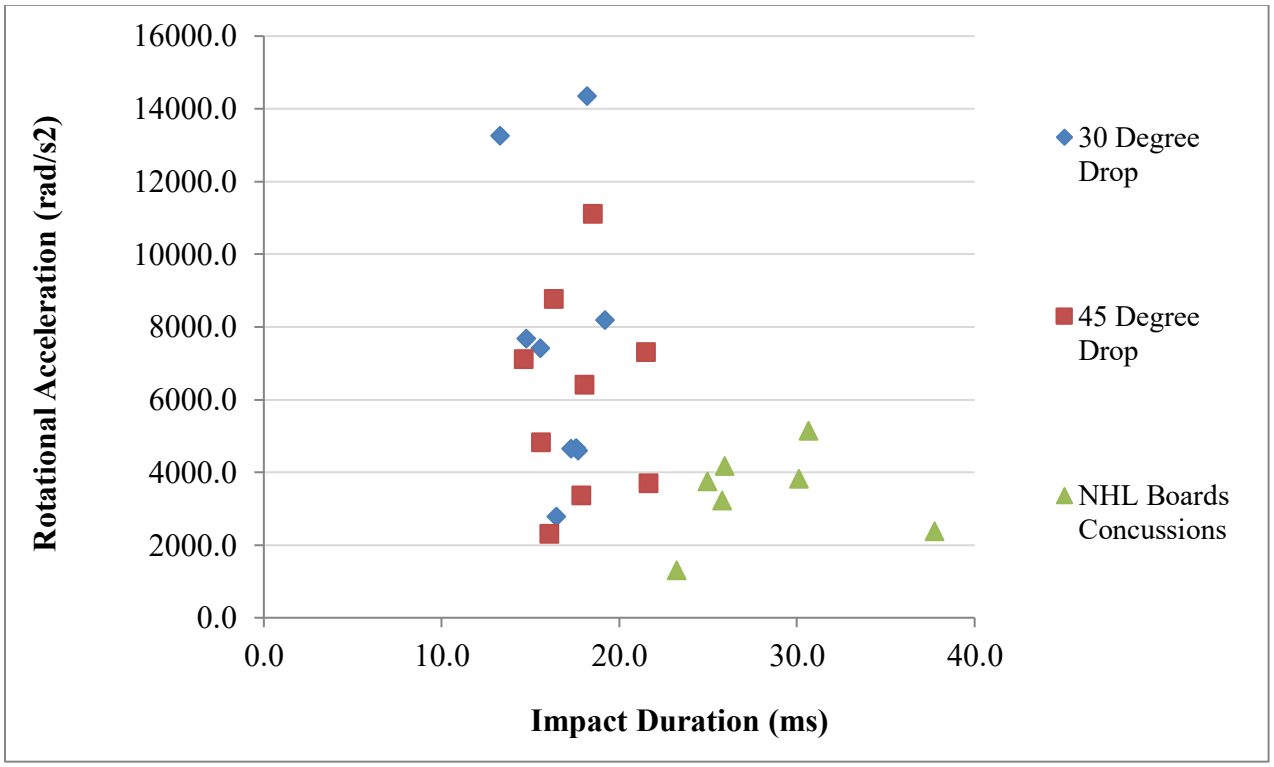

Figure H-2. Plot of rotational acceleration versus impact duration for the 30° Anvil Drop Test, 45° Anvil Drop Test, and PIH head-to-boards concussion reconstructions.

A graphical comparison of impact durations between the Medium Compliance Ram Test, High Compliance Ram Test, and PIH shoulder-to-head concussion reconstructions is presented in Figure I-3.

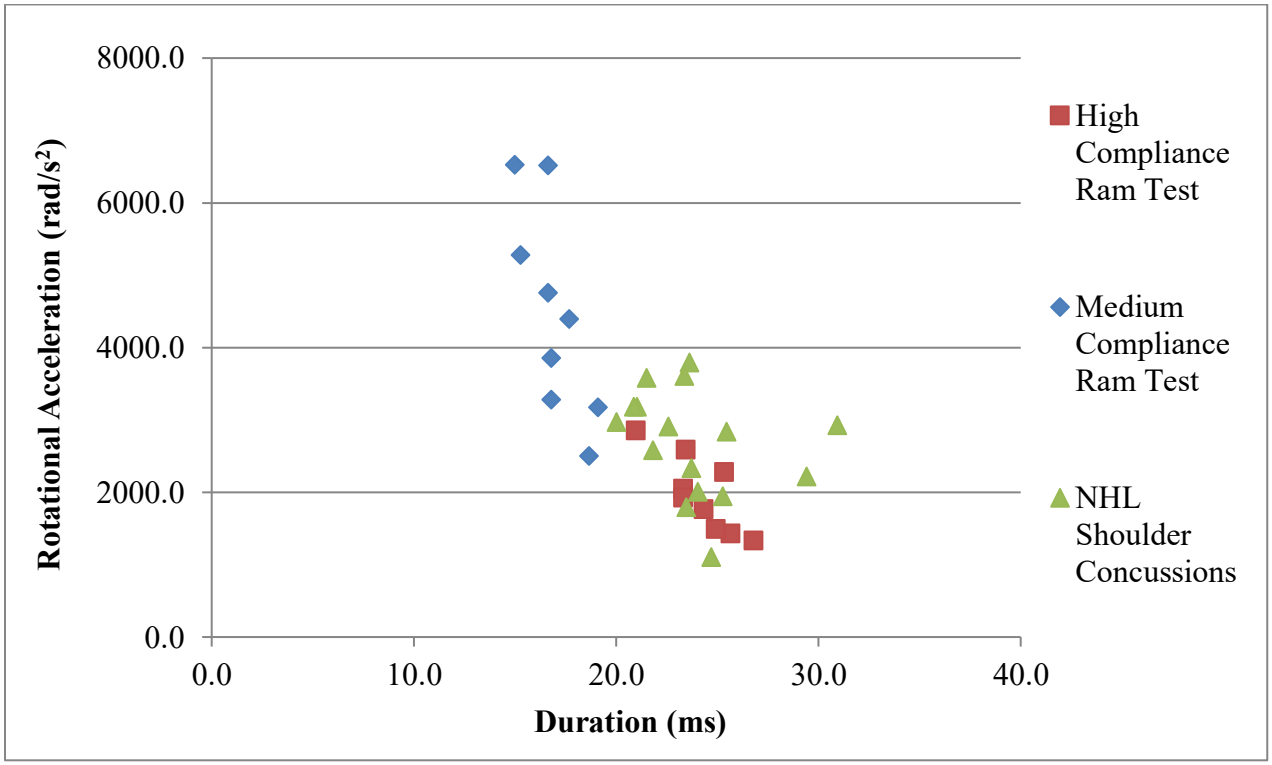

Figure H-3. Plot of rotational acceleration versus impact duration for the Medium Compliance Ram Test, High Compliance Ram Test, and PIH shoulder-to-head concussion reconstructions.

Appendix I

Results Separated by Impact Velocity and Location

Table I-1. Mean peak dynamic response and brain tissue deformation (±1 standard deviation) for the Flat Anvil Drop Test (*abbreviations explained below).

		Dynamic Response						*Brain Tissue Deformation*
		Linear Acceleration (g)		**Rotational Acceleration (rad/s^2)**		**Rotational Velocity (rad/s)**		**MPS (%)**
		Res.	**Dom.**	**Res.**	**Dom.**	**Res.**	**Dom.**	
3.0 m/s	FB	65.5 (2.2)	55.2 (12.3)	2883.0 (601.0)	2790.7 (632.1)	11.7 (1.9)	11.2 (2.2)	0.204 (0.038)
	RB	57.9 (8.0)	47.8 (4.2)	3913.7 (595.7)	3381.9 (752.8)	16.8 (2.0)	14.0 (2.4)	0.226 (0.021)
4.0 m/s	FB	88.1 (5.6)	76.4 (10.7)	4772.9 (1420.6)	4404.4 (1458.9)	18.0 (3.5)	16.6 (3.9)	0.329 (0.070)
	RB	119.9 (4.2)	95.8 (7.7)	8530.9 (797.7)	7360.3 (306.6)	25.6 (1.1)	22.3 (0.3)	0.400 (0.036)
5.0 m/s	FB	124.3 (9.0)	93.1 (19.5)	6128.6 (1271.3)	5284.0 (1540.2)	22.6 (3.6)	19.3 (4.5)	0.415 (0.052)
	RB	127.3 (5.0)	101.3 (14.5)	9688.8 (1071.9)	8422.1 (1346.9)	31.4 (0.9)	26.9 (2.2)	0.459 (0.078)

*Res. = Resultant; Dom. = Dominant

**FB = front boss; RB = rear boss

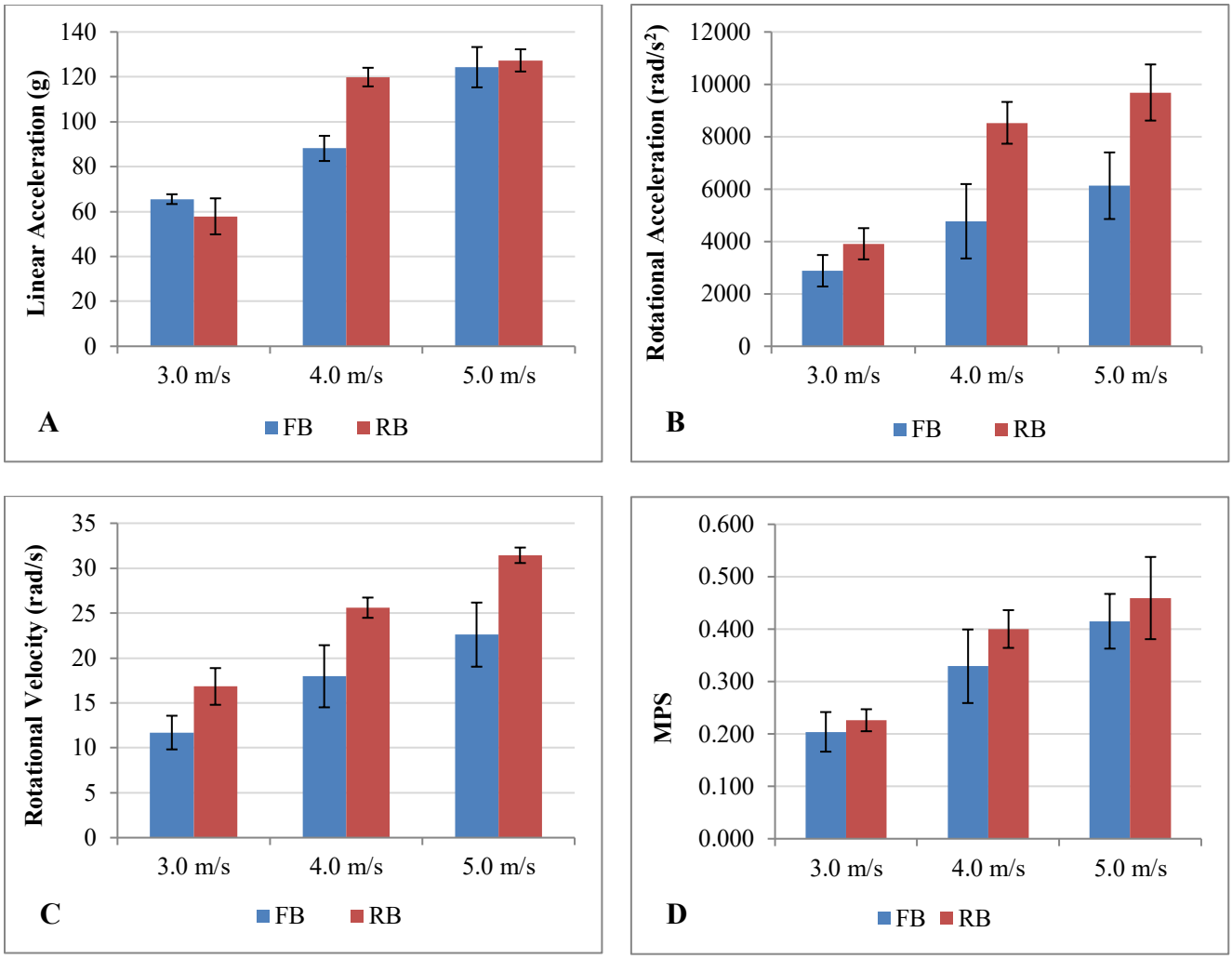

Figure I-1. Mean peak linear acceleration (A), rotational acceleration (B), rotational velocity (C), and MPS (D) for the Flat Anvil Drop Test, separated by impact velocity and location. Error bars indicate ± one standard deviation. FB = front boss; RB = rear boss.

Table I-2. Mean peak dynamic response and brain tissue deformation (±1 standard deviation) for the 30º Anvil Drop Test (*abbreviations explained below).

		Dynamic Response						*Brain Tissue Deformation*
		Linear Acceleration (g)		**Rotational Acceleration (rad/s^2)**		**Rotational Velocity (rad/s)**		**MPS (%)**
		Res.	**Dom.**	**Res.**	**Dom.**	**Res.**	**Dom.**	
3.0 m/s	S	46.4 (8.1)	36.3 (5.9)	4659.4 (376.9)	4450.3 (450.2)	22.3 (0.6)	21.5 (0.5)	0.331 (0.020)
	RB	45.4 (0.7)	37.8 (6.7)	4584.8 (428.4)	3678.3 (456.5)	22.0 (2.3)	17.9 (1.8)	0.308 (0.040)
	R	66.6 (9.4)	61.2 (7.0)	2775.7 (651.6)	2676.3 (515.3)	10.9 (1.3)	10.6 (1.2)	0.161 (0.026)
4.5 m/s	S	90.1 (6.9)	80.6 (12.8)	8187.2 (855.5)	7863.9 (1013.3)	31.3 (2.9)	29.7 (3.6)	0.497 (0.018)
	RB	89.8 (2.2)	70.5 (6.8)	7675.0 (309.8)	5992.0 (681.4)	30.6 (0.6)	23.1 (3.6)	0.427 (0.024)
	R	92.7 (3.3)	83.3 (3.9)	4649.1 (114.8)	4390.2 (76.9)	19.0 (0.6)	17.4 (2.3)	0.275 (0.001)
6.0 m/s	S	175.0 (3.0)	150.3 (21.8)	14342.1 (921.7)	13655.6 (785.9)	42.9 (1.8)	40.8 (1.3)	0.665 (0.032)
	RB	149.7 (7.6)	111.4 (7.0)	13256.7 (414.4)	8682.2 (97.9)	40.6 (0.6)	29.4 (1.7)	0.575 (0.014)
	R	126.5 (31.0)	103.9 (29.6)	7410.9 (1019.9)	5721.4 (1141.3)	29.6 (0.4)	22.3 (1.8)	0.410 (0.040)

*Res. = Resultant; Dom. = Dominant

**S = side; RB = rear boss; R = rear

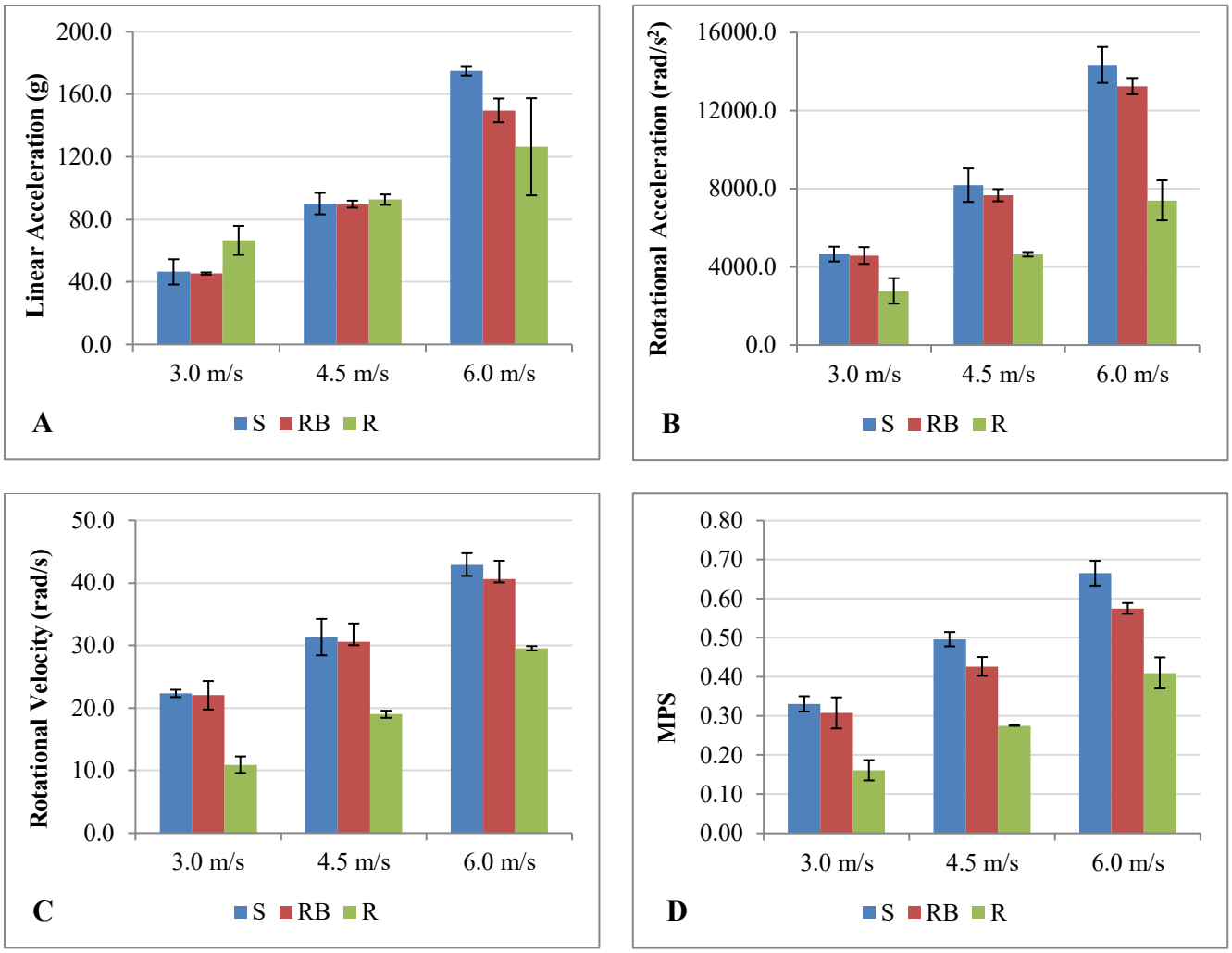

Figure I-2. Mean peak linear acceleration (A), rotational acceleration (B), rotational velocity (C), and MPS (D) for the 30° Anvil Drop Test, separated by impact velocity and location. Error bars indicate ± one standard deviation. S = side; RB = rear boss; R = rear.

Table I-3. Mean peak dynamic response and brain tissue deformation (±1 standard deviation) for the 45° Anvil Drop Test (*abbreviations explained below).

		Dynamic Response						*Brain Tissue Deformation*
		Linear Acceleration (g)		**Rotational Acceleration (rad/s^2)**		**Rotational Velocity (rad/s)**		**MPS (%)**
		Res.	**Dom.**	**Res.**	**Dom.**	**Res.**	**Dom.**	
3.0 m/s	S	25.1 (5.8)	18.8 (5.5)	3675.4 (594.9)	3382.8 (750.4)	25.3 (1.2)	23.6 (1.9)	0.365 (0.034)
	RB	30.8 (7.4)	22.3 (6.6)	3343.2 (288.7)	2592.5 (254.9)	20.2 (1.0)	16.2 (1.7)	0.265 (0.002)
	R	44.2 (12.6)	37.0 (11.7)	2291.8 (711.6)	2102.9 (836.0)	9.9 (4.8)	9.5 (5.0)	0.152 (0.084)
4.5 m/s	S	63.2 (3.8)	53.0 (5.8)	7277.5 (117.6)	6998.8 (298.6)	34.8 (0.7)	33.9 (0.7)	0.515 (0.008)
	RB	62.6 (11.3)	49.6 (7.5)	6393.4 (289.7)	4839.2 (365.0)	29.5 (3.6)	22.8 (2.8)	0.392 (0.050)
	R	78.2 (9.7)	58.7 (9.1)	4797.2 (710.6)	4756.2 (749.3)	24.1 (1.6)	23.7 (1.9)	0.332 (0.022)
6.0 m/s	S	123.3 (53.5)	100.0 (46.8)	11092.1 (3843.7)	10569.7 (4292.3)	42.0 (1.7)	39.6 (4.0)	0.639 (0.076)
	RB	86.0 (14.4)	66.5 (20.7)	8747.1 (1441.9)	6828.0 (902.5)	41.4 (5.4)	33.3 (2.7)	0.543 (0.042)
	R	134.1 (13.4)	117.9 (9.1)	7099.5 (481.1)	6901.9 (341.1)	25.1 (2.1)	24.5 (1.7)	0.371 (0.036)

*Res. = Resultant; Dom. = Dominant

**S = side; RB = rear boss; R = rear

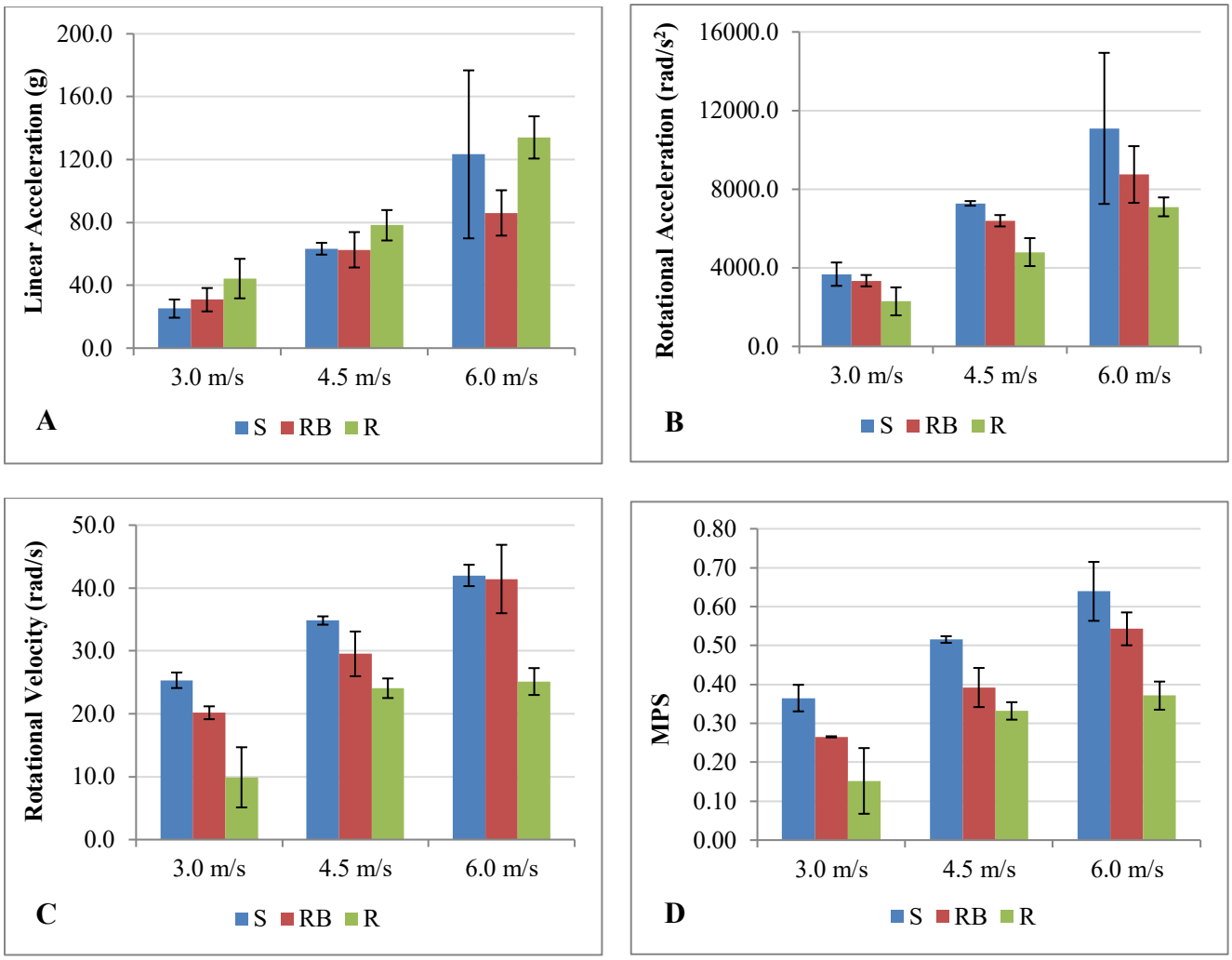

Figure I-3. Mean peak linear acceleration (A), rotational acceleration (B), rotational velocity (C), and MPS (D) for the 45° Anvil Drop Test, separated by impact velocity and location. Error bars indicate ± one standard deviation. S = side; RB = rear boss; R = rear.

Table I-4. Mean peak dynamic response and brain tissue deformation (±1 standard deviation) for the Medium Compliance Ram Test (*abbreviations explained below).

		Dynamic Response						*Brain Tissue Deformation*
		Linear Acceleration (g)		**Rotational Acceleration (rad/s^2)**		**Rotational Velocity (rad/s)**		**MPS (%)**
		Res.	**Dom.**	**Res.**	**Dom.**	**Res.**	**Dom.**	
6.0 m/s	FBPA	36.9 (0.2)	35.9 (0.1)	3169.3 (138.1)	2693.5 (100.8)	25.8 (0.2)	22.1 (0.2)	0.333 (0.005)
	S	41.1 (0.1)	41.1 (0.1)	2498.1 (43.9)	2492.9 (46.9)	26.3 (0.7)	26.2 (0.7)	0.270 (0.006)
	RBNA	33.9 (0.3)	33.5 (0.2)	3851.3 (36.1)	3230.0 (51.4)	31.1 (0.6)	25.6 (0.5)	0.323 (0.006)
7.5 m/s	FBPA	47.5 (0.5)	46.7 (0.4)	4391.3 (127.8)	3281.9 (67.3)	31.3 (0.7)	25.0 (0.4)	0.446 (0.011)
	S	54.7 (1.1)	54.6 (1.2)	3273.0 (92.1)	3158.4 (60.6)	26.9 (0.4)	26.6 (0.4)	0.328 (0.006)
	RBNA	42.9 (0.6)	42.2 (0.7)	5280.1 (57.0)	4849.5 (71.1)	33.9 (1.2)	29.2 (1.1)	0.356 (0.019
9.0 m/s	FBPA	64.8 (2.3)	63.7 (2.4)	6517.2 (242.8)	4771.1 (104.8)	36.6 (1.0)	27.8 (1.0)	0.565 (0.010)
	S	67.1 (1.8)	67.0 (1.8)	4207.8 (111.6)	4189.0 (125.1)	28.3 (0.1)	28.1 (0.0)	0.360 (0.005)
	RBNA	57.3 (3.6)	56.8 (3.7)	6521.7 (490.3)	5926.4 (444.3)	38.9 (2.6)	32.6 (2.3)	0.425 (0.020)

*Res. = Resultant; Dom. = Dominant

**FBPA = front boss positive azimuth; S = side; RBNA = rear boss negative azimuth

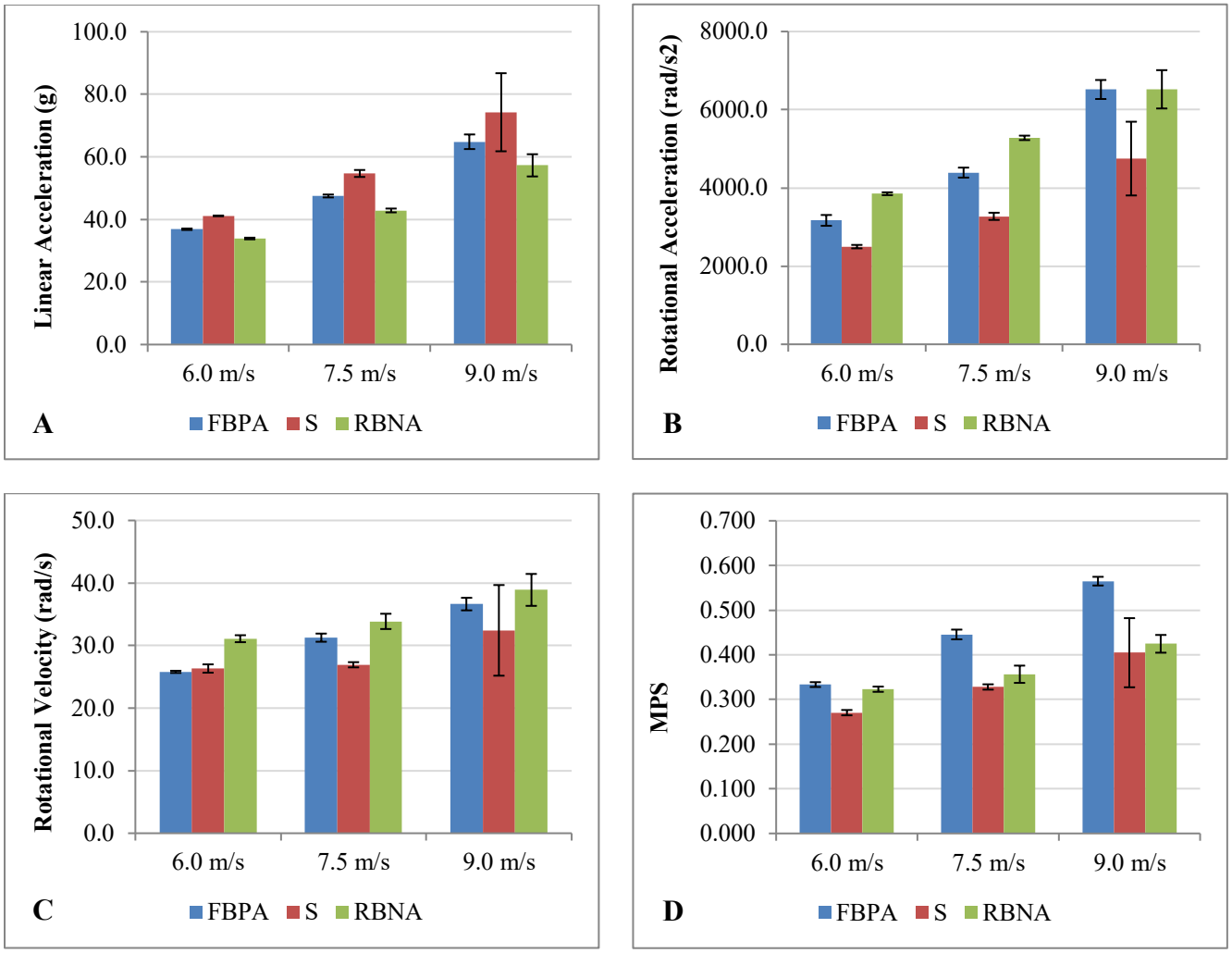

Figure I-4. Mean peak linear acceleration (A), rotational acceleration (B), rotational velocity (C), and MPS (D) for the Medium Compliance Ram Test, separated by impact velocity and location. Error bars indicate ± one standard deviation. FBPA = front boss positive azimuth; S = side; RBNA = rear boss negative azimuth.

Table I-5. Mean peak dynamic response and brain tissue deformation (±1 standard deviation) for the High Compliance Ram Test (*abbreviations explained below).

		Dynamic Response						*Brain Tissue Deformation*
		Linear Acceleration (g)		**Rotational Acceleration (rad/s^2)**		**Rotational Velocity (rad/s)**		**MPS (%)**
		Res.	**Dom.**	**Res.**	**Dom.**	**Res.**	**Dom.**	
6.0 m/s	FBPA	14.1 (0.3)	14.0 (0.2)	1757.8 (16.5)	1371.8 (2.4)	15.9 (0.3)	12.4 (0.2)	0.193 (0.005)
	S	16.6 (0.7)	16.6 (0.7)	1323.2 (53.8)	1186.1 (46.5)	14.3 (0.8)	13.6 (0.8)	0.155 (0.007)
	RBNA	14.1 (0.4)	14.1 (0.5)	1423.4 (46.9)	1108.6 (38.4)	19.2 (0.6)	13.9 (0.5)	0.168 (0.003)
7.5 m/s	FBPA	19.5 (1.0)	19.4 (1.1)	2270.5 (91.8)	1727.3 (72.1)	20.7 (1.3)	15.3 (0.9)	0.239 (0.012)
	S	20.4 (0.4)	20.3 (0.4)	1480.6 (7.7)	1478.5 (7.0)	16.3 (0.4)	16.3 (0.4)	0.155 (0.005)
	RBNA	16.1 (0.4)	16.0 (0.3)	2039.8 (84.2)	1867.6 (51.9)	24.2 (1.2)	19.5 (0.8)	0.201 (0.004)
9.0 m/s	FBPA	22.4 (0.8)	22.2 (0.8)	2580.9 (87.8)	1932.2 (70.7)	20.3 (0.7)	14.5 (0.5)	0.248 (0.010)
	S	23.9 (0.8)	23.9 (0.8)	1916.9 (40.7)	1911.5 (39.9)	17.1 (0.7)	17.0 (0.7)	0.174 (0.006)
	RBNA	20.4 (0.6)	20.4 (0.6)	2845.9 (100.4)	2514.7 (129.0)	27.0 (0.9)	21.8 (1.0)	0.235 (0.005)

*Res. = Resultant; Dom. = Dominant

**FBPA = front boss positive azimuth; S = side; RBNA = rear boss negative azimuth

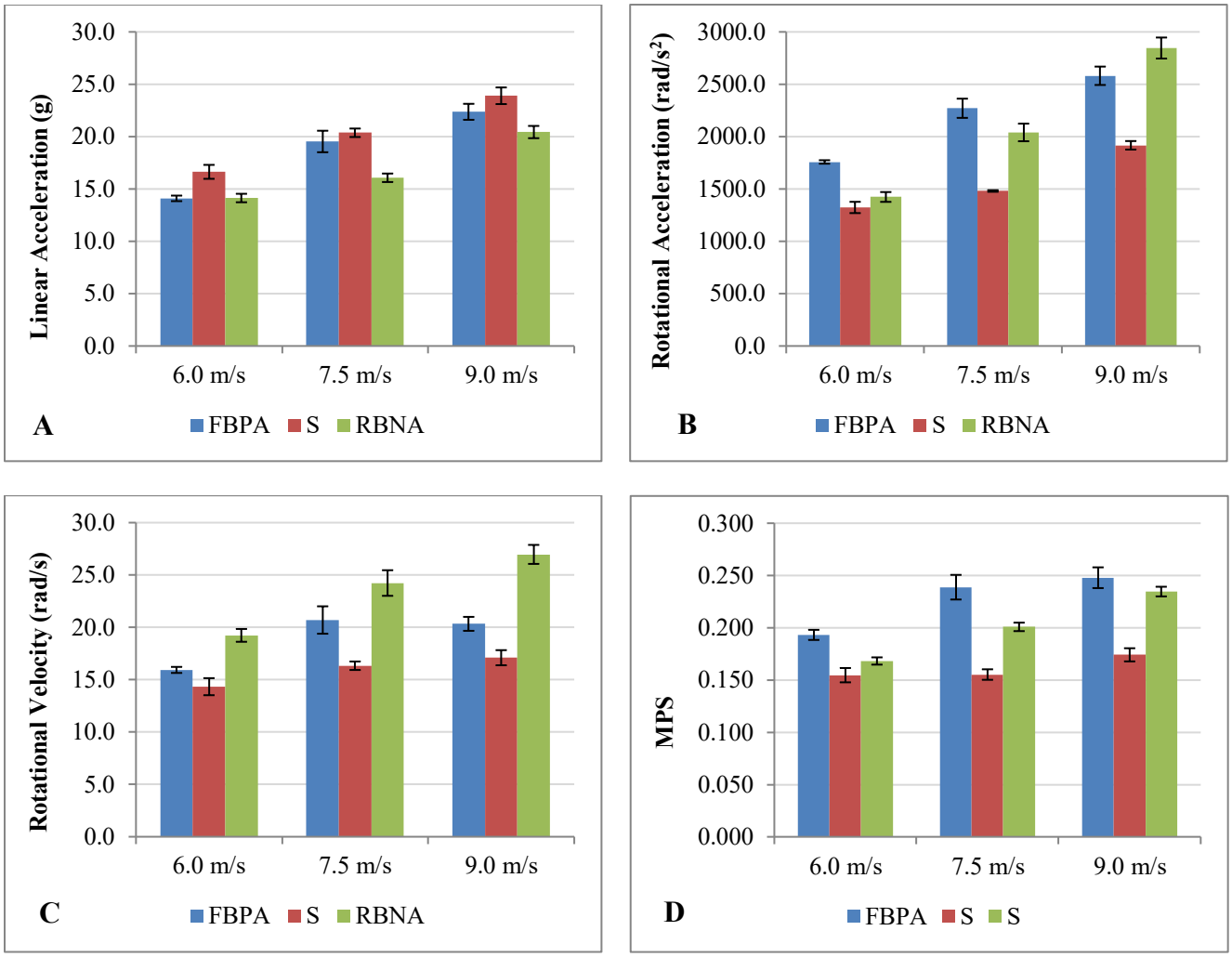

Figure I-5. Mean peak linear acceleration (A), rotational acceleration (B), rotational velocity (C), and MPS (D) for the High Compliance Ram Test, separated by impact velocity and location. Error bars indicate ± one standard deviation. FBPA = front boss positive azimuth; S = side; RBNA = rear boss negative azimuth.

Appendix J

Repeatability of Helmet Impact Tests

The flat anvil drop test used two impact locations and three impact velocities (six unique impact conditions). For each of the six conditions, the coefficient of variation $\left(CV = \frac{\sigma}{\mu}\right)$ was calculated for each dynamic response variable and MPS. Next, all coefficients of variation for linear acceleration were averaged, producing one number representing the overall repeatability of linear acceleration for the flat anvil drop test. This process was continued, producing one number representing the overall repeatability for each of the remaining dynamic response variables and MPS. A smaller average coefficient of variation indicates a more repeatable measure with little variation from one impact to the next. In contrast, a larger average coefficient of variation indicates a less repeatable measure with more variable results from one impact to the next. This process was repeated to evaluate the repeatability of the 30° anvil drop test, 45° anvil drop test, medium compliance ram test, and high compliance ram test (Table J-1).

Table J-1. Average coefficients of variation for each dependent variable for each helmet test.

	LA, Res.	**LA, Dom.**	**RA, Res.**	**RA, Dom.**	**RV, Res.**	**RV, Dom.**	**MPS**
Flat Anvil Drop	6.4%	14.7%	17.8%	21.2%	11.7%	15.5%	14.6%
30° Anvil Drop	8.7%	13.9%	9.0%	10.5%	5.1%	9.0%	6.8%
45° Anvil Drop	20.2%	24.2%	15.0%	17.6%	11.6%	13.2%	12.9%
Medium Compliance Ram	2.07%	2.07%	3.08%	2.81%	2.42%	2.56%	2.56%
High Compliance Ram	3.12%	3.13%	2.89%	2.87%	3.93%	3.96%	3.20%

* LA = linear acceleration; RA = rotational acceleration; RV = rotational velocity;
Res. = resultant; Dom. = dominant.

The average coefficients of variation for the 45° drop test are higher than the 30° drop test, indicating less repeatability. This is primarily due to the external geometry of the helmet interacting with the angled steel anvil and producing variability in the results. Both the medium and high compliance ram tests produced consistent results with low average coefficients of variation.